2002

The Classical Limit of the Quantum Baker's Map

Mark Morgan-Tracy

The classical limit of the quantum baker's map

by

Mark M. Tracy

B.S., Physics, University of Cincinnati, 1994
B.A., Mathematics, University of Cincinnati, 1994

THESIS

Submitted in Partial Fulfillment of the
Requirements for the Degree of

Doctor of Philosophy
Physics

The University of New Mexico

Albuquerque, New Mexico

December, 2002

Dedication

To my wife Kristin and daughter Emily.

Acknowledgments

I would like to thank all of those who have made this thesis possible.

Beginning with my advisor, Dr. Carlton M. Caves for giving the first draft of this work the pummeling it deserved and for many useful discussions, especially those on the non-physics topics of weather and GMO foods.

Dr. Ivan Deutsch has been extremely helpful in reading a first draft of this work and providing helpful comments (in pdf format no less).

I would like to thank the other members of my committee, Dr. Cris Moore and Dr. David Dunlap for taking time from their busy schedules to participate in the fun that is a thesis defense.

To Dr. Andrew Scott for being a great friend and bringing with him the last piece of the mathematical puzzle; the method of steepest descent (as well as a wealth of useful references and so may other useful tips and tricks. Thank You!!).

To my office cohorts who have provided me with hours of interesting conversation and lunch time fun. Thanks to Joe Renes, Kiran Manne, Shohini Ghose, Rene Stock, Tracey Tessier, and Pranaw Rungta.

I would also like to thank the former graduate students who have helped me in too many ways to list here: Michael Nielsen, Tom Pannuti, Howard Barnum, Cris Fuchs, Amy Stevenson, Audra Rice, Michael O'Brian, Eric Moore, Gavin Brennen, John Grondalski, and the others whom I can't recall at this point.

It would be remiss of me to forgot those who really help make a thesis happen: my mom and dad (for obvious reasons), and the office staff of Mary DeWitt, Betty Fry, and Eleanor Maes. It would have been impossible without your help.

And lastly, I would like to again thank my wife Kristin for not minding sleeping alone while I was up late writing this thing, and to my daughter Emily for sleeping until 8:00AM most of the time.

The classical limit of the quantum baker's map

by

Mark M. Tracy

ABSTRACT OF THESIS

Submitted in Partial Fulfillment of the
Requirements for the Degree of

Doctor of Philosophy
Physics

The University of New Mexico

Albuquerque, New Mexico

December, 2002

The classical limit of the quantum baker's map

by

Mark M. Tracy

B.S., Physics, University of Cincinnati, 1994
B.A., Mathematics, University of Cincinnati, 1994

Ph.D., Physics, University of New Mexico, 2002

Abstract

This work concerns the finding of the semi-classical form of the coherent state representation for the class of quantum baker's maps defined by Schack and Caves.

It begins by introducing the finite-dimensional Hilbert space on which the quantum baker's map is defined. Its pertinent features including the all important symmetry operators are introduced and given a full explanation. We also introduce the finite-dimensional phase space which will give the semi-classical limit a geometrical interpretation. For a D dimensional Hilbert space, the finite-dimensional phase space is found to be a grid with D^2 points. Each point corresponds to a particular pair of position and momentum displacement operator eigenphases.

We then detail the derivation of the finite-dimension version of the Wigner function, a quasi-distribution for the finite-dimensional phase space. We show that its

most "irregular" feature, mainly its property of having more values than was thought necessary, can be explained by its correct behavior under the symmetry operations, a feature lacking in other Wigner candidates. However, even this special choice for the Wigner function proves unusable in the semi-classical limit as it is found to have a non-convergent limit.

We then turn to another possible phase space function: the Q-function. It being necessary to find a suitable coherent state for the finite-dimensional Hilbert space, we begin by studying the properties of the periodically continued Gaussian states. These are the typical Weyl coherent states made periodic in both position and momentum such as to make them legitimate finite-dimensional states. Developing certain mathematical techniques allows us to show that they have compatible position and momentum representations, that a subset of them are complete and can be used to define a Q-function, and that this function obeys all of the symmetry properties.

Finally, we use these coherent states to find a representation for the propagator of the quantum baker's map. In the semi-classical limit, *i.e.* the large dimension limit, this representation is found, for most of the maps, to take a form of the exponentiation of the classical map's generating function. This form was predicted long ago by Van Vleck as indicator of an operator's classical limit. Therefore, we assert that these maps limit to the classically chaotic baker's map. In certain limiting schemes, however, the Schack-Caves maps do not reach this form and must be given a different interpretation.

Contents

List of Figures

List of Tables

Glossary

$\mathcal{H}_D$	Finite-dimensional Hilbert space with Dimension D.
$\mathcal{L}_2$	Space of square integrable functions.
$\hat{U}$	Momentum displacement operator in $\mathcal{H}_D$.
$\hat{V}$	Position displacement operator in $\mathcal{H}_D$.
$\hat{F}$	Fourier transform operator in $\mathcal{H}_D$.
$\hat{T}$	Time reversal antiunitary operator in $\mathcal{H}_D$.
$\Phi(\xi, \eta)$	The characteristic function for continuous Hilbert space.
$W(x, p)$	The Wigner function for continuous Hilbert space.
$\hat{\rho}$	A system's density operator.
$\hat{B}_{M,L}$	The characteristic function operator in $\mathcal{H}_D$.
$\hat{W}_{M/2,S/2}$	The Wigner function for $\mathcal{H}_D$.
$\hat{A}_{M/2,S/2}$	The Wigner function operator in $\mathcal{H}_D$.
$\big\lvert a\big\rangle$	The coherent state for $\mathcal{H}_D$ centered at $a = x_0 + ip_0$.
$Q(a)$	The Q-function for $\mathcal{H}_\mathcal{D}$.

Glossary

$\big\|\sigma\big\rangle$	The squeezed state for $\mathcal{H}_D$ centered at $\sigma = x_0 + ip_0$.
$\hat{B}_n$	The class of quantum baker's maps, $n = 1, \ldots, N-1$.
$\hat{B}_{\theta,s}$	The class of quantum baker's maps with altered notation.

Chapter 1

Introduction

> If your wish is to become really a man of science and not merely a petty experimentalist, I should advise you to apply to every branch of natural philosophy, including mathematics.
>
> –*Frankenstein*, Mary Shelley

1.1 A brief history of the classical limit, chaos, and quantum mechanics in general

The path which leads from the quirky yet captivating world of quantum mechanics to our mundane classical existence is murky. Is classical mechanics really an emergent phenomena arising from the more fundamental quantum mechanics, and if so, what physical mechanism separates the two? Is there a region of overlap between the two theories where one may sometimes find classical behavior and sometimes quantum? Questions of these sorts have puzzled physicists since the inception of quantum mechanics.

Most physicists' notion of a classical limit, *i.e.* a procedure which yields a classical counterpart to a quantum mechanical system, comes from the correspondence principle. This principle states that for systems which are described by a quantum number, like the harmonic oscillator or the Bohr atom, that as this quantum number becomes large[1], classical dynamics is restored. The "proof" of the correspondence principle relies mostly on analyzing the wavefunctions that can be explicitly found for the simple systems stated before. For example, the harmonic oscillator's probability density is found for large quantum number n to be contained inside an envelope. The function for this envelope is determined by the time interval a classically oscillating object spends at a point in space. This is a wonderful measure of the probability[2] of finding the oscillator at a certain point in space; hence, the correspondence principle's common acceptance.

While the correspondence principle works well for simple systems, it fails when considering systems without convenient quantum numbers that can be set arbitrarily high. Given that the Bohr atom and harmonic oscillator's quantum numbers measure the system's energy, a natural generalization is to examine systems in the high energy regime. For reasons which will become clear shortly, this regime is called semi-classical. The inspiration for this type of research was the work of Van Vleck. He proposed that in the very high energy limit the classical behavior of a system would re-assert itself; the position matrix representation for a quantum propagator would have a form dependent on the classical system's action [1]. Later Einstein, Brillouin, and Keller would each seize upon this idea of working in the semi-classical regime while devising a program for finding the quantum counterpart to a classical system [2, 3, 4]. The backbone of EBK, as it became known, was the quantization of the classical system's action. The end result being the approximation of the energy eigenvalues for systems in the semi-classical regime. In this way, one could study the

[1] Or equivalently as the action of the system becomes much larger than Plank's constant.
[2] Assuming that the function has been normalized.

lingering effects of the classical world on a quantum system. Unfortunately, EBK worked only for systems whose classical dynamics were integrable, *i.e.* systems in which all constants of motion are known thus making their motion easy to predict. It remained uncertain how to continue until the development of chaos theory.

The theory of chaos is a field of study with an enormous body of theoretical work and variety of application. To detail its salient points would take more space than is available. For our purposes it shall suffice to define chaos as the motion of systems in which small changes in initial conditions quickly create large differences in the final states thus making their motion difficult to predict. Many math historians trace the existence of chaos back to 19th century work of Poincaré[3]. Poincaré's use of the phase space to represent the motion of a system and his study of systems near unstable fixed points would not only help later spur the development of chaos but would have a profound impact on how physicists and mathematicians view the subject of mechanics. Poincaré's work helped Einstein realize that the EBK theory would fail for non-integrable systems. Physicists as a whole, however, remained mostly unaware of the work of Poincaré and later the development of chaos theory until it was brought to their attention in the early 1960's when the numerical studies of two astrophysicists, Hénon and Heiles [6] showed the existence of chaos in the motion of stars. This brought about a new interest in the field. In the following years there would be numerous findings of chaos in physical systems. From the motion of Saturn's moons to the turbulent vertices of liquid hydrogen, chaos seemed to be everywhere. But was chaos in quantum mechanics?

The new field of "quantum chaos" set out to determine the answer to this question. At first it seemed impossible that chaos could survive the transition from the classical world. Classical chaos depends on the phenomena of sensitivity to initial conditions, the exponential divergence of trajectories in phase space. In quantum

[3]Of course there were many others who helped this fledgling field. A short list would include Birkoff, Kovalevskaya, and Liapunov. See Percival's article in [5] for more details.

mechanics, we have vectors in a Hilbert space that are propagated in time by unitary operators. The natural measure of distance between states in Hilbert space is the inner product. The unitarity of the time propagator makes it impossible for this distance to change, thus making the concept of a quantum sensitivity to initial conditions moot. Luckily though, there is an alternative classical mechanics framework which would provide hope for solving the quantum chaos problem. Classical dynamics can be reformulated as the evolution of a probability density in phase space. This density's dynamics is determined by the Liouville equation, a linear partial differential equation which preserves the overlap between different densities, therefore masking sensitivity to initial conditions. Chaos manifests itself by its stretching and folding of the Liouville density to such a fine degree that it ends mixed completely over phase space. For the quantum case, an immediate analogy is made between the Liouville density and the quantum mechanical density operator. While this analogy was not seen by skeptics as a proof for the existence of quantum chaos, it was sufficiently encouraging for further work [7, 8, 9, 10, 11, 12, 13, 14].

In the early 1970's, quantum chaos was advanced tremendously when Gutzwiller invented his periodic orbit theory[4] that could find the semi-classical energy eigenvalues for classically chaotic systems [15]. Periodic orbit theory's name is derived from its dependence on summing over the periodic orbits of a classical system. Later, Berry and Tabor would show that EBK quantization could be recast as a sum over periodic orbits for an integrable system [16]. The work of EBK had been completed and quantum chaos had a new tool. The eventual result of this new ability to find the semi-classical eigenenergies was the belief that the lingering effect of classical chaos would be found in the distribution of these energies [17]. This new program, called eigenvalue statistics, had a theoretical motivation in Wigner's random matrix

[4]Of course at that time the field of chaos, much less quantum chaos, had not been developed yet. It would take a decade before Gutzwiller's impact on quantum chaos would become apparent.

theory [18]; a procedure for predicting the statistical properties of a quantum system by replacing its Hamiltonian with an appropriate ensemble of random matrices[5]. It was believed that the randomness of the matrices would distill the essence of classical chaos. The appeal of eigenvalue statistics was that it allowed one to simply determine whether a quantum system was chaotic. A chaotic system's eigenenergies would display repulsion from each other while an integrable system's eigenenergies would be attractive [17]. This behavior is represented in Figure 1.1 which plots the population as a function of the energy eigenvalue difference for an idealized chaotic and integrable system. The integrable system's eigenvalues are attractive, *i.e.* many of its values are nearly equal, thus making their difference approximately zero. Their statistical distribution reflects this by being peaked at zero. The chaotic system's eigenvalues, on the other hand, display repulsion hence their distribution is peaked away from zero.

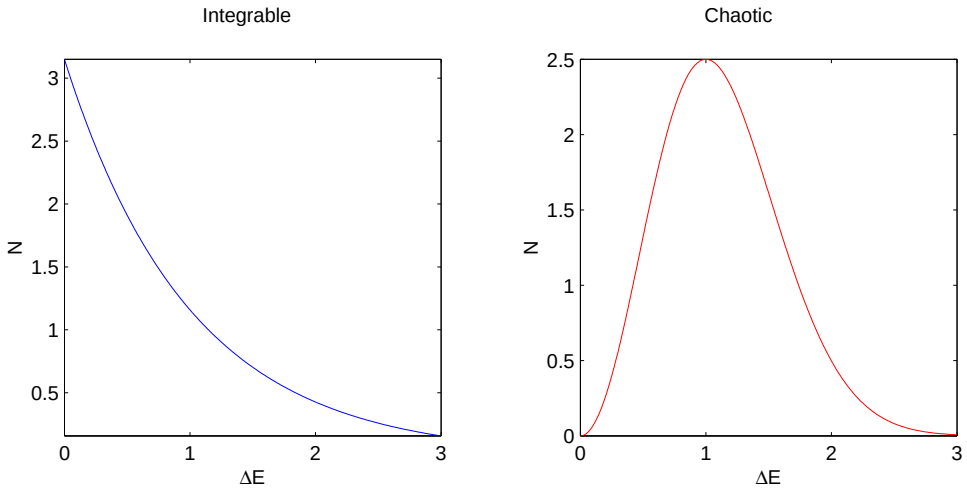

Figure 1.1: The energy eigenvalue difference Histogram for an integrable and chaotic system. The functional form for each is explained by the attractive (repulsive) nature of the eigenvalues.

While the eigenvalue statistics program was useful for characterizing a quantum

[5]This ensemble was chosen such as to have the same symmetries as the studied system.

system as chaotic, it could not establish a correspondence between a quantum and classical system, the necessary task for finding the classical limit. There seemed to be no procedure for starting from a classical system and finding its quantum analog, besides the trivial cases where the system's Hamiltonian could be quantized by operator replacement of variables. Even the simplest "toy" model systems, those with discrete time evolution such that the dynamics is given by a simple function on phase space, had no algorithm for finding their quantum counterpart. Given their simplicity, however, an attempt to derive a quantum version of these "toy" models, usually called maps, seemed inevitable.

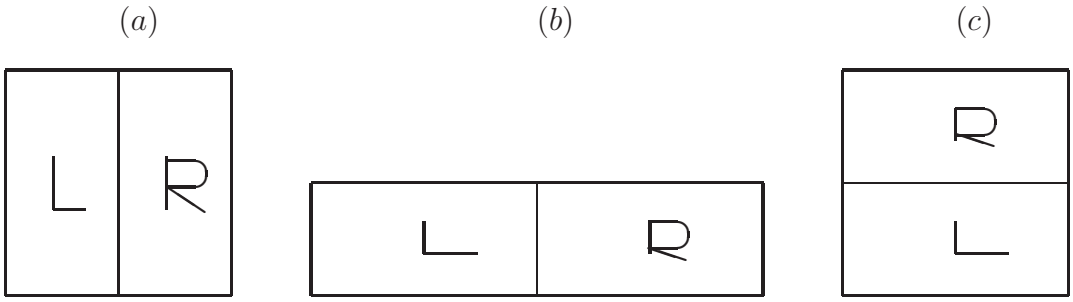

Figure 1.2: The classical baker's map: (a) the unit square is dived into left and right, (b) the square is squeezed in one dimension and stretched in the other, (c) the resultant right hand side is stacked onto the left to preserve area.

A famous example of a classical map is the baker's map [19]. As shown in Figure 1.2, the map operates on the unit square with an action that stretches by a factor of two in position, squeezes by the same amount in momentum, and then stacks the resultant right hand side on top of the left. In this way, its action is supposed to mimic a baker kneading dough. Despite the difficulties discussed earlier, in 1989 Balazs and Voros created an operator[6] which they claimed was a quantum version

[6]Given that the baker's map time evolution is a phase space mapping, the obvious quantum analog is a unitary time evolution operator.

of the baker's map [20]. Later Saraceno, by using anti-periodic boundary conditions, would improve the symmetry properties of this operator [21]. In the following years other versions of the quantum baker's map were to follow. In 1994 Hannay devised an optical analogy to the baker's map [22], a so called canonical quantization[7] was devised by Rubin and Lesniewski [23, 24]. Quantum computing realizations have been proposed by Schack and Brun [25, 26]. A quantum baker's mapping on the sphere has also been defined [27]. More recently, an entire class of quantum baker's maps was proposed by Schack and Caves using two-level systems *i.e.* qubits [28]. The Balazs-Voros quantization is but one member of this class. These works often contained a heuristic argument about why these operators were in fact a quantum version of the baker's map, but it remained to be shown in a compelling mathematical way that these statements were true.

1.2 The classical limit of the quantum baker's map

The thrust of this work is to find the classical limit for the class of quantum baker's maps defined by Shack and Caves and thereby to find out if these maps limit to the classical map. The classical limit for the Schack-Caves baker's map has already been studied by Soklakov and Schack using the decoherent histories apparatus [29]. Decoherent histories, developed by Griffiths, Omnès, and Gell-Mann and Hartle [30, 31, 32], is an alternate program for finding the classical limit. Unlike the semi-classical approach of this work, it arrives at classical dynamics by an appropriate coarse graining over phase space. We feel that our program, while using a different technique, builds upon Soklakov and Schack's work by studying different possible

[7]Meaning that Rubin and Lesniewski implemented a covering of the classical map, *i.e.* an extension to the entire plane; therefore, their quantum version uses the canonical position and momentum operators.

ways of approaching the classical limit[8].

Beginning with the Balazs-Voros-Saraceno map and continuing to the Schack-Caves maps, the quantum baker's has been defined on a finite-dimensional Hilbert space[9] of dimension D. This space, sometimes called $\mathcal{H}_D$, has a long history of use by physicists and mathematicians. A summary of its properties can be found in Weyl [33] as well as Schwinger [34] and Perelemov [35] who were all instrumental in developing it. The finite-dimensional Hilbert space is an abstract space; unlike the more familiar angular momentum states, there need not be a physical system motivating its existence. We begin with a complete set of orthonormal states, which we call for convenience the "position" basis. Using the discrete Fourier transform, we create a conjugate basis called "momentum," and from there, we construct the corresponding finite phase space. For reasons which will be elaborated in Chapter 2, the finite nature of the Hilbert space prevents the existence of a position and momentum operator with the canonical "$i\hbar$" commutator. There are, however, position and momentum displacement operators whose commutator has the same form as in the continuous Hilbert space. These operators allow us to associate eigenvalues with the position and momentum basis states. In the semi-classical, *i.e.* large dimension limit, these eigenvalues approach continuously-valued bounded variables. With proper scaling, it is possible to recover the unit square, a very important thing when working with the baker's map.

Our classical limit program relies on finding the semi-classical form of the quantum baker's map's propagator. It is inspired by the work of Van Vleck, Gutzwiller, and even Feynman's path integral formulation of quantum mechanics [36]. Using Gutzwiller's periodic orbit theory, the Balazs-Voros-Saraceno quantum baker's map's energy eigenvalues have been extensively investigated [37, 38, 39, 40, 41, 42, 43, 44, 45]. Our inspiration is from Van Vleck's original work [1]. His hypothesis was that

[8] See Figure 6.3 for details.

[9] The canonical version of the quantum baker's map [23, 24] being an exception

in the semi-classical regime a quantum propagator $\hat{U}$ should have a position matrix element approaching a delta function centered at the classical dynamics' action. For a map, the quantity equivalent to the action is another generating function W, thereby leaving the expression

$$\left\langle x' \middle| \hat{U} \middle| x \right\rangle \approx \left(2\pi\hbar\right)^{-1/2} \left| \frac{\partial^2 W}{\partial x' \partial x} \right| \exp\left[-iW(x', x)/\hbar\right].$$

The lack of a canonical position operator in the finite dimensional Hilbert space, however, forces a modification of this Van Vleck ansatz as it was called by Saraceno and Voros [39].

Rubin and Salwen's work on the canonical quantum baker's map [23] suggested that the necessary modification to the Van Vleck ansatz could be found using the Wigner function; a quasi-distribution found by tracing a system's density operator against the Fourier transform of the symmetrically ordered displacement operator. The symmetrically ordered displacement operator has the form $\exp\left[i\left(\eta\hat{q} - \xi\hat{p}\right)/\hbar\right]$ where the constants η and ξ specify displacement amounts. Rubin and Salwen showed that when η and ξ are multiples of $2\pi\hbar$, the $\hbar \to 0$ limit for the trace of the symmetrically ordered displacement operator with the Weyl coherent state projector is equal to a phase. In which case, the coherent state's Wigner function for these special η and ξ values limits to a delta function[10]. In the finite-dimensional Hilbert space, $2\pi\hbar$ is proportional to $1/D$, the fundamental unit of displacement. It therefore seemed reasonable that by finding a Wigner function and coherent states for the finite Hilbert space, one would be assured of a delta function limit for these coherent states' Wigner function, thus creating an analogy between the coherent states and phase space points. In this way, the Van Vleck ansatz would be modified to deal with phase space points instead of the generating function: if the Wigner function of a quantum map's propagator acting on these coherent states also limited to phase space points then a classical counterpart to the quantum map was obtained. Un-

[10]The location of this delta function is at the center of the coherent state.

fortunately, the existence of a finite-dimensional Wigner function was uncertain[11]. Undaunted, we began work to find such a function.

Aided by the work of Wootters [47] and Leonhardt [48], our program for finding a finite dimensional Wigner function relied on the natural connection between the finite-dimensional Hilbert space and the set of all doubly periodic wavefunctions. Demanding that a wavefunction be periodic in both position and momentum restricts the possible values of Plank's constant to be an integer. This has the effect of restricting the phase space area between orthogonal states, a quantity equal to Plank's constant, to be equal to an integer. The same situation is found in the finite-dimensional phase space where Plank's constant must be equal to the dimension of the Hilbert space, another integer. This connection, made precise through the use of an isomorphism, between the two spaces allows one to give a finite-dimensional reinterpretation of a doubly periodic wavefunction's Wigner function. Unfortunately, it was found that every state's finite dimensional Wigner function must necessarily have regions of rapid oscillation. There are various reasons for these oscillations, including proper symmetry properties and quantum interference. See Chapter 3 for details. In the large dimension limit, these oscillations' frequency increase apace making a convergent expression impossible. It seemed that the Wigner function was not the correct phase space function to use.

The other popular choice for phase space representation is the so called Q-function, often called a Husimi representation by mathematicians. A state's Q-function is given by the square modulus of its coherent state representation[12]. Using spin coherent states Kuś [49] as well as Scott [50] had found examples of angular momentum systems whose semi-classical propagator had taken a form reminiscent of

[11] After our work on the finite Wigner function was completed, it would become clear that Hannay and Berry [46] were aware of its existence in 1980. This fact seems to be relatively unknown in the physics literature.

[12] Assuming that the set of coherent states are complete.

the Van Vleck ansatz. When modified for use with a quantum map $\hat{B}$ and the $\mathcal{H}_D$ coherent states, this form is

$$\langle b|\hat{B}|a\rangle \propto \exp\Big[W(b^*,a)/2\hbar\Big]\exp\Big[-\big(|a|^2+|b|^2\big)/4\hbar\Big] \tag{1.1}$$

where $|a\rangle$ and $|b\rangle$ are the coherent states. This expression is a combination of the original Van Vleck ansatz and its modification to the phase space; its content is that in the semi-classical regime, the action of the quantum propagator on the point[13] a is non-zero only when b has the value specified by the classical map. To use this idea in the finite-dimensional Hilbert space of the quantum baker's map required finding appropriate coherent states. Literature on the subject indicated that a promising choice would be the complete set of periodically continued states of Shau-Jin and Shi [51]. Here, the traditional Weyl coherent states are periodically continued, making them legitimate states in the finite-dimensional Hilbert space. While there are other possibilities for coherent states, we have found that these states have many characteristics which make their use preferable, the least of which is the ease with which their analytic form can be manipulated in calculation.

It remained an open question whether these periodically continued coherent states would yield the appropriate semi-classical form for the quantum baker's map until the completion of this work. Using the method of steepest descent, a mathematical technique for finding an integral's asymptotic form, we calculated the left hand side of Equation 1.1 in the large dimensional limit for the class of maps defined by Schack and Caves. To define these maps, Schack and Caves created states for Hilbert space of dimension 2^N that have varying position and momentum localization. These states are labelled by an integer n. They are strictly position localized in a region of width $1/2^n$ and roughly localized[14] in a momentum region of width $1/2^{N-n}$. The parameter n, the number of position bits, ranges from 0 for momentum eigenstates

[13] As was the case with the Wigner function, the coherent states can be seen as limiting to phase space points.

[14] See Figure 5.4 for a plot of the momentum probability distribution.

to N for position eigenstates. The Schack-Caves class of quantum baker's maps are constructed by mapping[15] the set of "n-localized" states to the set of localized states with $n-1$. The change in localization from the n to $n-1$ states is such that the position localization is doubled while the corresponding momentum localization is halved. In this way, the Schack-Caves maps mimic the classical baker's map. Calculating the semi-classical form of the propagator is equivalent to letting N become infinite; however, one has complete freedom in determining the rate at which n and $N-n$, the number of momentum bits, approach infinity. Moreover, by choosing the appropriate rate either n or $N-n$ can be kept fixed in the limit. We found that as long as $N-n$ is not kept fixed then the semi-classical propagator has the desired form of Equation 1.1. Therefore, we assert that these maps have the proper classical limit. It is possible for most of the Schack-Caves maps, however, to fix the number of momentum bits in the limit[16]. We find that for these classically incorrect maps their propagator's matrix element has non-zero values for a finite set of states. In the language of Equation 1.1, there is more than one state b for which the matrix element $\langle b|\hat{U}|a\rangle$ is non-zero. An obvious interpretation of this result is a limit to a classical stochastic mapping which produces one of the phase space points analogous to b with a probability determined by the non-zero matrix element. However, it remains an open question whether this interpretation is valid.

It should be noted that the success for these maps is not a guarantee of this program working for all maps. Baranger [52] has shown that in general one should expect extra terms in the exponent of Equation 1.1. Also, we calculate the propagator for one time step to avoid complications which will arise after many iterations of the mapping. For long time scales, simple quantum-to-classical correspondences will break down [53]. In which case, another classical limit program such as decoherence

[15]The center's of the prior and resultant states are chosen to mimic the classical baker's map.

[16]This is the difference between our work and that of Soklakov and Schack. They did not allow for this case and thus did not realize the possibility of a different classical limit.

[54, 55, 56] or continuous measurement [57, 58] will be necessary to restore the classical dynamics.

1.3 Thesis outline

This thesis is organized in the following way. Chapter 2 introduces the finite-dimensional Hilbert space and its corresponding phase space. We begin with a summary of the basic features of the finite Hilbert space, the position basis vectors and the discrete Fourier transform's creation of momentum states. As the question of creating position and momentum operators is often raised by those unfamiliar with this space, an explicit calculation of the commutator for the obvious Hermitian operators is given. We find, as it has been shown in many places before, that the position representation of the commutator has non-zero off diagonal values; thus, proving that the canonical commutation relation is not obeyed. Next, we introduce the position and momentum displacement operators which act on states in the discrete Hilbert space. We find that their commutator is of the same form as the continuous space. This allows us to define an finite analog to the symmetrically ordered displacement operator. The displacement operators also allow us to show that the basis vectors are periodic, up to phases. From this periodicity, we realize that the finite-dimensional phase space corresponding to the Hilbert space is a torus. Finally, we introduce the symmetry operators, Fourier transform and time reversal, for the finite-dimensional Hilbert space and define them by their action on the position basis vectors. By demanding that these two operators produce basis vectors when operating on momentum states, we find these operators can be given a geometrical interpretation in phase space only for the special choice of periodic or anti-periodic boundary conditions. This interpretation being 90° rotation and reflection through the position axis respectively. Using the geometrical interpretation as a guide allows us to classify the

other possible symmetry operations. We find that every symmetry operation can be performed by combinations of Fourier and time reversal, thus making their study paramount.

Chapter 3 concerns the finite-dimensional Wigner functions; its derivation and relevant properties. As there seems to be a great degree of repetition in the field, we begin with a summary of the huge body of literature on the finite-dimensional Wigner function. Next, we introduce the motivation and the actual form of the isomorphism which maps between $\mathcal{H}_D$ and the subset of doubly periodic wavefunctions. With this isomorphism, we calculate the finite-dimensional characteristic function and from it, the finite-dimensional Wigner function. As the Wigner function plays a large role in this work, its salient features are studied in great detail. In particular, we show how the Wigner function produces the correct position and momentum marginal distribution and investigate its puzzling $4D^2$ values. As the phase space is a D^2 valued grid, it was originally assumed that the corresponding Wigner function would have the same number of values. Instead, it has 4 times as many values[17]. We have forwarded two explanations for these extra "pieces". One explanation is that these extra values are necessary to give the Wigner function the same geometrical interpretation in phase space as the symmetry operators of Chapter 2. The other explanation comes from the periodicity of the phase space, a characteristic which must be mirrored in the Wigner function. This periodicity of the Wigner function creates quantum interference and results in regions of phase space where the Wigner function's values oscillate rapidly[18]. Neither explanation can be proven to be the "real" reason for the $4D^2$ values and must instead be viewed as complimentary

[17]This statement is controversial. Many researchers believe in Leonhardt's result that this is true only for even-dimensional Hilbert spaces. We, on the other hand, have found that the Wigner function has $4D^2$ values for all dimensions but that it is possible, in odd dimensions only, to create from this function one with D^2 values.

[18]This is the same rapid oscillation which made the Wigner function unsuitable for use in the semi-classical calculation.

features of a phase space function.

Chapter 4 details the pertinent characteristics of the finite-dimensional Q-function. We first introduce the periodically continued coherent states and give their position basis representation. With our mathematical technique of finding the Fourier series representation of the periodically continued coherent states, we show that these states have the expected momentum basis representation and are able to give a simple expression for the normalization of the coherent state subset used in defining our Q-function. We also explicitly prove the completeness of these coherent states and thus define our Q-function. This Q-function is seen to almost trivially have the phase space geometrical interpretation that was so difficult to find for the discrete Wigner function. The periodically continued coherent states are easily modified to create a finite-dimensional squeezed state, so these states are introduced and shown to be complete as well. This chapter concludes with a derivation of the fact that a discrete Gaussian convolution links our choices for the Wigner and Q-function. While this fact is not directly related to finding the classical limit of the quantum baker's map, it is included as it gives greater weight to our belief that these functions are the proper ones for use in the finite-dimensional Hilbert space.

Chapter 5 introduces the quantum baker's map. Starting from the Balazs-Voros-Saraceno map, we motivate the Schack-Caves class of baker's maps. Balazs and Voros' quantum baker's map was defined using the partial Fourier transform operator which, to paraphrase Balazs and Voros, is an operator which, "Fourier transform half of the sites." Using the Q-function, we clarify this statement; we find that in phase space the partial Fourier transform operator creates states which are position localized in either the left or right hand side of the phase space and momentum localized to within the limits of the uncertainty relation. Their baker's map recreates the classical map by taking these states and mapping them to momentum eigenstates

whose position localization is twice that of the previous states[19]. Realizing this interpretation, Schack and Caves created the n-localized states discussed earlier. We detail the action of these maps and also show the importance of the Schack-Caves choice of anti-periodic boundary conditions. Lastly, we investigate the eigenvalues for the $n = N$ Schack-Caves map. Its eigenvalues are found to be completely regular, *i.e.* they are all roots of unity, a characteristic not found in the other maps. It is hypothesized that this difference in eigenvalue behavior could have been seen as an indicator that this map has a different classical limit.

Finally, Chapter 6 details the calculation of the semi-classical coherent state representation of the propagator for the Schack-Caves class of quantum baker's maps. As stated previously, we find that for limiting schemes which allow the number of momentum bits to become infinite the propagator's coherent state representation has a limiting form of Equation 1.1. Hence, we claim these maps have the proper classical limit. However, one has complete freedom in taking this limit, thus it is possible to fix the number of momentum bits and have a map without the correct classical limit. This is always true for the $n = N$ Schack-Caves map as its input is a position eigenstate. For these maps, we introduce the possibility and derive an expression for the probabilities of a stochastic classical interpretation.

Chapter 7 concludes this work by offering insight into the construction of this document as well as providing topics for future work.

[19]Where the mapping is chosen such that the center of the prior and resultant states mimics the classical baker's map.

Chapter 2

The quantum phase space

2.1 Discrete quantum phase space

The basis of work in this thesis is the discrete phase space corresponding to a D-dimensional Hilbert space $\mathcal{H}_D$. In a finite D-dimensional Hilbert space, there are no real position and momentum operators. The reason for this is that the canonical commutation relationship, $[q, p] = i\hbar$, is no longer true. Instead of relying on Hermitian position and momentum operators, we instead base our phase space on the unitary displacement operators[1].

We begin with a basis $\big|e_j\big\rangle$, $j = 0 \ldots D-1$, which will act as our "position" eigenstates. This assumption is made formal by having them be the eigenstates of the momentum displacement operator, $\hat{U}$,

$$\hat{U}\big|e_j\big\rangle = \exp\left[2\pi i(j+\beta)/D\right]\big|e_j\big\rangle. \tag{2.1}$$

This basis is complete, $\sum_{j=0}^{D-1}\big|e_j\big\rangle\big\langle e_j\big| = 1$ and orthonormal, $\big\langle e_j\big|e_l\big\rangle = \delta_{j,l}$.

[1]These operators, like in the continuous case, still obey the Wigner-Weyl commutation relation.

While labelled by variable j, the eigenstate $\left|e_j\right\rangle$ can be thought of as having a "position eigenvalue" $e_j = (Q/D)(j+\beta)$. Geometrically, we represent our Hilbert space in a configuration space as a discrete set of D points which are equally spaced between 0 and Q. Each point is offset by an constant amount β which must necessarily be in the range $[0, 1)$.

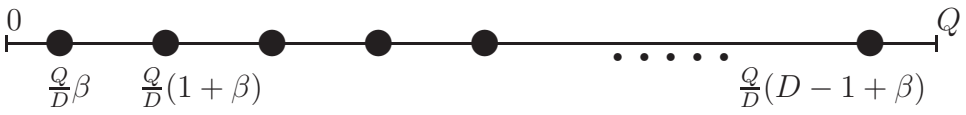

Figure 2.1: Geometrical interpretation of the position eigenstates: D equally spaced states along a line of length Q, each offset by an amount $(Q/D)\beta$. Their eigenvalues determined by their length from the origin.

We now wish to make a connection with the familiar constant $\hbar$. To do this, we make an analogy between the operator $\hat{U}$ and the continuous displacement operator $\exp[iP\hat{q}p/\hbar]$ which displaces by the amount Pp. The constant P sets an overall momentum scale and p is the displacement amount relative to P. If we naively operate upon a state[2] $\left|e_j\right\rangle$, we have

$$\exp\left[\frac{iP}{\hbar}\hat{q}p\right]\left|e_j\right\rangle = \exp\left[\frac{iQP}{\hbar D}(j+\beta)p\right]\left|e_j\right\rangle.$$

Now we must make some assumptions about the variable p. We know that in $\mathcal{H}_D$, the eigenvalues differ by $1/D$; therefore, if we set $p = 1/D$, we get

$$\exp\left[\frac{iP}{\hbar}\hat{q}p\right]\left|e_j\right\rangle = \exp\left[\frac{iQP}{\hbar D^2}(j+\beta)\right]\left|e_j\right\rangle.$$

For consistency of units *i.e.* to get Equation 2.1, we must have that

$$QP = 2\pi\hbar D. \tag{2.2}$$

[2]We will assume that $\hat{q}$ is the operator whose eigenstate is $\left|e_j\right\rangle$ with eigenvalue e_j.

This relationship simply states that the phase space area per orthogonal state QP/D is given by $2\pi\hbar = h$.

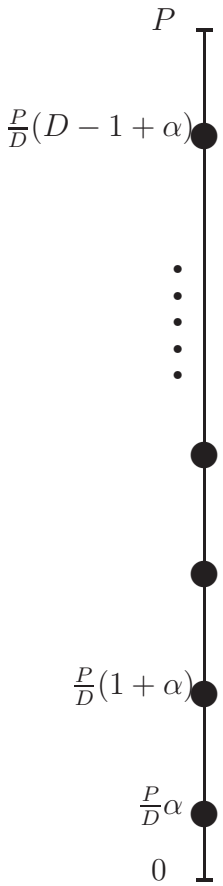

Figure 2.2: Geometrical interpretation of the momentum eigenstates: D equally spaced states along a vertical line of length P, each offset by an amount $(P/D)\alpha$. Their eigenvalues determined by their length from the origin.

Conjugate to position is momentum. We shall create a conjugate basis through the use of the quantum Fourier transform,

$$\big|p_k\big\rangle = \sum_{j=0}^{D-1} \big|e_j\big\rangle\big\langle e_j\big|p_k\big\rangle \equiv \frac{1}{\sqrt{D}} \sum_{j=0}^{D-1} \exp\left[\frac{2\pi i}{D}(j+\beta)(k+\alpha)\right] \big|e_j\big\rangle, \qquad (2.3)$$

which defines the inner product $\langle e_j | p_k \rangle$. This equation can also be written as

$$\begin{aligned} |p_k\rangle &= \sum_{j=0}^{D-1} |e_j\rangle\langle e_j|p_k\rangle = \sum_{j=0}^{D-1} |e_j\rangle \exp\left[\frac{i}{\hbar} e_j p_k\right] \\ &= \sum_{j=0}^{D-1} |e_j\rangle \exp\left[iQ(j+\beta)p_k/\hbar D\right], \end{aligned} \tag{2.4}$$

where $p_k = (P/D)(k+\alpha)$. Using Equation 2.2, we see that the momentum eigenstates have "momentum eigenvalues" $p_k = (P/D)(k+\alpha)$. Not surprisingly, the momentum representation of the Hilbert space is also a discrete set of points, but equally spaced between 0 and P. They are offset by a different constant $\alpha \in [0, 1)$. We shall see that the constants α and β are related to the periodicity of our space.

Equation summary for section 2.1

$$\hat{U}\left|e_j\right\rangle = \exp\left[\frac{2\pi i}{D}(j+\beta)\right]\left|e_j\right\rangle = \exp\left[\frac{i}{\hbar}e_j(P/D)\right]\left|e_j\right\rangle$$

$$e_j = \frac{Q}{D}(j+\beta)$$

$$\sum_{j=0}^{D-1}\left|e_j\right\rangle\left\langle e_j\right| = 1$$

$$\left\langle e_j|e_l\right\rangle = \delta_{j,l}$$

$$\left\langle e_j|p_k\right\rangle = \frac{1}{\sqrt{D}}\exp\left[\frac{2\pi i}{D}(j+\beta)(k+\alpha)\right] = \frac{1}{\sqrt{D}}\exp\left[\frac{i}{\hbar}e_j p_k\right]$$

$$p_k = \frac{P}{D}(k+\alpha)$$

$$QP = 2\pi\hbar D$$

2.1.1 Non-canonical position and momentum operators

With the mathematics already developed, we can see why it is impossible to define a position and momentum operator in $\mathcal{H}_D$ which satisfy the canonical commutation

relationship[3]. If we define a position operator, we can write it as

$$\hat{q} = \sum_{j=0}^{D-1} e_j \left|e_j\right\rangle\!\left\langle e_j\right|, \tag{2.5}$$

where e_j is shorthand for $(Q/D)(j+\beta)$. Likewise, we can write a momentum operator

$$\hat{p} = \sum_{k=0}^{D-1} p_k \left|p_k\right\rangle\!\left\langle p_k\right| \tag{2.6}$$

with $p_k = (P/D)(k+\alpha)$. From these definitions, we see that

$$\begin{aligned} \hat{q}\hat{p} &= \sum_{j,k=0}^{D-1} e_j p_k \left|e_j\right\rangle\!\left\langle e_j|p_k\right\rangle\!\left\langle p_k\right| \\ &= \frac{1}{\sqrt{D}} \sum_{j,k=0}^{D-1} e_j p_k \, \exp\left[\frac{2\pi i}{D}(j+\beta)(k+\alpha)\right] \left|e_j\right\rangle\!\left\langle p_k\right|. \end{aligned} \tag{2.7}$$

Inserting a resolution of the identity, we can write the operator in the position representation[4] as

$$\begin{aligned} \hat{q}\hat{p} &= \frac{1}{\sqrt{D}} \sum_{j,k=0}^{D-1} \sum_{l=0}^{D-1} e_j p_k \exp\left[\frac{2\pi i}{D}(j+\beta)(k+\alpha)\right] \left|e_j\right\rangle\!\left\langle p_k|e_l\right\rangle\!\left\langle e_l\right| \\ &= \frac{1}{D} \sum_{j,k,l=0}^{D-1} e_j p_k \exp\left[\frac{2\pi i}{D}(k+\alpha)(j-l)\right] \left|e_j\right\rangle\!\left\langle e_l\right|. \end{aligned} \tag{2.8}$$

We can divide the sum over the l variable into two pieces: $l = j$ and $l \neq j$. For the former case, we have

$$\sum_{j=0}^{D-1} \frac{e_j}{D} \left|e_j\right\rangle\!\left\langle e_j\right| P \sum_{k=0}^{D-1} \frac{k+\alpha}{D} = \frac{P}{D}\left(\frac{D-1}{2}+\alpha\right) \sum_{j=0}^{D-1} e_j \left|e_j\right\rangle\!\left\langle e_j\right| \tag{2.9}$$

where we have used the summation formula

$$\sum_{m=0}^{N} m = \frac{N(N+1)}{2}.$$

[3]This topic has been much discussed and is included mostly as a summary of other work. For a recent review along with a proof of the re-emergence of the canonical commutation relation in infinite dimension see de la Torre [59].

[4]A similar treatment in the momentum representation yields similar results.

For the $l \neq j$ case, we need to be a little trickier. We can write the sum of interest as

$$\sum_{k=0}^{D-1}(k+\alpha)\exp\left[\frac{2\pi i}{D}(k+\alpha)(j-l)\right] = \frac{D}{2\pi i}\frac{\partial}{\partial x}\left(\sum_{k=0}^{D-1}\exp\left[\frac{2\pi i}{D}(k+\alpha)x\right]\right)\Bigg|_{x=j-l}.$$

Using the summation formula for a geometric sum,

$$\sum_{r=0}^{a} x^r = \frac{1-x^{a+1}}{1-x}, \tag{2.10}$$

we see that

$$\sum_{k=0}^{D-1}(k+\alpha)\exp\left[\frac{2\pi i}{D}(k+\alpha)(j-l)\right] = \frac{D}{2\pi i}\frac{\partial}{\partial x}\left(\frac{\exp\left[2\pi i\alpha x/D\right]\left(1-\exp\left[2\pi i x\right]\right)}{1-\exp\left[2\pi i x/D\right]}\right).$$

After taking the derivative and setting $x = j-l$, we have

$$\sum_{k=0}^{D-1}(k+\alpha)\exp\left[\frac{2\pi i}{D}(k+\alpha)(j-l)\right] = -D\frac{\exp\left[2\pi i\alpha(j-l)/D\right]}{1-\exp\left[2\pi i(j-l)/D\right]} \tag{2.11}$$

giving

$$\hat{q}\hat{p} = \frac{P}{D}\sum_{j=0}^{D-1} e_j\left(\frac{D-1+2\alpha}{2}\left|e_j\right\rangle\!\left\langle e_j\right| - \sum_{l\neq j}\frac{\exp\left[2\pi i\alpha(j-l)/D\right]}{1-\exp\left[2\pi i(j-l)/D\right]}\left|e_j\right\rangle\!\left\langle e_l\right|\right). \tag{2.12}$$

From this expression, we find the commutator matrix elements,

$$\hat{q}\hat{p} - \hat{p}\hat{q} = -\frac{P}{D}\sum_{j=0}^{D-1}\sum_{l\neq j} e_j\left(\frac{\exp\left[2\pi i\alpha(j-l)/D\right]}{1-\exp\left[2\pi i(j-l)/D\right]}\left|e_j\right\rangle\!\left\langle e_l\right| - h.c.\right), \tag{2.13}$$

where *h.c.* stands for hermitian conjugate. We see that not only is the commutator not proportional to the identity matrix, its diagonal elements are zero.

For an infinite-dimensional Hilbert space, the analogous expression for the $\hat{q}\hat{p}$ operator contains the term

$$\int dp\, p\, \exp\left[-\frac{i}{\hbar}p(x-x')\right] = i\hbar\frac{\partial}{\partial x}\delta(x-x').$$

This Dirac-delta function derivative is necessary to create the canonical commutation relation. In the finite case, the sums are not sufficient to create them[5]; therefore, the idea of having canonical position and momentum operators is impossible.

Equation summary for section 2.1.1

$$\sum_{r=0}^{a} x^r = \frac{1-x^{a+1}}{1-x}$$

$$\hat{q}\hat{p} - \hat{p}\hat{q} = -\frac{P}{D}\sum_{j=0}^{D-1}\sum_{l\neq j} e_j \left(\frac{\exp\left[2\pi i\alpha(j-l)/D\right]}{1-\exp\left[2\pi i(j-l)/D\right]} \left|e_j\right\rangle\left\langle e_l\right| - h.c. \right)$$

2.1.2 Displacement operators and periodicity

The action of $\hat{U}$ on the momentum states can easily be calculated as

$$\begin{aligned} \hat{U}\left|p_k\right\rangle &= \frac{1}{\sqrt{D}}\sum_{j=0}^{D-1} \exp\left[\frac{2\pi i}{D}(j+\beta)(k+\alpha)\right] \hat{U}\left|e_j\right\rangle \\ &= \frac{1}{\sqrt{D}}\sum_{j=0}^{D-1} \exp\left[\frac{2\pi i}{D}(j+\beta)(k+1+\alpha)\right] \left|e_j\right\rangle \\ &= \left|p_{k+1}\right\rangle. \end{aligned} \tag{2.14}$$

Hence $\hat{U}$'s earlier title of "momentum displacement operator."

By reversing the roles of position and momentum, we define a position displacement operator, $\hat{V}$. Its eigenvectors are the momentum basis vectors $\left|p_k\right\rangle$, and its action on them is defined by

$$\hat{V}\left|p_k\right\rangle = \exp\left[-\frac{2\pi i}{D}(k+\alpha)\right]\left|p_k\right\rangle = \exp\left[-\frac{i}{\hbar}p_k(Q/D)\right]\left|p_k\right\rangle. \tag{2.15}$$

[5]As will be shown in an upcoming section, sums of the form $\sum_{j=0}^{D-1}\exp\left[2\pi ijk/D\right]$ are Kronecker-delta functions, but one cannot create from them a function with the necessary Dirac-delta function derivative properties.

A similar calculation to the one above verifies its name,

$$\hat{V}\big|e_j\big\rangle = \big|e_{j+1}\big\rangle. \tag{2.16}$$

From their definition, it is easy to calculate the commutator of the two displacement operators. The calculation is

$$\begin{aligned}\hat{U}\hat{V}\sum_{j=0}^{D-1}\big|e_j\big\rangle\big\langle e_j\big| &= \sum_{j=0}^{D-1}\exp\left[\frac{2\pi i}{D}(j+1)\right]\big|e_{j+1}\big\rangle \\ \hat{V}\hat{U}\sum_{j=0}^{D-1}\big|e_j\big\rangle\big\langle e_j\big| &= \sum_{j=0}^{D-1}\exp\left[\frac{2\pi i}{D}j\right]\big|e_{j+1}\big\rangle\end{aligned} \tag{2.17}$$

such that $\hat{U}\hat{V} = \exp\left[2\pi i/D\right]\hat{V}\hat{U}$. This procedure can be generalized for arbitrary powers; we find that the operators obey the Wigner-Weyl commutation relationship,

$$\hat{U}^j\hat{V}^k = \exp\left[\frac{2\pi i}{D}jk\right]\hat{V}^k\hat{U}^j. \tag{2.18}$$

This leads to the idea of a symmetrically ordered displacement operator. If we define an operator $\hat{B}_{j,k}$ to be the following

$$\hat{B}_{j,k} \equiv \exp\left[\frac{i\pi}{D}jk\right]\hat{V}^j\hat{U}^k, \tag{2.19}$$

then we see that this chosen phase factor gives it the very nice property that

$$\hat{B}^\dagger_{j,k} = \hat{B}_{-j,-k}.$$

This is analogous to the continuous case where the symmetrically ordered displacement operator is $\hat{D}(\eta,\xi) = \exp\Big[i(\eta\hat{q} - \xi\hat{P})/\hbar\Big]$, which trivially satisfies the condition $\hat{D}^\dagger(\eta,\xi) = \hat{D}(-\eta,-\xi)$.

But what happens if one tries to displace out of the space, *i.e.* what is $\hat{U}\big|p_D\big\rangle$ or $\hat{V}\big|e_D\big\rangle$? There are many ways to answer this question. Perhaps the easiest way

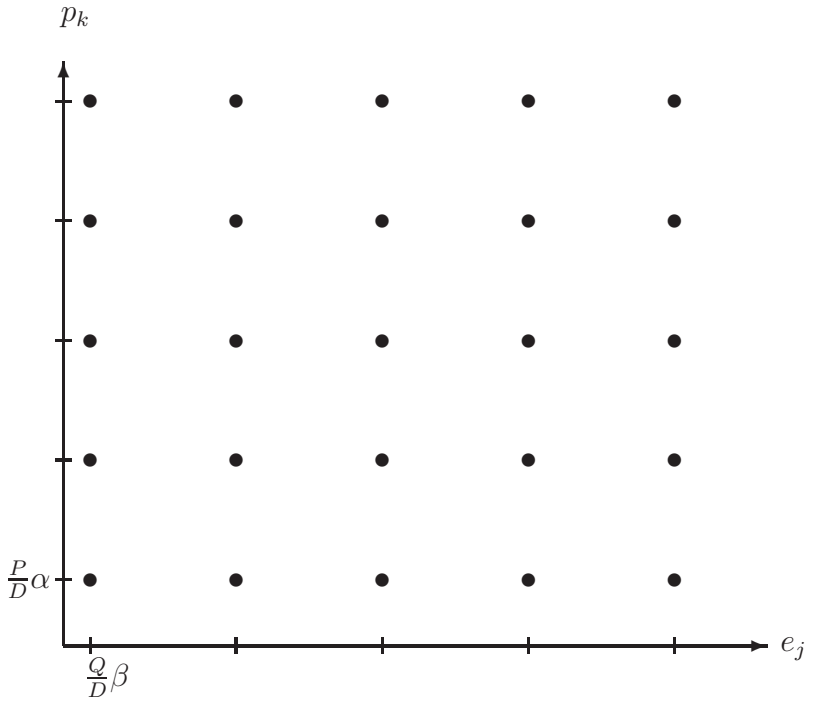

Figure 2.3: A representation of the phase space for a $D = 5$ dimensional Hilbert space. Each point on the lattice corresponds to a particular eigenvalue pair (e_j, p_k).

is to look at the equivalent problem of finding the action of $\hat{U}^D\big|p_0\big\rangle$. Repeating the calculation of equation 2.14, we see the following

$$\hat{U}^D\big|p_0\big\rangle = \frac{1}{\sqrt{D}}\sum_{j=0}^{D-1}\exp\left[\frac{2\pi i}{D}(j+\beta)D\right]\exp\left[\frac{2\pi i}{D}(j+\beta)(k+\alpha)\right]\big|e_j\big\rangle. \tag{2.20}$$

Now, there are two equivalent ways to continue. We can do as before and say that $\hat{U}^D\big|p_0\big\rangle = \big|p_D\big\rangle$, or we can use the fact that $\exp\left[2\pi i(j+\beta)D/D\right] = \exp\left[2\pi i\beta\right]$ to conclude that $\hat{U}^D\big|p_0\big\rangle = \exp\left[2\pi i\beta\right]\big|p_0\big\rangle$. This argument can be applied to any of the momentum basis vectors; therefore, we are led to the fact that our Hilbert space is periodic[6] in momentum

$$\big|p_{k+D}\big\rangle = \exp\left[2\pi i\beta\right]\big|p_k\big\rangle. \tag{2.21}$$

[6]Periodic with the phase β would be a more accurate statement.

A similar argument shows that the Hilbert space is also periodic in position

$$\left|e_{j+D}\right\rangle = \exp\left[-2\pi i\alpha\right]\left|e_j\right\rangle. \tag{2.22}$$

The constants α and β are boundary conditions, sometimes called Floquet angles, that determine the kind of periodicity of our phase space. Since this space is periodic[7] in both conjugate variables we can identify it to be a torus. While any combination α and β is possible *a priori*, there are two sets of boundary conditions which are used most often. These are $\alpha = \beta = 0$, which is periodic boundary conditions: $\left|e_{j+D}\right\rangle = \left|e_j\right\rangle$, $\left|p_{k+D}\right\rangle = \left|p_k\right\rangle$, and $\alpha = \beta = 1/2$, which is anti-periodic boundary conditions: $\left|e_{j+D}\right\rangle = -\left|e_j\right\rangle$, $\left|p_{k+D}\right\rangle = -\left|p_k\right\rangle$.

From this construction of conjugate position and momentum variables, we create a phase space for our finite-dimensional Hilbert space (Figure 2.3). It consists of a lattice of D^2 evenly spaced points. Each point represents a pair of position and momentum eigenstates. Given the toroidal nature of the phase space, we must keep in mind that these points are the fiducial choice for the states and that this grid extends infinitely in all directions.

[7] Up to irrelevant phases.

Equation summary for section 2.1.2

$$\frac{1}{D}\sum_{j=0}^{D-1}\exp\left[\frac{2\pi i}{D}j(k-l)\right]=\sum_{m=-\infty}^{\infty}\delta_{k-l,mD}$$

$$\hat{U}\left|e_j\right\rangle=\exp\left[\frac{2\pi i}{D}(j+\beta)\right]\left|e_j\right\rangle=\exp\left[\frac{i}{\hbar}e_j(P/D)\right]\left|e_j\right\rangle$$

$$\hat{U}\left|p_k\right\rangle=\left|p_{k+1}\right\rangle$$

$$\hat{U}^D\left|p_k\right\rangle=\left|p_{k+D}\right\rangle=\exp\left[2\pi i\beta\right]\left|p_k\right\rangle$$

$$\hat{V}\left|p_k\right\rangle=\exp\left[-\frac{2\pi i}{D}(k+\alpha)\right]\left|p_k\right\rangle=\exp\left[-\frac{i}{\hbar}p_k(Q/D)\right]\left|p_k\right\rangle$$

$$\hat{V}\left|e_j\right\rangle=\left|e_{j+1}\right\rangle$$

$$\hat{V}^D\left|e_j\right\rangle=\left|e_{j+D}\right\rangle=\exp\left[-2\pi i\alpha\right]\left|e_j\right\rangle$$

$$\hat{U}^j\hat{V}^k=\exp\left[\frac{2\pi i}{D}jk\right]\hat{V}^k\hat{U}^j$$

$$\hat{B}_{j,k}=\exp\left[\frac{i\pi}{D}jk\right]\hat{V}^j\hat{U}^k$$

$$\hat{B}_{j,k}^{\dagger}=\hat{B}_{-j,-k}$$

2.2 Special operators

2.2.1 Fourier transform

In $\mathcal{H}_D$ there are operators whose use is so common that they deserve special attention. The first is the Fourier transform operator, $\hat{F}$. It is defined through its action upon a position eigenstate,

$$\hat{F}\big|e_j\big\rangle \equiv \big|p_j\big\rangle. \tag{2.23}$$

Its matrix elements are given by the discrete Fourier transform,

$$\big\langle e_j\big|\hat{F}\big|e_k\big\rangle = \big\langle e_j\big|p_k\big\rangle = \frac{1}{\sqrt{D}}\exp\left[\frac{2\pi i}{D}(j+\beta)(k+\alpha)\right]. \tag{2.24}$$

Unfortunately, not all boundary conditions can be used with this Fourier operator. The reason for this becomes apparent when we look at the action of the parity operator, $\hat{F}^2$. Given parity's definition, we demand that its operation on a position eigenstate be another position eigenstate[8]; therefore, the $\big\langle e_k\big|\hat{F}^2\big|e_j\big\rangle$ matrix element should equal a Kronecker-delta function.

From the earlier definition,

$$\big\langle e_k\big|\hat{F}^2\big|e_j\big\rangle = \sum_{l=0}^{D-1}\big\langle e_k\big|\hat{F}\big|e_l\big\rangle\big\langle e_l\big|\hat{F}\big|e_j\big\rangle = \exp\left[\frac{2\pi i}{D}\alpha(k+\beta)\right]\exp\left[\frac{2\pi i}{D}\beta(j+\alpha)\right] \frac{1}{D}\sum_{l=0}^{D-1}\exp\left[\frac{2\pi i}{D}l(k+j+\alpha+\beta)\right]. \tag{2.25}$$

The sum over l will be a delta function only if $\alpha+\beta$ is an integer.

To see this we shall prove the following fact

$$\frac{1}{D}\sum_{j=0}^{D-1}\exp\left[\frac{2\pi i}{D}j\mu\right] = \sum_{m=-\infty}^{\infty}\delta_{\mu,mD} \tag{2.26}$$

[8]This requirement is equivalent to demanding that the action of the Fourier operator on a momentum eigenstate be a position eigenstate.

given that μ is an integer.

The proof is quite simple and relies on the expression for a geometric sum, Equation 2.10. First it is obvious that if μ is a multiple of D, say $\mu = mD$, then

$$\exp\left[\frac{2\pi i}{D} j\mu\right] = \exp\left[2\pi i j m\right] = 1$$

such that

$$\frac{1}{D}\sum_{j=0}^{D-1} \exp\left[\frac{2\pi i}{D} j\mu\right] = 1.$$

Otherwise, the geometrical sum formula gives

$$\begin{aligned}\frac{1}{D}\sum_{j=0}^{D-1} \exp\left[\frac{2\pi i}{D} j\mu\right] &= \frac{1}{D}\sum_{j=0}^{D-1} \left(\exp\left[\frac{2\pi i}{D}\mu\right]\right)^j \\ &= \frac{1}{D}\left(\frac{1-\exp\left[2\pi i\mu D/D\right]}{1-\exp\left[2\pi i\mu/D\right]}\right).\end{aligned} \tag{2.27}$$

If μ is an integer then $\exp\left[2\pi i\mu D/D\right] = 1$ such that numerator above must be zero. In which case we have a function whose value is 1 when μ is a multiple of D and 0 otherwise[9]. By definition, this function is the Kronecker-delta sum of Equation 2.26.

Some care must be used when using Equation 2.26. As was made clear during the derivation, its content is, "If μ is equal to 0 *modulo* D then the sum's value is unity; otherwise, its value is zero." Many times when using this sum, the possible values of μ will be restricted such that there can only be at most one or two possible values of m in the resulting Kronecker-delta sum. Throughout this work, the author has taken pains to note places where the sum in Equation 2.26 may seem to create mathematical difficulties.

With the proof of Equation 2.26 completed, we now see that the sum from Equation 2.25 yields the Kronecker-delta function,

$$\frac{1}{D}\sum_{l=0}^{D-1} \exp\left[\frac{2\pi i}{D} l(k+j+\alpha+\beta)\right] = \sum_{m=-\infty}^{\infty} \delta_{k+j+\alpha+\beta,mD}, \tag{2.28}$$

[9]If μ is not an integer then Equation 2.27 is the best we can do.

only when $\alpha+\beta$ is an integer. Our choice of boundary conditions have been restricted.

Assuming that $\alpha + \beta$ is an integer, simplifies the $\hat{F}^2$ matrix element to be

$$\left\langle e_k \middle| \hat{F}^2 \middle| e_j \right\rangle = \sum_{m=-\infty}^{\infty} \exp\left[2\pi i m\beta\right] \exp\left[\frac{2\pi i}{D}(j+\alpha)(\beta-\alpha)\right] \delta_{k+j+\alpha+\beta,mD}. \tag{2.29}$$

If we choose j and k to be in the fiducial 0 to $D-1$ range then the only possible value for m is 0; in which case

$$\left\langle e_k \middle| \hat{F}^2 \middle| e_j \right\rangle = \left\langle e_k \middle| \hat{F} \middle| p_j \right\rangle = \exp\left[\frac{2\pi i}{D}(j+\alpha)(\beta-\alpha)\right] \delta_{k,-j-\alpha-\beta}. \tag{2.30}$$

If we also wish to have the Fourier operator be the geometrical phase space 90° rotation then the situation is further simplified. As Figure 2.4 shows, to have the position state rotate to the proper momentum state, we must have α and β equal.

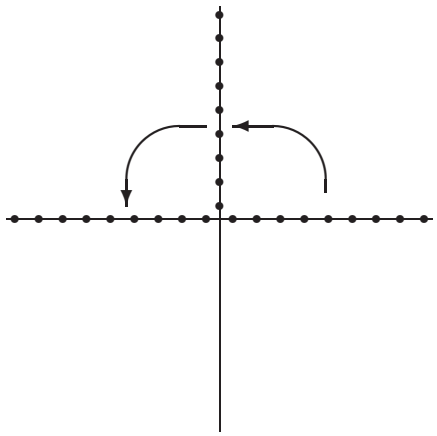

Figure 2.4: The Fourier transform operator is counter-clockwise 90° rotation.

Combining this restriction with the $\alpha + \beta$ equal to an integer condition, gives us our possible boundary conditions. Since α and β have values restricted to the $[0, 1)$ range, the only possible boundary conditions are: $\alpha = \beta = 0$ (periodic) or $\alpha = \beta = 1/2$ (anti-periodic). For these two special case, Equation 2.23 and Equation

2.30 imply that the action of the Fourier operator is

$$\begin{aligned}\hat{F}\big|e_j\big\rangle &= \big|p_j\big\rangle, \\ \hat{F}\big|p_k\big\rangle &= \big|e_{-k-\alpha-\beta}\big\rangle.\end{aligned} \tag{2.31}$$

To see that this is the proper behavior, we need to remember that the eigenstates' "eigenvalues" are placed in the phase space at $e_j = Q(j+\beta)/D$ and $p_k = P(k+\alpha)/D$. In the periodic case, we have the following map for the eigenvalues,

$$\begin{aligned}e_j = \frac{Q}{D}j \to p_j = \frac{P}{D}j, \\ p_k = \frac{P}{D}k \to e_{-k} = \frac{Q}{D}(-k) = -e_k,\end{aligned} \tag{2.32}$$

which is the definition of a 90° rotation.

The anti-periodic case works as well. Here, we have the mapping

$$\begin{aligned}e_j = \frac{Q}{D}(j+\frac{1}{2}) \to p_j = \frac{P}{D}(j+\frac{1}{2}) \\ p_k = \frac{P}{D}(k+\frac{1}{2}) \to e_{-k-1} = \frac{Q}{D}(-k-1+\frac{1}{2}) = \frac{Q}{D}(-k-\frac{1}{2}) = -e_k.\end{aligned} \tag{2.33}$$

The additional $\alpha+\beta$ term in resultant Fourier transformed state ensures that the eigenvalues are rotated to the correct values.

A compact of writing these final results is that

$$\begin{aligned}\hat{F}\,\big|e_j\big\rangle &= \big|p_j\big\rangle \\ \hat{F}\,\big|p_k\big\rangle &= \big|-e_k\big\rangle\end{aligned} \tag{2.34}$$

for periodic and anti-periodic boundary conditions.

As a final note on the Fourier operator. We see that its interpretation as a 90° rotation holds for repeated applications (not just $\hat{F}$ and $\hat{F}^2$). This can be shown directly

$$\hat{F}^4\big|e_j\big\rangle = \hat{F}^3\big|p_j\big\rangle = \hat{F}^2\big|e_{-j-\alpha-\beta}\big\rangle = \hat{F}\big|p_{-j-\alpha-\beta}\big\rangle = \big|e_{j+\alpha+\beta-\alpha-\beta}\big\rangle = \big|e_j\big\rangle. \tag{2.35}$$

As is required by a geometry, four 90° rotations is identity.

2.2.2 Time reversal

The other operator of interest is time reversal, $\hat{T}$. It is an anti-unitary operator which means that it is anti-linear and unitary [60]. An anti-linear operator is one which operates on a linear combination of states in the following way

$$\hat{T}\left(\sum_{j=0}^{D-1} a_j \big|e_j\big\rangle\right) = \sum_{j=0}^{D-1} a_j^* \hat{T}\big|e_j\big\rangle \tag{2.36}$$

where a_j^* is the complex conjugate of a_j. The unitarity of this operator still means that $\hat{T}\hat{T}^\dagger = \hat{T}^\dagger\hat{T} = 1$. Time reversal is defined by its action being invariant on a position eigenstate, *i.e.*

$$\hat{T}\big|e_j\big\rangle = \big|e_j\big\rangle \tag{2.37}$$

for all values of j. Its operation on a momentum state can easily be found with a resolution of identity,

$$\begin{aligned}
\hat{T}\big|p_k\big\rangle &= \hat{T}\left(\sum_{j=0}^{D-1} \big\langle e_j\big|p_k\big\rangle \big|e_j\big\rangle\right) \\
&= \frac{1}{\sqrt{D}}\hat{T}\left(\sum_{j=0}^{D-1} \exp\left[\frac{2\pi i}{D}(j+\beta)(k+\alpha)\right]\big|e_j\big\rangle\right) \\
&= \frac{1}{\sqrt{D}}\sum_{j=0}^{D-1} \exp\left[-\frac{2\pi i}{D}(j+\beta)(k+\alpha)\right]\big|e_j\big\rangle.
\end{aligned} \tag{2.38}$$

By rewriting this expression, we see that the reasonable demand that time reversal produce an eigenstate when operating on a momentum state restricts the choices of boundary condition,

$$\hat{T}\big|p_k\big\rangle = \frac{1}{\sqrt{D}}\sum_{j=0}^{D-1} \exp\left[\frac{2\pi i}{D}(j+\beta)(-k-2\alpha+\alpha)\right]\big|e_j\big\rangle = \big|p_{-k-2\alpha}\big\rangle. \tag{2.39}$$

It is obvious that 2α must be an integer for this last statement to be true; therefore, we must choose either periodic or anti-periodic boundary conditions for momentum. The logical choice would be to choose either of these boundary conditions for both

position and momentum. In which case, the Fourier operator would be rotation in phase space, and we can give time reversal a similar interpretation. A similar analysis to the one done before on the eigenvalues shows that the action of time reversal is

$$\begin{aligned} \hat{T}\left|e_j\right\rangle &= \left|e_j\right\rangle \\ \hat{T}\left|p_k\right\rangle &= \left|-p_k\right\rangle. \end{aligned} \tag{2.40}$$

Not surprisingly, as shown in Figure 2.5 time reversal is reflection through the

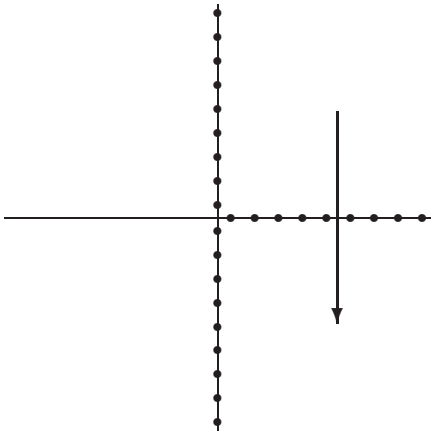

Figure 2.5: Time reversal is reflection through the position axis.

position axis.

It is interesting to note that it would be possible without appealing to a geometrical interpretation to have one exist regardless. Demanding that both the Fourier and time reversal operator produce eigenstates when acting on momentum states is enough to restrict the choice of boundary conditions to either periodic or anti-periodic. The Fourier operator restricts us to $\alpha + \beta$ being an integer, and time reversal forces 2α to be an integer. Obviously, the second restriction implies that α must be either 0 or $1/2$, and the first then forces β to be 0 and $1/2$ respectively. The drawing of a picture to analyze the behavior of these operators is unnecessary, but as always a useful tool for reaching a deeper understanding of the principles involved.

2.2.3 Other symmetries

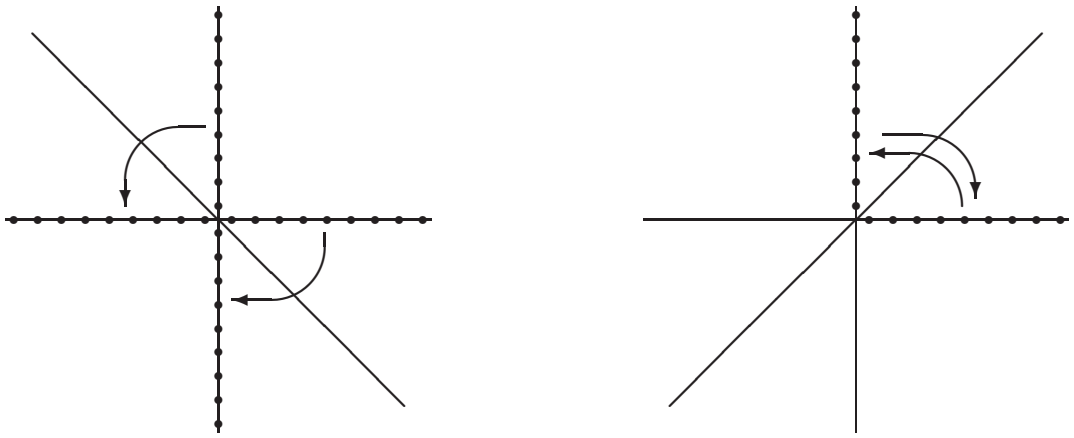

Figure 2.6: The action of the operators $\hat{T}\hat{F}$ and $\hat{F}\hat{T}$ respectively. Each is found to be a reflection through a different diagonal (represented by the solid line).

The geometrical interpretation of the Fourier and time reversal operators immediately suggests that other interesting operators may be found by considering the possible symmetries of the square[10]. The remaining symmetry operations are reflection through the momentum axis and the diagonal. Fortunately, it can be shown that these operations can be created from combinations of the ones previously defined. For example, the operator $\hat{T}\hat{F}$ has the following action

$$\begin{aligned} \hat{T}\hat{F}\left|e_j\right\rangle &= \hat{T}\left|p_j\right\rangle = \left|-p_j\right\rangle, \\ \hat{T}\hat{F}\left|p_k\right\rangle &= \hat{T}\left|-e_k\right\rangle = \left|-e_k\right\rangle \end{aligned} \tag{2.41}$$

where we assumed either periodic or anti-periodic boundary conditions such that both Fourier and time reversal are defined. We see that this operation is reflection about the diagonal, $y = -x$ (Figure 2.6).

[10]Give the freedom of choosing Q and P, the symmetries of the rectangle may be a more semantic yet truer statement of what we wish to find.

The other operator, $\hat{F}\hat{T}$ acts as

$$\begin{aligned} \hat{F}\hat{T}\left|e_j\right\rangle &= \hat{F}\left|e_j\right\rangle = \left|p_j\right\rangle, \\ \hat{F}\hat{T}\left|p_k\right\rangle &= \hat{F}\left|-p_k\right\rangle = \left|e_k\right\rangle \end{aligned} \tag{2.42}$$

which is reflection about the other diagonal, $y = x$ (Figure 2.6).

To get the operator which is reflection about the momentum axis (Figure 2.7), we need to rotate the state which has been reflected about the positive diagonal. That is, we use the operator, $\hat{F}\hat{F}\hat{T}$. Its action is

$$\begin{aligned} \hat{F}\hat{F}\hat{T}\left|e_j\right\rangle &= \hat{F}\left|p_j\right\rangle = \left|-e_j\right\rangle, \\ \hat{F}\hat{F}\hat{T}\left|p_k\right\rangle &= \hat{F}\left|e_k\right\rangle = \left|p_k\right\rangle. \end{aligned} \tag{2.43}$$

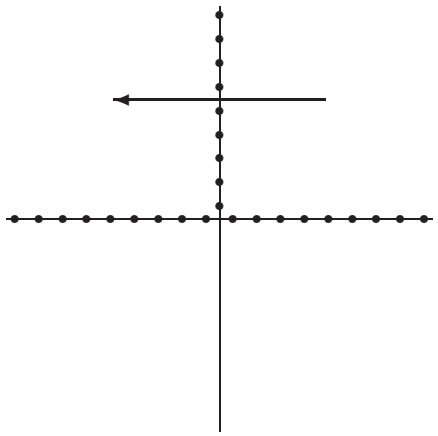

Figure 2.7: The action of the operator $\hat{F}\hat{F}\hat{T}$; reflection through the momentum axis.

A list if all possible symmetry operations have been compiled in Table 2.1. These operations will be revisited when discussing the finite-dimensional Wigner function of Chapter 3.

Symmetry	**Operator**
Position Translation	$\hat{V}$
Momentum Translation	$\hat{U}$
90° Rotation	$\hat{F}$
Reflection about Position	$\hat{T}$
Reflection about Momentum	$\hat{F}\hat{F}\hat{T}$
180° Rotation (Inversion)	$\hat{F}^2$
Reflection about $y = x$	$\hat{F}\hat{T}$
Reflection about $y = -x$	$\hat{T}\hat{F}$

Table 2.1: A summary of all possible symmetry operations including translations, which were not explicitly discussed in the previous section, but can easily be seen as such.

Summary of the symmetry operations
from section 2.2
for periodic and anti-periodic boundary conditions

$$\hat{F}\left|e_j\right\rangle = \left|p_j\right\rangle$$

$$\hat{F}\left|p_k\right\rangle = \left|-e_k\right\rangle$$

$$\hat{T}\left|e_j\right\rangle = \left|e_j\right\rangle$$

$$\hat{T}\left|p_k\right\rangle = \left|-p_k\right\rangle$$

$$\hat{F}\hat{T}\left|e_j\right\rangle = \left|p_j\right\rangle$$

$$\hat{F}\hat{T}\left|p_k\right\rangle = \left|e_k\right\rangle$$

$$\hat{T}\hat{F}\left|e_j\right\rangle = \left|-p_j\right\rangle$$

$$\hat{T}\hat{F}\left|p_k\right\rangle = \left|-e_j\right\rangle$$

$$\hat{F}\hat{F}\hat{T}\left|e_j\right\rangle = \left|-e_j\right\rangle$$

$$\hat{F}\hat{F}\hat{T}\left|p_k\right\rangle = \left|p_k\right\rangle$$

Chapter 3

A Wigner function for finite-dimensional Hilbert spaces

3.1 A history of the finite Wigner function: Re-inventing the wheel

The quasi-probability function that bears his name was first introduced by E. P. Wigner in 1932 [61]. It is a real function of position and momentum, $W(q,p)$, whose marginals give the probability distribution of the conjugate variable, *i.e.*

$$\int dp\, W(q,p) = P(q), \qquad \int dq\, W(q,p) = \tilde{P}(p).$$

The Wigner function is called a quasi-probability function because there are systems for which it has negative values; hence, it cannot be a true joint probability function. The Wigner function is defined as the two-dimensional Fourier transform of a characteristic function, $\Phi(\eta,\xi)$, which is the expectation value of the symmetrically

ordered displacement operator,

$$\Phi(\xi,\eta) = \mathrm{tr}\Big(\hat{\rho}\exp\left[i(\eta\hat{q} - \xi\hat{p})/\hbar\right]\Big) = \mathrm{tr}\Big(\hat{\rho}\exp\left[i\eta\xi/2\hbar\right]\exp\left[-i\xi\hat{p}/\hbar\right]\exp\left[i\eta\hat{q}/\hbar\right]\Big). \tag{3.1}$$

$$W(q,p) = \frac{1}{(2\pi\hbar)^2}\int d\eta\, d\xi\, \exp\left[i\xi p/\hbar\right]\exp\left[-i\eta q/\hbar\right]\Phi(\xi,\eta). \tag{3.2}$$

Contrary to what is reported in much of the physics literature, the first work[1] on a Wigner function for finite-dimensional Hilbert spaces was not done by Wootters [47]. In 1980, Hannay and Berry developed a Wigner function, by in their words, "a straightforward application of the definition [of the continuous Wigner function] it is found that provided irrelevant infinite normalization difficulties are ignored the Wigner function ... is a $2N \times 2N$ periodic 'δ brush' on the phase plane." [46] Not only did Hannay and Berry develop the Wigner function before Wootters, they were the first to see that finite-dimensional Wigner functions have $4D^2$ values. We shall see that the derivation of a finite Wigner function in this work avoids the infinite normalization difficulties mentioned above.

Having missed the Hannay and Berry paper, Wootters developed his own more limited version of a finite Wigner function seven years later [47]. He created a D^2 valued discrete function, $W_{l,m}$, for Hilbert spaces of prime dimensionality D. The indices label possible position and momentum eigenstates. The sum over one of the indices gives the probability for the system to be in the eigenstate labelled by the other index (Figure 3.1). The argument for prime dimensions was based upon the Wigner function's projection property, which states that projecting the Wigner function onto a line in phase space gives the probability distribution for an observable orthogonal to that line[2]. It is only possible in prime dimensions to construct a unique set of discrete "lines;" therefore, only prime dimensional spaces could have Wigner

[1] We are ignoring the continuous angle variable approach for finding Wigner functions of spin systems. The interested reader is urged to check the references contained within Leonhardt [62].

[2] The marginals are the extreme cases of the projection property.

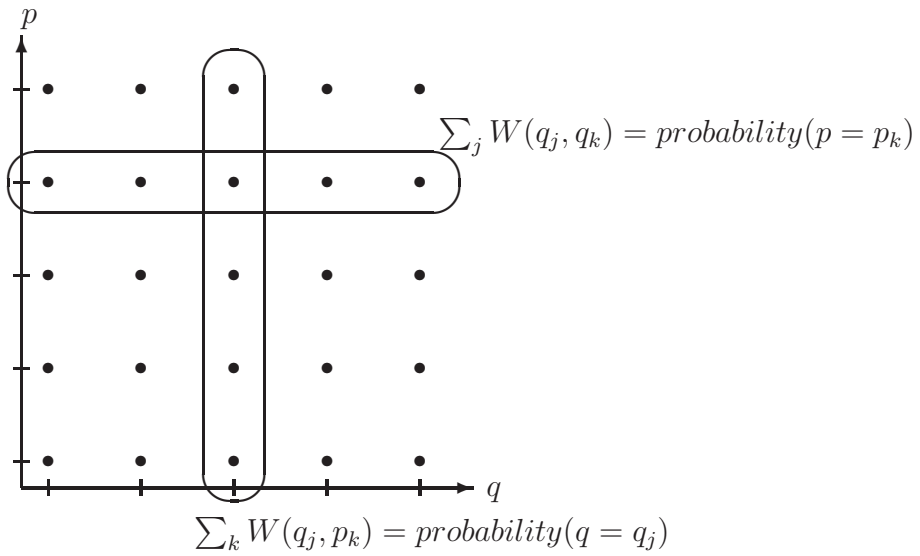

Figure 3.1: A schematic rendering of Wootters' Wigner function for a finite-dimensional Hilbert space. The Wigner function has a real value at each point of the lattice. Marginal distributions are found by summing over a row or column.

functions defined on them. There was the possibility of factoring composite spaces into their prime factors, but Wootters was unable to define a Wigner function for them from first principles.

In the following years, progress was slow [63, 64] until the work by Leonhardt [48][3]. His approach was to find an operator on the finite-dimensional Hilbert space which is the analogue to the symmetrically ordered displacement operator. With this operator, he was able to define a characteristic function and by taking a discrete Fourier transform, a Wigner function. During the derivation, it became clear that even and odd dimensional Hilbert spaces needed to be treated separately. For odd dimensional spaces the Wigner function has D^2 values and exists at integer lattice sites; while for even spaces, it has $4D^2$ values and exists at half-integer lattice sites [62].

This half-integer nature of the Wigner function is now becoming widely accepted.

[3]Who also did not reference Hannay and Berry

This type of Wigner function was recently used by Bianucci *et al.* [65] to study Grover's algorithm, an exciting development in quantum computation. The author's approach to finding a Wigner function for finite-dimensional Hilbert spaces relies on there being an isomorphism between the finite-dimensional Hilbert space and the space of doubly periodic (unnormalized) wavefunctions. With this map, one can use the continuous phase space definition of the Wigner function to define a Wigner function for finite dimensions. This approach also makes clear why the Wigner function has $4D^2$ values for all dimensions and how a D^2 valued version can be constructed in odd dimensions.

Of course, not all researchers missed the seminal Hannay and Berry paper. Its influence can be seen in the works of Dana [66] and Lakshminarayan [67], for example. However, most physicists continue to begin the Wigner function journey with the works of Wootters or at best Leonhardt.

3.2 The isomorphism

In the infinite-dimensional Hilbert space, $\mathcal{L}_2$, we have position and momentum basis vectors, $\big|\overline{q}\big\rangle$ and $\big|\overline{p}\big\rangle$, with Dirac-delta function normalization, $\big\langle\overline{q}\big|\overline{q}'\big\rangle = \delta(q-q')$ and $\big\langle\overline{p}\big|\overline{p}'\big\rangle = \delta(p-p')$. The basis vectors are related by a continuous Fourier transform

$$\big\langle\overline{p}\big|\overline{q}\big\rangle = \frac{1}{\sqrt{2\pi\hbar}}\exp\left[-\frac{i}{\hbar}qp\right].$$

There is a natural connection between $\mathcal{H}_D$ and the subspace of $\mathcal{L}_2$ consisting of doubly periodic states $\big|\psi\big\rangle$, whose position and momentum wavefunctions satisfy

$$\big\langle\overline{x+Q}\big|\psi\big\rangle = \exp\left[2\pi i\alpha\right]\big\langle\overline{x}\big|\psi\big\rangle, \tag{3.3}$$

$$\big\langle\overline{p+P}\big|\psi\big\rangle = \exp\left[-2\pi i\beta\right]\big\langle\overline{p}\big|\psi\big\rangle, \tag{3.4}$$

where Q and P are the periodicity scales in position and momentum[4]. The periodicity defines a D-dimensional subspace, provided $QP/(2\pi\hbar) = D$ is an integer, as we will now show.

Consider a wavefunction whose position representation, $\psi(x)$, is periodic as in Equation 3.3. Being periodic, it must have a Fourier series representation

$$\psi(x) = \langle \overline{x} | \psi \rangle = \sum_{n=-\infty}^{\infty} a_n \exp\left[\frac{2\pi i}{Q}(n+\alpha)x\right], \tag{3.5}$$

where the expansion coefficients, a_n, are found in the usual way. If we substitute this relationship into the momentum representation, we get

$$\begin{aligned}
\widetilde{\psi}(p) &= \langle \overline{p} | \psi \rangle \\
&= \sqrt{\frac{1}{2\pi\hbar}} \sum_{n=-\infty}^{\infty} a_n \int dx \, \exp\left[2\pi i x \left(\frac{n+\alpha}{Q} - \frac{p}{2\pi\hbar}\right)\right] \\
&= \sqrt{2\pi\hbar} \sum_{n=-\infty}^{\infty} a_n \, \delta\left(p - \frac{2\pi\hbar}{Q}(n+\alpha)\right).
\end{aligned} \tag{3.6}$$

From this last expression, we see that

$$\begin{aligned}
\widetilde{\psi}(p+P) &= \sqrt{2\pi\hbar} \sum_{n=-\infty}^{\infty} a_n \, \delta\left(p + P - \frac{2\pi\hbar}{Q}(n+\alpha)\right) \\
&= \sqrt{2\pi\hbar} \sum_{n=-\infty}^{\infty} a_n \, \delta\left(p - \frac{2\pi\hbar}{Q}(n - \frac{QP}{2\pi\hbar} + \alpha)\right).
\end{aligned} \tag{3.7}$$

We see that unless $QP/2\pi\hbar$ is an integer, this expression can never be periodic. It should be noted in the interest of completeness (and for the interested reader) that the correct periodicity (Equation 3.4) is enforced by the condition $a_{n+D} = \exp\left[-2\pi i\beta\right] a_n$.

We shall now show that the expansion coefficients for a general state vector in the $\mathcal{H}_D$ and the subspace of $\mathcal{L}_2$ are simply related. This will allow us to create an

[4]There is a small problem with these doubly periodic functions; their periodicity makes them impossible to normalize. However, these states, just like plane waves, can be used (with care) in theoretical calculations.

isomorphism between the two spaces. Take an arbitrary vector in $\mathcal{H}_D$,

$$\left|\psi\right\rangle = \sum_{j=0}^{D-1} c_j \left|e_j\right\rangle = \sum_{k=0}^{D-1} d_k \left|p_k\right\rangle. \tag{3.8}$$

By using the completeness relationship $\sum_{k=0}^{D-1} \left|p_k\right\rangle\!\left\langle p_k\right| = 1$, we find the relation between expansion coefficients,

$$\begin{aligned} c_j = \left\langle e_j|\psi\right\rangle &= \sum_{k=0}^{D-1} \left\langle e_j|p_k\right\rangle\!\left\langle p_k|\psi\right\rangle \\ &= \frac{1}{\sqrt{D}} \sum_{k=0}^{D-1} \exp\left[\frac{i}{\hbar} p_k e_j\right] d_k. \end{aligned} \tag{3.9}$$

Within the doubly periodic subspace of $\mathcal{L}_2$, we construct a state $\left|\overline{\psi}\right\rangle$ which has support only on those q and p whose values are the same as those from the finite-dimensional subspace. That is, we take $q = Q(j+\beta)/D$, $p = P(k+\alpha)/D$ and create the state

$$\left|\overline{\psi}\right\rangle = \sum_{j=-\infty}^{\infty} c'_j \left|\overline{q_j}\right\rangle = \sum_{k=-\infty}^{\infty} d'_k \left|\overline{p_k}\right\rangle. \tag{3.10}$$

The periodicity of the subspace allows us to rewrite these expressions as

$$\begin{aligned} \left|\overline{\psi}\right\rangle &= \sum_{j=0}^{D-1} c'_j \left(\sum_{n=-\infty}^{\infty} \exp\left[2\pi i \alpha n\right] \left|\overline{q_j + nQ}\right\rangle \right) \\ &= \sum_{k=0}^{D-1} d'_k \left(\sum_{m=-\infty}^{\infty} \exp\left[-2\pi i \beta m\right] \left|\overline{p_k + mP}\right\rangle \right). \end{aligned} \tag{3.11}$$

Now we'll find the relationship between c'_j and d'_k. We'll start by using the position wavefunction,

$$\left\langle \overline{x}|\overline{\psi}\right\rangle = \sum_{j=0}^{D-1} \sum_{n=-\infty}^{\infty} c'_j \exp\left[2\pi i \alpha n\right] \delta(x - q_j - nQ),$$

which we'll relate to the momentum wavefunction,

$$\begin{aligned}\langle\overline{x}|\overline{\psi}\rangle &= \int dp\, \langle\overline{x}|\overline{p}\rangle\langle\overline{p}|\overline{\psi}\rangle \\ &= \frac{1}{\sqrt{2\pi\hbar}} \int dp\, \exp\left[\frac{i}{\hbar}xp\right] \sum_{k=0}^{D-1}\sum_{m=-\infty}^{\infty} d'_k \exp\left[-2\pi i m\beta\right] \delta(p - p_k - mP) \\ &= \frac{1}{\sqrt{2\pi\hbar}} \sum_{k=0}^{D-1}\sum_{m=-\infty}^{\infty} \exp\left[\frac{i}{\hbar}x(p_k + mP)\right] d'_k \exp\left[-2\pi i m\beta\right] \\ &= \frac{1}{\sqrt{2\pi\hbar}} \sum_{k=0}^{D-1} \exp\left[\frac{i}{\hbar}xp_k\right] d'_k \sum_{m=-\infty}^{\infty} \exp\left[2\pi i m(Dx/Q - \beta)\right].\end{aligned} \tag{3.12}$$

In the last step, we have used the fact that $QP = 2\pi\hbar D$.

This expression can be simplified by using the Poisson formula,

$$\sum_{m=-\infty}^{\infty} \exp\left[2\pi i m(x-y)\right] = \sum_{l=-\infty}^{\infty} \delta(x - y - l). \tag{3.13}$$

After doing the sum,

$$\sum_{m=-\infty}^{\infty} \exp\left[2\pi i m\left(\frac{D}{Q}x - \beta\right)\right] = \sum_{l=-\infty}^{\infty} \delta\left(\frac{D}{Q}x - \beta - l\right) = \frac{Q}{D}\sum_{l=-\infty}^{\infty} \delta(x - q_l),$$

we insert the resulting delta into Equation 3.12 to give

$$\langle\overline{x}|\overline{\psi}\rangle = \sqrt{\frac{Q}{P}}\frac{1}{\sqrt{D}} \sum_{k=0}^{D-1}\sum_{l=-\infty}^{\infty} d'_k \exp\left[\frac{i}{\hbar}q_l p_k\right] \delta(x - q_l).$$

We then separate the summing variable l into two pieces

$$\begin{aligned}\langle\overline{x}|\overline{\psi}\rangle &= \sqrt{\frac{Q}{P}}\frac{1}{\sqrt{D}} \sum_{k=0}^{D-1}\sum_{j=0}^{D-1}\sum_{n=-\infty}^{\infty} \exp\left[\frac{i}{\hbar}q_j p_k\right] d'_k \exp\left[2\pi i\alpha\right] \delta(x - q_j - nQ) \\ \implies \qquad \frac{c'_j}{\sqrt{Q}} &= \frac{1}{\sqrt{D}} \sum_{k=0}^{D-1} \exp\left[\frac{i}{\hbar}q_j p_k\right] \frac{d'_k}{\sqrt{P}}.\end{aligned} \tag{3.14}$$

Equations 3.9 and 3.14 verify that the expansion coefficients $c'_j/\sqrt{Q}$ and $d'_k/\sqrt{P}$ are related in the same way as c_j and d_k, thus establishing an isomorphism between

$\mathcal{H}_D$ and the doubly periodic subspace of $\mathcal{L}_2$. Comparing equations 3.8 and 3.11 gives a general form for the isomorphism,

$$\begin{aligned} \big|e_j\big\rangle &\leftrightarrow \sqrt{Q}\sum_{n=-\infty}^{\infty}\exp\left[2\pi i\alpha n\right]\big|\overline{q_j+nQ}\big\rangle \\ \big|p_k\big\rangle &\leftrightarrow \sqrt{P}\sum_{m=-\infty}^{\infty}\exp\left[-2\pi i\beta m\right]\big|\overline{p_k+mP}\big\rangle. \end{aligned} \tag{3.15}$$

3.2.1 An improvement to the isomorphism

The different inner products for states in $\mathcal{H}_D$ and states in $\mathcal{L}_2$ forces us to be more careful in defining this map,

$$\begin{aligned} \big\langle e_k\big|e_j\big\rangle &= \delta_{j,k} \\ &\to Q\sum_{n,n'=-\infty}^{\infty}\exp\left[2\pi i\alpha(n-n')\right]\big\langle\overline{q_k+n'Q}\big|\overline{q_j+nQ}\big\rangle \\ &= Q\sum_{n,n'=-\infty}^{\infty}\exp\left[2\pi i\alpha(n-n')\right]\delta(q_j-q_k+Q(n-n')) \\ &= \delta(q_j-q_k)\sum_{n,n'=-\infty}^{\infty}\delta(n-n')\exp\left[2\pi i\alpha(n-n')\right]. \end{aligned} \tag{3.16}$$

Thus the simple isomorphism maps the Kronecker-delta inner product to a delta-function multiplied by a highly divergent series.

To avoid this problem, we use a slightly altered form for the isomorphism,

$$\big|e_j\big\rangle \to \sum_{n=-\infty}^{\infty}\exp\left[2\pi in\alpha\right]\int_{-\infty}^{\infty}dq\,F(q)G(q-q_j-nQ)\big|\overline{q}\big\rangle. \tag{3.17}$$

$F(q)$ is a very broad real windowing function whose width is much greater than Q, while $G(u)=\sqrt{D/Q}\Theta(Du/Q)$ is a very narrow windowing function with the form

$$\Theta(x)=\begin{cases} 1/\sqrt{\epsilon} & \text{for } -\epsilon/2<x<\epsilon/2 \\ 0 & \text{else} \end{cases}. \tag{3.18}$$

Using this form for the isomorphism, we see that the inner product will be mapped to

$$\langle e_k | e_j \rangle \rightarrow \sum_{n,n'=-\infty}^{\infty} \exp\left[2\pi i \alpha (n-n')\right] \int dq\, F^2(q) G(q - q_j - nQ) G(q - q_k - n'Q).$$

The width of Θ is assumed small enough to ensure no overlap ($\epsilon \ll 1$); therefore, the integral is non-zero only when $q_j = q_k$ and $n = n'$,

$$\begin{aligned}
\langle e_k | e_j \rangle &\rightarrow \delta_{j,k} \sum_{n=-\infty}^{\infty} \int dq\, F^2(q) G^2(q - q_j - nQ) \\
&= \delta_{j,k} \sum_{n=-\infty}^{\infty} \int du\, F^2(u + q_j + nQ) G^2(u) \\
&= \delta_{j,k} \sum_{n=-\infty}^{\infty} \frac{D}{\epsilon Q} \int_{-\epsilon Q/2D}^{\epsilon Q/2D} du\, F^2(u + q_j + nQ).
\end{aligned}$$

This leads to a normalization condition

$$\sum_{n=-\infty}^{\infty} \int_{-\epsilon Q/2D}^{\epsilon Q/2D} du\, F^2(u + q_j + nQ) = \epsilon \frac{Q}{D} \tag{3.19}$$

for all q_j. Unfortunately, this condition cannot be satisfied for all j and we must instead make some approximations. These approximations will be made clear after we develop an expression for $F(u)$.

To find this expression, we demand that the map for $|p_k\rangle$ have the same form as that for $|e_j\rangle$. We start with the quantum Fourier transformation in $\mathcal{H}_D$,

$$|p_k\rangle = \frac{1}{\sqrt{D}} \sum_{j=0}^{D-1} \exp\left[\frac{i}{\hbar} p_k e_j\right] |e_j\rangle$$

which gets mapped by Equation 3.17 to

$$\frac{1}{\sqrt{D}} \sum_{j=0}^{D-1} \exp\left[\frac{i}{\hbar} p_k e_j\right] \sum_{n=-\infty}^{\infty} \exp\left[2\pi i n \alpha\right] \int dq\, F(q) G(q - q_j - nQ) |\overline{q}\rangle.$$

We now find the expansion of the last piece in the infinite-dimensional momentum basis

$$\begin{aligned} & \int dq \int dp \left|\overline{p}\right\rangle\left\langle\overline{p}\middle|\overline{q}\right\rangle F(q)G(q-q_j-nQ) \\ = & \int dp \left|\overline{p}\right\rangle \int dq \frac{1}{\sqrt{2\pi\hbar}} \exp\left[-\frac{i}{\hbar}pq\right] F(q)G(q-q_j-nQ). \end{aligned}$$

We can simplify by taking the Fourier transform of $G(q-q_j-nQ)$,

$$\frac{1}{\sqrt{2\pi\hbar}} \int dp\, dq \left|\overline{p}\right\rangle \exp\left[-ipq/\hbar\right] F(q) \frac{1}{\sqrt{2\pi\hbar}} \int dp'\, \tilde{G}(p') \exp\left[\frac{i}{\hbar}p'(q-q_j-nQ)\right].$$

Combining terms, we get

$$\begin{aligned} & \int dq\, F(q)G(q-q_j-nQ)\left|\overline{q}\right\rangle \\ = & \frac{1}{\sqrt{2\pi\hbar}} \int dp\, dp' \left|\overline{p}\right\rangle \tilde{G}(p') \exp\left[-\frac{i}{\hbar}p'(q_j+nQ)\right] \frac{1}{\sqrt{2\pi\hbar}} \int dq\, F(q) \exp\left[-\frac{i}{\hbar}(p-p')q\right] \\ = & \frac{1}{\sqrt{2\pi\hbar}} \int dp\, dp' \left|\overline{p}\right\rangle \tilde{G}(p') \exp\left[-\frac{i}{\hbar}p'(q_j+nQ)\right] \tilde{F}(p-p'). \end{aligned}$$

Now that we have that expansion, we can substitute into the rest of the expression and find the map for a momentum eigenstate,

$$\begin{aligned} \left|p_k\right\rangle \rightarrow & \frac{1}{\sqrt{2\pi\hbar D}} \sum_{j=0}^{D-1} \exp\left[\frac{i}{\hbar}p_k q_j\right] \sum_{n=-\infty}^{\infty} \exp\left[2\pi i n\alpha\right] \int dp \left|\overline{p}\right\rangle \\ & \times \int dp'\, \tilde{F}(p-p')\tilde{G}(p') \exp\left[-\frac{i}{\hbar}p'(q_j+nQ)\right] \\ = & \frac{1}{\sqrt{2\pi\hbar D}} \sum_{j=0}^{D-1} \int dp \left|\overline{p}\right\rangle \int dp'\, \tilde{F}(p-p')\tilde{G}(p') \exp\left[\frac{i}{\hbar}q_j(p_k-p')\right] \\ & \times \sum_{n=-\infty}^{\infty} \exp\left[-2\pi i\left(\frac{D}{P}p'-\alpha\right)n\right]. \end{aligned}$$

From the Poisson formula,

$$\begin{aligned} \sum_{n=-\infty}^{\infty} \exp\left[-2\pi i\left(p'\frac{D}{P}-\alpha\right)n\right] &= \frac{P}{D} \sum_{r=-\infty}^{\infty} \delta\left(p'-\frac{P}{D}(r+\alpha)\right) \\ &= \frac{P}{D} \sum_{l=0}^{D-1} \sum_{m=-\infty}^{\infty} \delta\left(p'-p_l-mP\right), \end{aligned}$$

we get rid of the sum over the n variable and find that

$$\begin{aligned}\big|p_k\big\rangle \;\rightarrow\; \frac{P}{\sqrt{2\pi\hbar D}D}\sum_{m=-\infty}^{\infty}\sum_{j,l=0}^{D-1}\exp\left[\frac{i}{\hbar}q_j(p_k-p_l-mP)\right]\tilde{G}(p_l+mP)\\ \times\int dp\,\tilde{F}(p-p_l-mP)\big|\overline{p}\big\rangle.\end{aligned}$$

This expression can be simplified further using

$$\exp\left[-\frac{i}{\hbar}q_jmP\right]=\exp\left[-2\pi i(j+\beta)m\right]=\exp\left[-2\pi im\beta\right]$$

and[5]

$$\sum_{j=0}^{D-1}\exp\left[\frac{i}{\hbar}q_j(p_k-p_l)\right]=D\delta_{k,l}$$

to give

$$\big|p_k\big\rangle\rightarrow\frac{P}{\sqrt{2\pi\hbar D}}\sum_{m=-\infty}^{\infty}\exp\left[-2\pi im\beta\right]\tilde{G}(p_k+mP)\int dp\,\tilde{F}(p-p_k-mP)\big|\overline{p}\big\rangle. \quad (3.20)$$

The Fourier transform of $G(q)$ is easily calculated to be

$$\tilde{G}(p)=\sqrt{\frac{2\pi}{P}}\tilde{\Theta}\left(\frac{2\pi p}{P}\right)=\sqrt{\frac{\epsilon}{P}}\frac{\sin(\epsilon\pi p/P)}{\epsilon\pi p/P},$$

and thus we find that

$$\big|p_k\big\rangle\rightarrow\sqrt{\frac{2\pi}{Q}}\sum_{m=-\infty}^{\infty}\exp\left[-2\pi im\beta\right]\tilde{\Theta}\left(\frac{2\pi}{P}(p_k+mP)\right)\int dp\,\tilde{F}(p-p_k-mP)\big|\overline{p}\big\rangle. \quad (3.21)$$

Upon inspection, we see that the functions Θ and F in the map for $\big|e_j\big\rangle$ have been replaced by $\tilde{F}$ and $\tilde{\Theta}$ in $\big|p_k\big\rangle$ respectively. In order that the momentum map have the same form as the position map, we need to choose $F(q)\propto\tilde{\Theta}(q)$.

[5]This is another use of Equation 2.26. The restricted value of k and l collapses the sum of delta functions to one term.

Let's assume that $F(q) = A\sqrt{2\pi/Q}\tilde{\Theta}(2\pi q/Q)$ and $\tilde{F}(p) = A\sqrt{D/P}\Theta(Dp/P)$ where the constant A is determined from the normalization condition

$$\begin{aligned}\epsilon\frac{Q}{D} &= \sum_{n=-\infty}^{\infty}\int_{-\epsilon Q/2D}^{\epsilon Q/2D} du\, F^2(u+q_j+nQ) \\ &= A^2\frac{2\pi}{Q}\sum_{n=-\infty}^{\infty}\int_{-\epsilon Q/2D}^{\epsilon Q/2D} du\,\tilde{\Theta}^2\left(\frac{2\pi}{Q}(u+q_j+nQ)\right).\end{aligned}$$

It is not possible to satisfy this condition for all q_j without $F(q)$ being constant, but this is the situation that lead to an infinite inner product in Equation 3.16. Therefore, we shall have to make some approximations that are valid in the limit of small ϵ. First, we shall assume that $\tilde{\Theta}(q)$ is constant over ranges smaller than Q (by choosing ϵ small enough) so that we can approximate

$$\tilde{\Theta}^2\left(\frac{2\pi}{Q}(u+q_j+nQ)\right) \approx \tilde{\Theta}^2(2\pi n).$$

This leads to a normalization condition of

$$\epsilon\frac{Q}{D} = A^2\frac{2\pi}{Q}\frac{\epsilon Q}{D}\sum_{n=-\infty}^{\infty}\tilde{\Theta}^2(2\pi n) = A^2\frac{2\pi\epsilon}{D}\sum_{n=-\infty}^{\infty}\tilde{\Theta}^2(2\pi n).$$

Second, we shall approximate the sum over n with an integral

$$\sum_{n=-\infty}^{\infty}\tilde{\Theta}^2(2\pi n) = \sum_{n=-\infty}^{\infty}\frac{\epsilon}{2\pi}\left(\frac{\sin(\pi n\epsilon)}{\pi n\epsilon}\right)^2 \overset{\epsilon\ll 1}{\approx} \frac{1}{2\pi}\int_{-\infty}^{\infty} dv\,\left(\frac{\sin v}{v}\right)^2 = \frac{1}{2\pi}.$$

Therefore, we see that $A = \sqrt{Q}$, and that the map we should use is the following

$$\begin{aligned}\left|e_j\right\rangle &\leftrightarrow \sqrt{\frac{2\pi D}{Q}}\sum_{n=-\infty}^{\infty}\exp\left[2\pi i n\alpha\right]\tilde{\Theta}(2\pi n)\int dq\,\left|\overline{q}\right\rangle\,\Theta\left(\frac{D}{Q}(q-q_j-nQ)\right), \\ \left|p_k\right\rangle &\leftrightarrow \sqrt{\frac{2\pi D}{P}}\sum_{m=-\infty}^{\infty}\exp\left[-2\pi i m\beta\right]\tilde{\Theta}(2\pi m)\int dp|\overline{p}\rangle\Theta\left(\frac{D}{P}(p-p_k-mP)\right).\end{aligned} \tag{3.22}$$

We recover the simple form of the map by taking the limit $\epsilon \to 0$

$$\lim_{\epsilon\to 0} \frac{1}{\sqrt{\epsilon}} \Theta\left(\frac{D}{Q}(q - q_j - nQ)\right) = \frac{Q}{D}\delta(q - q_j - nQ).$$

This leads to

$$\left|e_j\right\rangle \to \sqrt{\frac{Q}{D}}\epsilon \sum_{n=-\infty}^{\infty} \exp\left[2\pi i n\alpha\right] \left|\overline{q_j + nQ}\right\rangle. \tag{3.23}$$

Identical considerations give

$$\left|p_k\right\rangle \to \sqrt{\frac{P}{D}}\epsilon \sum_{m=-\infty}^{\infty} \exp\left[-2\pi i m\beta\right] \left|\overline{p_k + mP}\right\rangle. \tag{3.24}$$

The factor of ϵ emphasizes that periodically continued states are not normalizable.

Equation summary for section 3.2

$$\sum_{m=-\infty}^{\infty} \exp\left[2\pi i m(x-y)\right] = \sum_{l=-\infty}^{\infty} \delta(x - y - l)$$

$$\left|e_j\right\rangle \leftrightarrow \sqrt{\frac{2\pi D}{Q}} \sum_{n=-\infty}^{\infty} \exp\left[2\pi i n\alpha\right] \tilde{\Theta}(2\pi n) \int dq \left|\overline{q}\right\rangle \Theta\left(\frac{D}{Q}(q - q_j - nQ)\right)$$

$$\left|p_k\right\rangle \leftrightarrow \sqrt{\frac{2\pi D}{P}} \sum_{m=-\infty}^{\infty} \exp\left[-2\pi i m\beta\right] \tilde{\Theta}(2\pi m) \int dp \left|\overline{p}\right\rangle \Theta\left(\frac{D}{P}(p - p_k - mP)\right)$$

$$\left\langle \overline{q} | \overline{q}' \right\rangle = \delta(q - q'), \quad \left\langle \overline{p} | \overline{p}' \right\rangle = \delta(p - p')$$

$$\left|e_j\right\rangle \xrightarrow{\epsilon\to 0} \sqrt{\frac{Q}{D}}\epsilon \sum_{n=-\infty}^{\infty} \exp\left[2\pi i n\alpha\right] \left|\overline{q_j + nQ}\right\rangle$$

$$\left|p_k\right\rangle \xrightarrow{\epsilon\to 0} \sqrt{\frac{P}{D}}\epsilon \sum_{m=-\infty}^{\infty} \exp\left[-2\pi i m\beta\right] \left|\overline{p_k + mP}\right\rangle$$

3.3 Derivation of the characteristic function

The strategy for calculating the Wigner function is to use the isomorphism developed in the last section to map a density matrix up to the doubly-periodic subspace of $\mathcal{L}_2$. Then we can use the infinite-dimensional Hilbert space definition for the characteristic and Wigner function.

Expand a finite-dimensional Hilbert space density matrix in the position basis and use the limiting case of Equation 3.23 for the isomorphism, *i.e* do not use the Θ functions from the last section

$$\begin{aligned} \hat{\rho} &= \sum_{j,k=0}^{D-1} \rho_{j,k} \big|e_j\big\rangle\big\langle e_k\big| \\ &\to \frac{Q}{D}\epsilon^2 \sum_{j,k=0}^{D-1} \sum_{n,n'=-\infty}^{\infty} \rho_{j,k} \exp\left[2\pi i\alpha(n-n')\right] \big|\overline{q_j + nQ}\big\rangle\big\langle\overline{q_k + n'Q}\big|. \end{aligned} \tag{3.25}$$

From the definition of the continuous characteristic function, Equation 3.1, we see

that

$$\begin{aligned}
\Phi(\xi,\eta) &= \frac{Q}{D}\epsilon^2 \sum_{j,k=0}^{D-1} \sum_{n,n'=-\infty}^{\infty} \rho_{j,k} \exp\left[2\pi i\alpha(n-n')\right] \\
&\qquad \times \left\langle \overline{q_k + n'Q} \right| \exp\left[\frac{i}{2\hbar}\eta\xi\right] \exp\left[-\frac{i}{\hbar}\xi\hat{p}\right] \exp\left[\frac{i}{\hbar}\eta\hat{q}\right] \left| \overline{q_j + nQ} \right\rangle \\
&= \frac{Q}{D}\epsilon^2 \sum_{j,k=0}^{D-1} \sum_{n,n'=-\infty}^{\infty} \rho_{j,k} \exp\left[2\pi i\alpha(n-n')\right] \exp\left[\frac{i}{2\hbar}\eta\xi\right] \\
&\qquad \times \exp\left[\frac{i}{\hbar}\eta(q_j + nQ)\right] \left\langle \overline{q_k + n'Q} \middle| \overline{q_j + nQ + \xi} \right\rangle \\
&= \frac{Q}{D}\epsilon^2 \sum_{j,k=0}^{D-1} \sum_{n,n'=-\infty}^{\infty} \rho_{j,k} \exp\left[2\pi i\alpha(n-n')\right] \exp\left[\frac{i}{\hbar}\eta(q_j + nQ)\right] \\
&\qquad \times \exp\left[\frac{i}{2\hbar}\eta(q_k - q_j + (n'-n)Q)\right] \delta\Big(\xi - (q_k - q_j + Qn' - Qn)\Big) \\
&= \frac{Q}{D}\epsilon^2 \sum_{j,k=0}^{D-1} \sum_{n,n'=-\infty}^{\infty} \rho_{j,k} \exp\left[2\pi i\alpha(n-n')\right] \exp\left[\frac{i}{2\hbar}\eta(q_k + q_j + (n'+n)Q)\right] \\
&\qquad \times \delta\Big(\xi - (q_k - q_j + Qn' - Qn)\Big).
\end{aligned} \tag{3.26}$$

Next we introduce two new summing variables, $N = n' - n$ and $\nu = n' + n$. This simplifies the above expression to

$$\begin{aligned}
\Phi(\xi,\eta) = \frac{Q}{D}\epsilon^2 \sum_{j,k=0}^{D-1} \sum_{N=-\infty}^{\infty} \sum_{\nu} \rho_{j,k} \exp\left[-2\pi i\alpha N\right] \exp\left[\frac{i}{2\hbar}\eta(q_k + q_j)\right] \\
\times \exp\left[\frac{i}{2\hbar}\eta\nu Q\right] \delta\Big(\xi - (q_k - q_j + NQ)\Big).
\end{aligned} \tag{3.27}$$

Notice that the delta function restricts the values of ξ to integral multiples of Q/D, regardless of what boundary conditions are used.

Using the relationship $QP = 2\pi\hbar D$, the sum over ν can be put into an equivalent form,

$$\sum_{\nu} \exp\left[\frac{i\eta\nu Q}{2\hbar}\right] = \sum_{\nu} \exp\left[2\pi i \frac{D}{P}\eta\frac{\nu}{2}\right].$$

This is in the form of the Poisson formula, but we must be careful because the variables N and ν are parity related. When N is even (odd), ν must be even (odd).

When N is even, $\nu = 2\nu'$, and the sum becomes

$$\sum_{\nu \text{ even}} \exp\left[\frac{i}{2\hbar}\eta\nu Q\right] = \sum_{\nu'=-\infty}^{\infty} \exp\left[2\pi i \frac{D}{P}\eta\nu'\right] = \sum_{L=-\infty}^{\infty} \delta\left(\frac{D}{P}\eta - L\right).$$

When N is odd, $\nu = 2\nu' + 1$, so we have

$$\begin{aligned}\sum_{\nu \text{ odd}} \exp\left[\frac{i}{2\hbar}\eta\nu Q\right] &= \sum_{\nu'=-\infty}^{\infty} \exp\left[2\pi i \frac{D}{P}\eta\nu'\right] \exp\left[\pi i \frac{D}{P}\eta\right] \\ &= \sum_{L=-\infty}^{\infty} \exp\left[\pi i L\right] \delta\left(\frac{D}{P}\eta - L\right).\end{aligned}$$

The difference between the two cases is a factor of $e^{\pi i L}$ when N is odd. This leads to the conclusion that

$$\begin{aligned}\sum_{\nu} \exp\left[\frac{i}{2\hbar}\eta\nu Q\right] &= \sum_{L=-\infty}^{\infty} \exp\left[\pi i L N\right] \delta\left(\frac{D}{P}\eta - L\right) \\ &= \frac{P}{D} \sum_{L=-\infty}^{\infty} \exp\left[\pi i L N\right] \delta\left(\eta - \frac{P}{D}L\right).\end{aligned} \tag{3.28}$$

The delta function here restricts η to integer multiples of P/D.

The expression for the characteristic function becomes

$$\begin{aligned}\Phi(\xi,\eta) = \frac{QP}{D^2}\epsilon^2 \sum_{j,k=0}^{D-1} \sum_{N,L=-\infty}^{\infty} \rho_{j,k} \exp\left[-2\pi i \alpha N\right] \exp\left[\pi i L N\right] \exp\left[\frac{i}{2D\hbar} P(q_k + q_j)L\right] \\ \times \delta\left(\eta - \frac{P}{D}L\right) \delta\Big(\xi - (q_k - q_j + NQ)\Big).\end{aligned} \tag{3.29}$$

Now, let's use the fact that $q_j = (Q/D)(j+\beta)$ and $q_k = (Q/D)(k+\beta)$ to produce

$$\begin{aligned}\Phi(\xi,\eta) = \frac{QP}{D^2}\epsilon^2 \sum_{j,k=0}^{D-1} \sum_{N,L=-\infty}^{\infty} \rho_{j,k} \exp\left[-2\pi i \alpha N\right] \exp\left[\frac{2\pi i}{D} L\beta\right] \exp\left[\pi i L N\right] \\ \times \exp\left[\frac{\pi i}{D}(j+k)L\right] \delta\left(\eta - \frac{P}{D}L\right) \delta\left(\xi - \frac{Q}{D}(k - j + ND)\right).\end{aligned} \tag{3.30}$$

Let's try to simplify the $k - j + ND$ expression that appears in the ξ delta function. We'll begin by introducing a new variable $l = k - j$. This substitution helps simplify our expression, but we must be careful to keep the proper limits on the sum over l. Our new expression for the characteristic function is

$$\begin{aligned}\Phi(\xi,\eta) = \frac{QP}{D^2}\epsilon^2 \sum_{N,L=-\infty}^{\infty} \sum_{j=0}^{D-1} \sum_{l=-j}^{-j+D-1} \rho_{j,j+l} \exp\left[-2\pi i\alpha N\right] \exp\left[\frac{2\pi i}{D}(j+\beta)L\right] \\ \times \exp\left[\frac{\pi i}{D}(l+ND)L\right] \delta\left(\eta - \frac{P}{D}L\right) \delta\left(\xi - \frac{Q}{D}(l+ND)\right).\end{aligned} \tag{3.31}$$

The sum over l can be split into two pieces,

$$\sum_{l=-j}^{-j+D-1} = \sum_{l=-j}^{-1} + \sum_{l=0}^{-j+D-1}.$$

For the first piece, let's make two more substitutions, $l' = l + D$ and $N' = N - 1$. Under these changes the N and l sums of the first piece become

$$\begin{aligned}\sum_{N'=-\infty}^{\infty} \sum_{l'=D-j}^{D-1} \rho_{j,j+l'-D} \exp\left[-2\pi i\alpha(N'+1)\right] \exp\left[\frac{2\pi i}{D}(j+\beta)L\right] \\ \times \exp\left[\frac{\pi i}{D}(l'+N'D)L\right] \delta\left(\eta - \frac{P}{D}L\right) \delta\left(\xi - \frac{Q}{D}(l'+N'D)\right).\end{aligned} \tag{3.32}$$

Given Equation 3.25, the density matrix has an extension consistent with the periodicity of our finite Hilbert space,

$$\rho_{j+nD,k+mD} = \left\langle e_{j+nD}\middle|\hat{\rho}\middle|e_{k+mD}\right\rangle = \exp\left[2\pi i(n-m)\alpha\right] \rho_{j,k}. \tag{3.33}$$

We will make use of this fact twice. First, we'll use Equation 3.33 to rewrite $\rho_{j,j+l'-D}$ as $\exp\left[2\pi i\alpha\right] \rho_{j,j+l'}$. This rewriting produces a phase which cancels the one in Equation 3.32, thus allowing us to recombine the sum over l,

$$\begin{aligned}\Phi(\xi,\eta) = \frac{QP}{D^2}\epsilon^2 \sum_{N,L=-\infty}^{\infty} \sum_{j,l=0}^{D-1} \rho_{j,j+l} \exp\left[-2\pi i\alpha N\right] \exp\left[\frac{2\pi i}{D}(j+\beta)L\right] \\ \times \exp\left[\frac{\pi i}{D}(l+ND)L\right] \delta\left(\eta - \frac{P}{D}L\right) \delta\left(\xi - \frac{Q}{D}(l+ND)\right).\end{aligned} \tag{3.34}$$

We use Equation 3.33 a second time to make the following observation,

$$\rho_{j,j+l} \exp\left[-2\pi i \alpha N\right] = \rho_{j,j+l+ND},$$

which simplifies the characteristic function to

$$\begin{aligned}\Phi(\xi,\eta) = \frac{QP}{D^2}\epsilon^2 \sum_{N,L=-\infty}^{\infty} \sum_{j,l=0}^{D-1} \rho_{j,j+l+ND} \exp\left[\frac{2\pi i}{D}(j+\beta)L\right] \\ \times \exp\left[\frac{\pi i}{D}(l+ND)L\right] \delta\left(\eta - \frac{P}{D}L\right) \delta\left(\xi - \frac{Q}{D}(l+ND)\right).\end{aligned} \tag{3.35}$$

We see that the two variables l and N can be combined into a single variable M to give our final expression,

$$\begin{aligned}\Phi(\xi,\eta) = \frac{QP}{D^2}\epsilon^2 \sum_{M,L=-\infty}^{\infty} \sum_{j=0}^{D-1} \rho_{j,j+M} \exp\left[\frac{2\pi i}{D}(j+\beta)L\right] \\ \times \exp\left[\frac{\pi i}{D}LM\right] \delta\left(\eta - \frac{P}{D}L\right) \delta\left(\xi - \frac{Q}{D}M\right).\end{aligned} \tag{3.36}$$

This expression has a simple interpretation. The characteristic function has Dirac-delta function singularities at the lattice of points given by $\eta = (P/D)L$, $\xi = (Q/D)M$, $M, L \in \mathcal{Z}$. When working in $\mathcal{H}_D$, however, we should think of the zero-limiting ϵ multiplying the Dirac-delta function as producing a finite, discrete value at the singularity, *i.e.*

$$\epsilon\, \delta\left(\eta - \frac{P}{D}L\right) = \epsilon\, \Theta^2\left(\eta - \frac{P}{D}L\right) \to \begin{cases} 0, & \eta \neq (P/D)L, \\ 1, & \eta = (P/D)L. \end{cases} \tag{3.37}$$

Thus the characteristic function becomes a discrete-valued function

$$\Phi_{M,L} = \Phi\left(\frac{Q}{D}M, \frac{P}{D}L\right) = \frac{QP}{D^2} \sum_{j=0}^{D-1} \rho_{j,j+M} \exp\left[\frac{\pi i}{D}LM\right] \exp\left[\frac{2\pi i}{D}(j+\beta)L\right]. \tag{3.38}$$

Using the fact that $\rho_{j,M+j} = \mathrm{tr}(\hat{\rho}\left|e_{M+j}\right\rangle\!\left\langle e_j\right|)$, we see that this characteristic function $\Phi_{M,L} = \mathrm{tr}(\hat{\rho}\hat{B}_{M,L})$ is the expectation value of an operator

$$\hat{B}_{M,L} = \frac{QP}{D^2} \sum_{j=0}^{D-1} \exp\left[\frac{\pi i}{D}LM\right] \exp\left[\frac{2\pi i}{D}L(j+\beta)\right] \left|e_{M+j}\right\rangle\!\left\langle e_j\right|.$$

Remembering the definition of the finite Hilbert space's displacement operators (Equations 2.14 and 2.16), this simplifies to

$$\hat{B}_{M,L} = \frac{QP}{D^2} \exp\left[\frac{\pi i}{D} LM\right] \hat{V}^M \hat{U}^L. \tag{3.39}$$

The form of this operator should come as no surprise. Comparison with Equation 2.19 shows that it is the symmetrically ordered displacement operator for $\mathcal{H}_D$, suitably normalized. It is the same as the operator used by Leonhardt [48, 62] and other works on finite Wigner functions [68, 69, 70].

One last item of note on the characteristic function is its periodicity. As noted above, the characteristic function does not sit at the same lattice points as the position and momentum eigenstates (which are offset by the constants α and β respectively). However, the original periodicity chosen on $\mathcal{H}_D$ is still expressed in the characteristic function in an altered form. A simple calculation shows that

$$\hat{B}_{M,L+D} = \exp\left[2\pi i\beta\right] (-1)^M \hat{B}_{M,L}.$$

The phase $(-1)^M$ prevents $\hat{B}_{M,L}$ from being "β"-periodic in its second index. An obvious solution is to advance by $2D$ which gives

$$\hat{B}_{M,L+2D} = \exp\left[2\pi i 2\beta\right] \hat{B}_{M,L}.$$

Similarly, we have $\hat{B}_{M+D,L} = \exp\left[-2\pi i\alpha\right] (-1)^L \hat{B}_{M,L}$ and

$$\hat{B}_{M+2D,L} = \exp\left[-2\pi i 2\alpha\right] \hat{B}_{M,L}.$$

The characteristic function is thus doubly periodic with period $2Q$ and $2P$. It acquires the same phase as would be expected from advancing a vector in the finite-dimensional Hilbert space by the same amount. Upon Fourier transforming the characteristic function, this twice periodicity produces the half-integer nature of the finite Wigner function. Notice that for the boundary conditions of greatest interest, periodic ($\alpha = \beta = 0$) and anti-periodic ($\alpha = \beta = 1/2$), the characteristic function is strictly periodic with period $2Q$ and $2P$.

Equation summary for section 3.3

$$\hat{\rho} = \sum_{j,k=0}^{D-1} \rho_{j,k} \big|e_j\big\rangle\big\langle e_k\big|$$

$$\rho_{j+nD,k+mD} = \exp\left[2\pi i(n-m)\alpha\right]$$

$$\Phi_{M,L} = \mathrm{tr}(\hat{\rho}\hat{B}_{M,L})$$

$$\hat{B}_{M,L} = \frac{QP}{D^2} \sum_{j=0}^{D-1} \exp\left[\frac{\pi i}{D} LM\right] \exp\left[\frac{2\pi i}{D} L(j+\beta)\right] \big|e_{M+j}\big\rangle\big\langle e_j\big|$$

$$\hat{B}_{M,L+2D} = \exp\left[2\pi i 2\beta\right] \hat{B}_{M,L}$$

$$\hat{B}_{M+2D,L} = \exp\left[-2\pi i 2\alpha\right] \hat{B}_{M,L}$$

3.4 Derivation of the Wigner function

Knowing the infinite-dimensional expression for the Wigner function, Equation 3.2, and having calculated the characteristic function, we can do a straightforward calculation to find the Wigner function.

Using Equation 3.36, we find the Wigner function to be

$$\begin{aligned} W(q,p) &= \frac{QP}{D^2}\epsilon^2 \frac{1}{(2\pi\hbar)^2} \sum_{j=0}^{D-1} \sum_{L,M=-\infty}^{\infty} \exp\left[\frac{i}{\hbar D} QMp\right] \exp\left[-\frac{i}{\hbar D} PLq\right] \rho_{j,M+j} \\ &\qquad \times \exp\left[\frac{2\pi i}{D} L(j+\beta)\right] \exp\left[\frac{\pi i}{D} LM\right] \\ &= \frac{\epsilon^2}{2\pi\hbar D} \sum_{j=0}^{D-1} \sum_{L,M=-\infty}^{\infty} \exp\left[\frac{2\pi i}{P} pM\right] \exp\left[-\frac{2\pi i}{Q} qL\right] \rho_{j,M+j} \\ &\qquad \times \exp\left[\frac{2\pi i}{D} L(j+\beta)\right] \exp\left[\frac{\pi i}{D} LM\right] \\ &= \frac{\epsilon^2}{2\pi\hbar D} \sum_{j=0}^{D-1} \sum_{M=-\infty}^{\infty} \exp\left[\frac{2\pi i}{P} pM\right] \rho_{j,M+j} \\ &\qquad \times \sum_{L=-\infty}^{\infty} \exp\left[2\pi i L\Big(-q/Q + \frac{j+\beta+M/2}{D}\Big)\right]. \end{aligned}$$

From the Poisson sum formula, we have

$$\sum_{L=-\infty}^{\infty} \exp\left[2\pi i L\Big(-q/Q + \frac{j+\beta+M/2}{D}\Big)\right] = \sum_{R=-\infty}^{\infty} \delta\left(\frac{q}{Q} - \frac{j+\beta+M/2}{D} - R\right).$$

Therefore, the Wigner function is

$$\begin{aligned} W(q,p) = \frac{\epsilon^2}{P} \sum_{j=0}^{D-1} \sum_{R,M=-\infty}^{\infty} &\exp\left[\frac{2\pi i}{P} pM\right] \rho_{j,M+j} \\ &\delta\left(q - \frac{Q}{D}\left(j + RD + M/2 + \beta\right)\right), \end{aligned} \tag{3.40}$$

where we have used the ever useful $QP = 2\pi\hbar D$ to simplify the factor in front of the sum. We see that the values of q are restricted to the same lattice sites as position eigenstates plus the points sitting halfway between these sites.

Let's simplify the expression in the delta function using the same technique employed in finding the characteristic function. We start by introducing a new variable,

$M' = 2j + 2RD + M$. This simplifies the Wigner function to

$$W(q,p) = \frac{\epsilon^2}{P}\sum_{j=0}^{D-1}\sum_{R,M'=-\infty}^{\infty}\rho_{j,M'-j-2RD}\exp\left[\frac{2\pi i}{P}p(M'-2j-2RD)\right] \times \delta\left(q - \frac{Q}{D}\left(M'/2+\beta\right)\right). \tag{3.41}$$

Next we use Equation 3.33 to rewrite $\rho_{j,M'-j-2RD}$ as $e^{2\pi i 2R\alpha}\rho_{j,M'-j}$ and combine terms to give

$$W(q,p) = \frac{\epsilon^2}{P}\sum_{j=0}^{D-1}\sum_{M'=-\infty}^{\infty}\exp\left[\frac{2\pi i}{P}p(M'-2j)\right]\rho_{j,M'-j} \times \delta\left(q - \frac{Q}{D}\left(M'/2+\beta\right)\right)\sum_{R=-\infty}^{\infty}\exp\left[2\pi i R(2\alpha - 2D\frac{p}{P})\right]. \tag{3.42}$$

We can do the sum over R by once again using the Poisson formula,

$$\sum_{R=-\infty}^{\infty}\exp\left[2\pi i R(2\alpha - 2D\frac{p}{P})\right] = \frac{P}{2D}\sum_{S=-\infty}^{\infty}\delta\left(p - \frac{P}{D}\left(S/2+\alpha\right)\right), \tag{3.43}$$

which shows that the values of p are restricting to a half-integer lattice based on the momentum eigenvalues. Inserting this value for p, we arrive at our final answer for the Wigner function

$$W(q,p) = \frac{1}{2D}\epsilon^2\sum_{S,M=-\infty}^{\infty}\sum_{j=0}^{D-1}\rho_{j,M-j}\exp\left[\frac{2\pi i}{D}(M-2j)(S/2+\alpha)\right] \times \delta\left(q - \frac{Q}{D}\left(M/2+\beta\right)\right)\delta\left(p - \frac{P}{D}\left(S/2+\alpha\right)\right). \tag{3.44}$$

Again this expression has a simple interpretation as a discrete valued function, we end up with

$$\begin{aligned} W_{M/2,S/2} = W\left(q_{M/2}, p_{S/2}\right) &= \frac{1}{2D}\sum_{j=0}^{D-1}\rho_{j,M-j}\exp\left[\frac{i}{\hbar}2\left(q_{M-j}-q_j\right)p_{S/2}\right] \\ &= \frac{1}{2D}\sum_{j=0}^{D-1}\rho_{j,M-j}\exp\left[\frac{2\pi i}{D}(M-2j)(S/2+\alpha)\right]. \end{aligned} \tag{3.45}$$

The indices label the lattice of points $e_{M/2}, p_{S/2}$, $M, S = 0, 1, \ldots 2D-1$. Unlike the work of Leonhardt, we find that the Wigner function has values at half-integer lattice points for all dimensions D, both even and odd. Comparing Equation 3.45 with the one for a continuous density matrix,

$$W(q,p) = \frac{2}{2\pi\hbar}\int dx\, \rho_{x,2q-x}\, \exp\left[\frac{i}{\hbar}2(q-x)p\right],$$

we see that apart from a different normalization our expression is equivalent to the continuous one with summation replacing integration.

As was the case for the characteristic function, the Wigner function can be written as the trace of an operator against the system's density operator,

$$W_{M/2,S/2} = \mathrm{tr}\left(\hat{\rho}A_{M/2,S/2}\right). \tag{3.46}$$

This operator is hermitian for each value of M and S, thus assuring the Wigner function is real valued and have a position representation given by

$$\hat{A}_{M/2,S/2} = \frac{1}{2D}\sum_{j=0}^{D-1}\exp\left[\frac{2\pi i}{D}(M-2j)(S/2+\alpha)\right]\left|e_{M-j}\right\rangle\left\langle e_j\right|. \tag{3.47}$$

Unlike the characteristic function's $\hat{B}_{M,L}$ operators, the $\hat{A}_{M/2,S/2}$ operators are strictly periodic for all boundary conditions,

$$\hat{A}_{M/2,S/2+D} = \hat{A}_{M/2+D,S/2} = \hat{A}_{M/2,S/2}. \tag{3.48}$$

Given that there are $4D^2$ of these operators, they must be overcomplete. A quick calculation reveals that

$$\begin{aligned}\hat{A}_{M/2,(S+D)/2} &= (-1)^M \hat{A}_{M/2,S/2},\\ \hat{A}_{(M+D)/2,S/2} &= (-1)^S \hat{A}_{M/2,S/2}.\end{aligned} \tag{3.49}$$

This behavior will ensure that the Wigner function recreates the proper marginal distributions. Its true purpose, however, is two-fold. One purpose, which will be

discussed in the next section, is to give the Wigner function a geometrical interpretation. The other purpose is to create phase space "interference." As was discussed in Chapter 2, the discrete phase space is represented by a D^2 lattice of points corresponding to position and momentum eigenvalue pairs; however, the phase space is toroidal so this grid can be extended infinitely in all directions. Equation 3.48 tells us that there will be copies of every Wigner function in the phase space's non-fiducial continuation[6]. The quantum mechanical interference between these copies will manifest itself in the series of sharp peaks described in Equation 3.49. An example of this interference can be seen in the Wigner function for the periodically continued coherent states of Chapter 4, Figure 4.1. As with the continuous case, these states have a Gaussian Wigner function centered at phase space point, (x_0, p_0). Equation 3.48 implies that there are also Gaussians centered at all points x_0+nQ and p_0+mP, the interference of which can clearly be seen in Figure 4.1.

The probability of finding the system at position $e_{M/2}$ is given by summing over the variable S. But what happens when M is odd? These points do not correspond to position eigenvalues, so they must have zero probability. We know that any sum can be broken up into its component pieces

$$\sum_{S=0}^{2D-1} \hat{A}_{M/2,S/2} = \sum_{S=0}^{D-1} \hat{A}_{M/2,S/2} + \sum_{S=D}^{2D-1} \hat{A}_{M/2,S/2}, \tag{3.50}$$

and by using Equations 3.49 and 3.47, we see that

$$\sum_{S=0}^{2D-1} \hat{A}_{M/2,S/2} = \left(1+(-1)^M\right) \frac{1}{2D} \sum_{j=0}^{D-1} \left|e_{M-j}\right\rangle\!\left\langle e_j\right| \sum_{S=0}^{D-1} \exp\left[\frac{2\pi i}{D}(M-2j)(S/2+\alpha)\right]. \tag{3.51}$$

When M is odd, this sum is 0. When M is even, Equation 2.26 collapses the sum

[6]This is the set of phase space grid points for position and momentum eigenvalues outside the 0 to $D-1$ fiducial range.

over j to one value[7] ,

$$\sum_{S=0}^{2D-1} \hat{A}_{M/2,S/2} = \begin{cases} 0, & \text{when } M \text{ is odd,} \\ \big|e_{M/2}\big\rangle\big\langle e_{M/2}\big|, & \text{when } M \text{ is even.} \end{cases} \tag{3.52}$$

Consequently, the value for the sum over S for the Wigner function will have the non-zero value of $\rho_{M/2,M/2}$ only when M is even. We find that there is no probability to be at the half-integer positions. For the integral positions, we get the position marginal probability.

A similar argument holds for summing over M. If we had started with the momentum representation of the density matrix,

$$\hat{\rho} = \sum_{l,m=0}^{D-1} \widetilde{\rho}_{l,m} \big|p_l\big\rangle\big\langle p_m\big|,$$

we would have found the Wigner function to be

$$W_{M/2,S/2} = \frac{1}{2D} \sum_{k=0}^{D-1} \widetilde{\rho}_{k,S-k} \exp\left[-\frac{2\pi i}{D}(S-2k)(M/2+\beta)\right] \tag{3.53}$$

and the $\hat{A}_{M/2,S/2}$ operator to have a momentum representation given by

$$\hat{A}_{M/2,S/2} = \frac{1}{2D} \sum_{k=0}^{D-1} \exp\left[-\frac{2\pi i}{D}(S-2k)(M/2+\beta)\right] \big|p_k\big\rangle\big\langle p_{S-k}\big|. \tag{3.54}$$

In an analogous calculation, we find that

$$\sum_{M=0}^{2D-1} \hat{A}_{M/2,S/2} = \begin{cases} 0, & \text{when } S \text{ is odd,} \\ \big|p_{S/2}\big\rangle\big\langle p_{S/2}\big|, & \text{when } S \text{ is even.} \end{cases} \tag{3.55}$$

Once again summing over the M index of the Wigner function gives the correct marginal, $\widetilde{\rho}_{S/2,S/2}$, for S even; there is no probability at the half-integer momentum

[7]The restricted values of M and j makes the sum over delta functions in Equation 2.26 irrelevant

values. The purpose of the Wigner function's half-integer values will be explored in the next section.

How does this Wigner function relate to the work done by previous authors? It should be noted that our Wigner function is equivalent to Hannay and Berry's Wigner function. Our Wigner function, however, was developed using a different technique and does not suffer from a problem with infinite normalization. Also, our function is the same as Leonhardt's for even dimensions. For odd-dimensional Hilbert spaces, Leonhardt's Wigner function operators can be found from the subset $\hat{A}_{M/2,S/2}$ for $M, S = 0, 2, 4, \ldots 2D-2$. This works because of the fundamental fact that odd numbers are not divisible by two. In even dimensions, this subset will contain both the $\hat{A}_{M/2,S/2}$ and $\hat{A}_{M/2,S/2+D/2}$ operators. By Equation 3.49, we know that these two operators are not linearly independent[8]. For a Wigner function with D^2 values to contain complete information about the system, its elements must necessarily be linearly independent. In odd dimensions, the M and S even subset selects the D^2 linearly independent operators and creates a valid Wigner function.

In 2 dimensions, Wootters [47] has found specific matrices $\hat{A'}_{M,S}$ which create his Wigner function. A quick calculation reveals the relationship between Wootters' matrices and our own,

$$\begin{aligned}
\hat{A}'_{0,0} &= (\hat{A}_{0,0} + \hat{A}_{1/2,0} + \hat{A}_{0,1/2} + \hat{A}_{1/2,1/2}) \\
\hat{A}'_{1,0} &= (\hat{A}_{1,0} + \hat{A}_{3/2,0} + \hat{A}_{1,1/2} + \hat{A}_{3/2,1/2}) \\
\hat{A}'_{0,1} &= (\hat{A}_{0,1} + \hat{A}_{1/2,1} + \hat{A}_{0,3/2} + \hat{A}_{1/2,3/2}) \\
\hat{A}'_{1,1} &= (\hat{A}_{1,1} + \hat{A}_{3/2,1} + \hat{A}_{3/2,1} + \hat{A}_{3/2,3/2}).
\end{aligned} \tag{3.56}$$

Here we have used periodic ($\alpha = \beta = 0$) boundary conditions. This suggests a method for creating a D^2-valued Wigner function by taking the linear combination

$$\hat{A}_{M/2,S/2} + \hat{A}_{M/2+1/2,S/2} + \hat{A}_{M/2,S/2+1/2} + \hat{A}_{M/2+1/2,S/2+1/2}$$

[8]In fact, they are equal half of the time.

for $M, S = 0, 2, \ldots, 2D-2$. This linear combination would still be hermitian and an index sum would produce the proper marginal, but as will be shown in the next section, this combination does not give the proper phase space geometrical interpretation. Hence, we reject its use.

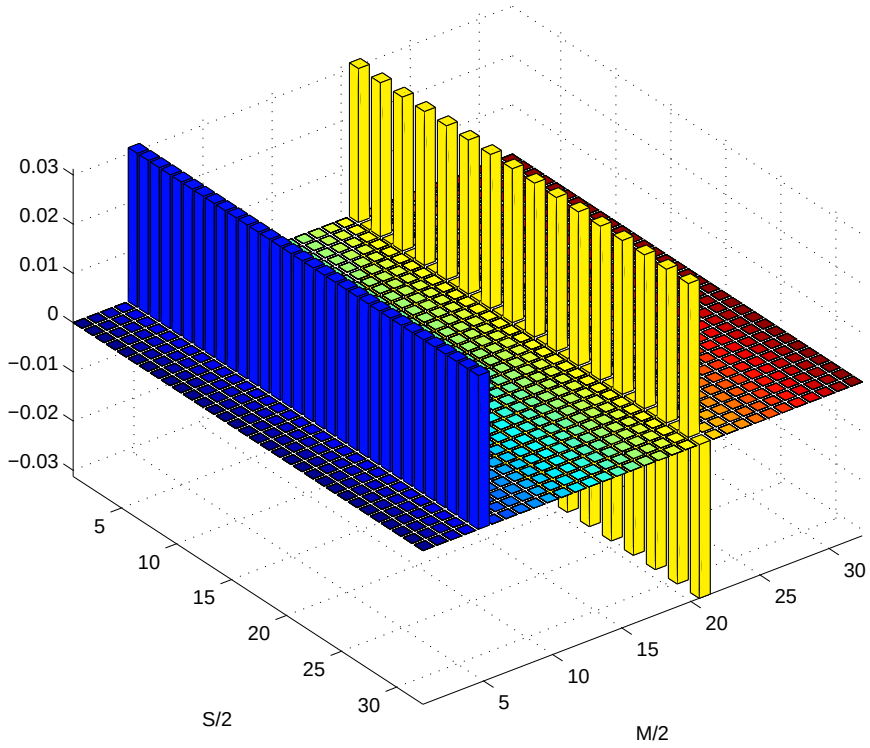

Figure 3.2: A true rendering of the Wigner function $W_{M/2,S/2}$ for the $\left|e_2\right\rangle$ position eigenstate in $D = 16$ dimensions with periodic boundary conditions. The height of each bin is determined by the Wigner function's value.

Finally, we conclude this section with a example. Figures 3.2 and 3.3 contrast two representations of the Wigner function for the $\left|e_2\right\rangle$ position eigenstate in $D = 16$ dimensions with periodic boundary conditions. Figure 3.2 is a true rendering of a discrete valued function with the height of each bar determined by our Wigner function $W_{M/2,S/2}$. The second plot is created by interpolating a continuous function between

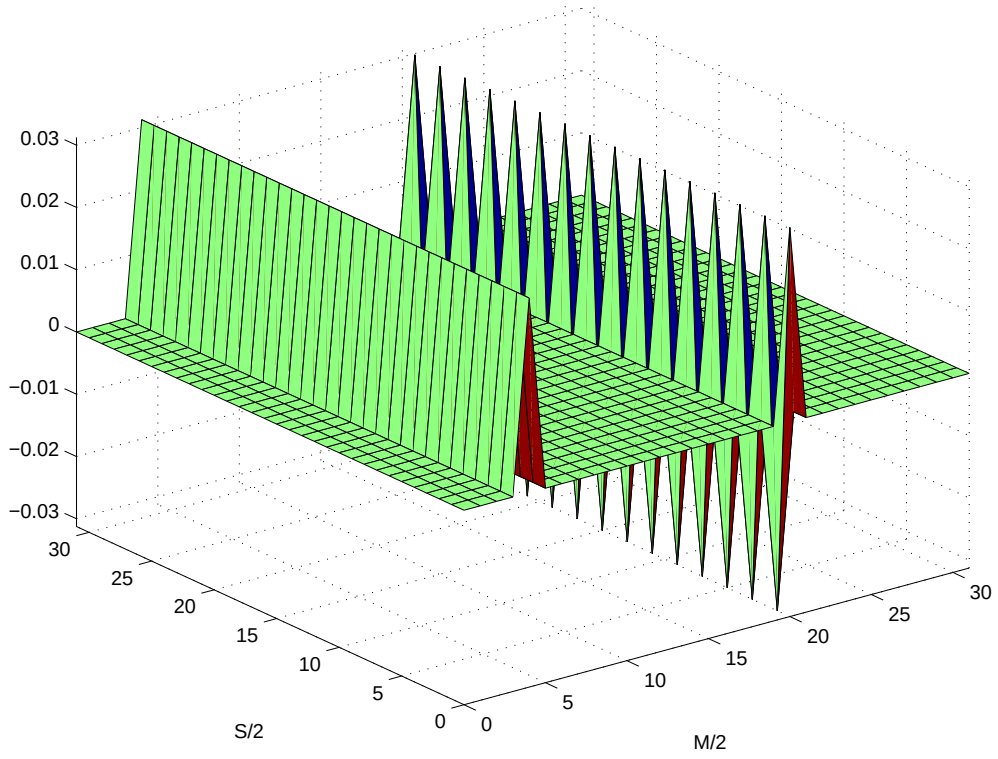

Figure 3.3: An interpretive rendering of the Wigner function $W_{M/2,S/2}$ for the $\left|e_2\right\rangle$ position eigenstate in $D = 16$ dimensions with periodic boundary conditions. A continuously valued function is extrapolated for undefined points, allowing for easier interpretation.

the grid points. As the second plot allows greater detail and easier interpretation, such plots will be used throughout this work.

For a position eigenstate, Figure 3.3 shows that the Wigner function has a uniform distribution along the momentum axis at the position of $\left|e_2\right\rangle$ as well as a series of sign-alternating "spikes" along the momentum axis at a position half a rectangle away. As was discussed earlier, these spikes are explained by Equation 3.49 and ensure the proper marginal distributions shown in Figure 3.4. The marginals are found by summing over the assorted indices of the Wigner function, and then ignoring the zero

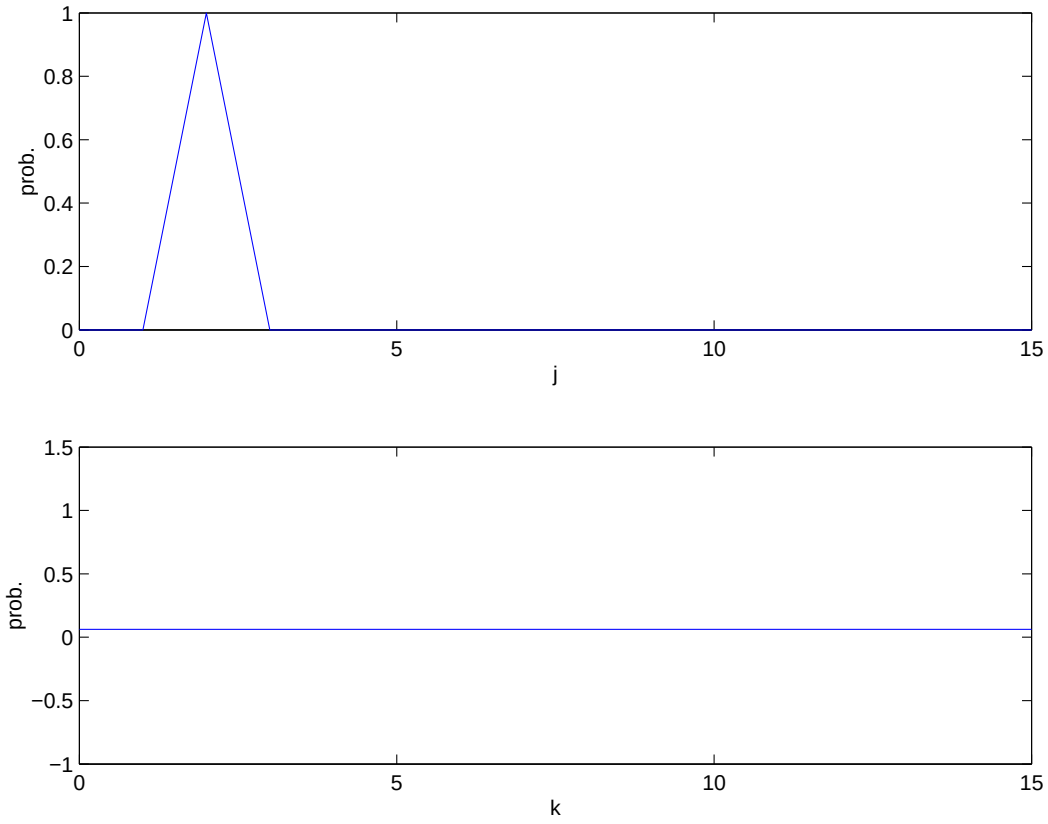

Figure 3.4: The unexciting, but necessary position and momentum marginal distributions of the $\left|e_2\right\rangle$ position eigenstate in $D = 16$ dimensions with periodic boundary conditions.

valued entries (Equations 3.52 and 3.55). We see that the marginals are correct for a position eigenstate which is strictly localized in position and completely delocalized in momentum.

Equation summary for section 3.4

$$W_{M/2,S/2} = \frac{1}{2D}\sum_{j=0}^{D-1} \rho_{j,M-j} \exp\left[\frac{2\pi i}{D}(M-2j)(S/2+\alpha)\right]$$

$$W_{M/2,S/2} = \frac{1}{2D}\sum_{k=0}^{D-1} \widetilde{\rho}_{k,S-k} \exp\left[-\frac{2\pi i}{D}(S-2k)(M/2+\beta)\right]$$

$$W_{M/2,S/2} = \mathrm{tr}\big(\hat{\rho}A_{M/2,S/2}\big)$$

$$\hat{A}_{M/2,S/2} = \frac{1}{2D}\sum_{j=0}^{D-1} \exp\left[\frac{2\pi i}{D}(M-2j)(S/2+\alpha)\right] \big|e_{M-j}\big\rangle\big\langle e_j\big|$$

$$\sum_{S=0}^{2D-1} W_{M/2,S/2} = \rho_{M/2,M/2} \text{ for } M \text{ even}$$

$$\sum_{M=0}^{2D-1} W_{M/2,S/2} = \widetilde{\rho}_{S/2,S/2} \text{ for } S \text{ even}$$

3.5 Symmetry properties of the Wigner function

In this section, we are going to explore the reason for the half-integer valued Wigner function. We believe that the reason for this has to do with the behavior of the Wigner function under symmetry transformations. This idea was first used by Luis and Peřina [69] in constructing a suitable finite-dimensional Wigner function. Since the Wigner function is defined on phase space, a symmetry operation acting on $\hat{\rho}$ should change the Wigner function in the way defined by the geometry of the

phase space. For example, in Chapter 2 we found that for periodic and anti-periodic boundary conditions, one could interpret the Fourier transform operator as a 90° rotation in phase space. We will find that the Wigner function's half-integer values allows us to make a similar interpretation for the $\hat{A}_{M/2,S/2}$ operators.

Let's begin with the simplest symmetry transformation: displacement. Our systems are described by a toroidal, finite-dimensional phase space, *i.e.* one which is periodic up to a phase. An overall phase does not affect probabilities, so the Wigner function should reflect this by being periodic with period D. As was already shown in Equation 3.48, this is a true statement,

$$W_{M/2+D,S/2} = W_{M/2,S/2+D} = W_{M/2,S/2}. \tag{3.57}$$

Another symmetry of interest is 90° rotation, *i.e.* Fourier transformation[9] (see Chapter 2). Given its definition, Equation 2.23, the Fourier operator's action upon the Wigner function is determined by

$$\hat{F}\hat{A}_{M/2,S/2}\hat{F}^\dagger = \frac{1}{2D}\sum_{j=0}^{D-1}\exp\left[\frac{2\pi i}{D}(M-2j)(S/2+\alpha)\right]\big|p_{M-j}\big\rangle\big\langle p_j\big|.$$

We can re-express this in the position basis as

$$\begin{aligned}\hat{F}\hat{A}_{M/2,S/2}\hat{F}^\dagger &= \frac{1}{2D}\sum_{j=0}^{D-1}\exp\left[\frac{2\pi i}{D}(M-2j)(S/2+\alpha)\right]\sum_{l,r=0}^{D-1}\big|e_l\big\rangle\big\langle e_l\big|p_{M-j}\big\rangle\big\langle p_j\big|e_r\big\rangle\big\langle e_r\big| \\ &= \frac{1}{2D}\sum_{l,r=0}^{D-1}\exp\left[\frac{2\pi i}{D}M(S/2+l+\alpha+\beta)\right]\exp\left[\frac{2\pi i}{D}\alpha(l-r)\right]\big|e_l\big\rangle\big\langle e_r\big| \\ &\qquad \times\frac{1}{D}\sum_{j=0}^{D-1}\exp\left[-\frac{2\pi i}{D}j\Big(S+l+r+2(\alpha+\beta)\Big)\right],\end{aligned}$$

[9]We should be calculating $\hat{F}^\dagger\hat{A}_{M/2,S/2}\hat{F}$, but given Equation 3.47, it is much simpler to calculate $\hat{F}\hat{A}_{M/2,S/2}\hat{F}^\dagger$. If we find that the operator rotates 90° clockwise under the latter transformation, then it must do the correct thing and rotate counter-clockwise under the former transformation.

and do the sum over j. We remember that the Fourier transform operator has the 90° rotation interpretation only for periodic and anti-periodic boundary conditions; therefore, $\alpha + \beta$ must be an integer; Equation 2.26 can be applied to give

$$\frac{1}{D}\sum_{j=0}^{D-1}\exp\left[-\frac{2\pi i}{D}j\Big(S+l+r+2(\alpha+\beta)\Big)\right] = \delta_{S+l+r+2(\alpha+\beta),tD}. \tag{3.58}$$

We can omit the sum over t because the values of S, l, r, and $\alpha+\beta$ are such that t ranges only between 0 and 3. Unfortunately, the values of t have no simple relation to those of the other variables; therefore, we must leave it undefined. Luckily we will find that all dependence upon t disappears in the final form. Inserting this delta function into our expression leaves us with

$$\begin{aligned}\hat{F}\hat{A}_{M/2,S/2}\hat{F}^\dagger &= \frac{1}{2D}\sum_{r=0}^{D-1}\exp\left[\frac{2\pi i}{D}\left(\frac{M}{2}+\alpha\right)(-S-2(\alpha+\beta)-2r)\right]\exp\left[2\pi i\alpha t\right] \\ &\qquad\qquad \times \left|e_{tD-S-2(\alpha+\beta)-r}\right\rangle\!\left\langle e_r\right| \\ &= \frac{1}{2D}\sum_{r=0}^{D-1}\exp\left[\frac{2\pi i}{D}\left(\frac{M}{2}+\alpha\right)(-S-2(\alpha+\beta)-2r)\right] \\ &\qquad\qquad \times \left|e_{-S-2(\alpha+\beta)-r}\right\rangle\!\left\langle e_r\right|,\end{aligned} \tag{3.59}$$

where we have used the fact that $\left|e_{tD+j}\right\rangle = \exp\left[-2\pi i\alpha t\right]\left|e_j\right\rangle$. From here we see that

$$\hat{F}\hat{A}_{M/2,S/2}\hat{F}^\dagger = \hat{A}_{-S/2-(\alpha+\beta),M/2}. \tag{3.60}$$

For the two cases for which Fourier transform has a geometric phase space interpretation, we get what we wanted: a 90° clockwise rotation,

$$\begin{aligned}\text{Periodic:} \quad & \hat{F}\hat{A}_{M/2,S/2}\hat{F}^\dagger = \hat{A}_{-S/2,M/2} \\ \text{Anti-periodic:} \quad & \hat{F}\hat{A}_{M/2,S/2}\hat{F}^\dagger = \hat{A}_{-S/2-1,M/2}.\end{aligned} \tag{3.61}$$

The other operator of interest is the anti-unitary time reversal operator $\hat{T}$. For periodic and anti-periodic boundary conditions it has the geometrical interpretation

of reflection through the position axis (See Chapter 2). In the position representation, its action is complex conjugation,

$$\begin{aligned}\hat{T}^\dagger \hat{A}_{M/2,S/2}\hat{T} &= \frac{1}{2D}\sum_{j=0}^{D-1}\exp\left[-\frac{2\pi i}{D}(M-2j)(S/2+\alpha)\right]\left|e_{M-j}\right\rangle\left\langle e_j\right| \\ &= \frac{1}{2D}\sum_{j=0}^{D-1}\exp\left[\frac{2\pi i}{D}\left(M-2j\right)\left(-S/2-2\alpha+\alpha\right)\right]\left|e_{M-j}\right\rangle\left\langle e_j\right| \\ &= \hat{A}_{M/2,-S/2-2\alpha}.\end{aligned} \tag{3.62}$$

Once again our Wigner function behaves correctly. Other possible geometrical operations can be performed using combinations of Fourier, time-reversal, and translation symmetries (Table 2.1); therefore, our Wigner function correctly expresses all possible symmetry transformations. It is an ideal candidate for use in calculation.

It appears that the set of operators $\hat{A}_{M/2,S/2}$ is the only one for which all of these symmetries can given the geometrical phase space interpretation for all dimensions. As was stated earlier, for odd dimensional Hilbert spaces, one can choose the subset $\hat{A}_{M/2,S/2},\ M,S=0,2,4,\ldots 2D-2$. Obviously, if the entire set of operators has the desired symmetry properties then this subset will behave accordingly. We will have a D^2 valued Wigner function with a well defined geometrical interpretation. In even dimensions, however, one cannot pick out the D^2 linearly independent operators and give them the desired geometrical interpretation. Both the symmetry behavior and the marginal calculation for the $\hat{A}_{M/2,S/2}$ operators are determined by their indices. Relabeling these indices to give a D^2-valued Wigner function which produces the proper marginals will give a Wigner function without the geometrical interpretation.

As was discussed in the previous section, there is the possibility of defining a D^2 valued Wigner function by taking a linear combination of the $\hat{A}_{M/2,S/2}$ operators. One could define a new operator $\hat{A}'_{M/2,S/2},\ M,S=0,2,4\ldots 2D-2$ with the definition

$$\hat{A}'_{M/2,S/2} = \hat{A}_{M/2,S/2} + \hat{A}_{M/2+1/2,S/2} + \hat{A}_{M/2,S/2+1/2} + \hat{A}_{M/2+1/2,S/2+1/2}. \tag{3.63}$$

This new operator created from four of the original operators would be hermitian, and a sum over an index would give the correct marginal. But this function does not obey all symmetry properties. As a counter-example, consider the Fourier transform acting upon one of these new operators. Fourier transformation is a linear operator; therefore, it will act upon each term of Equation 3.63 separately,

$$\begin{aligned}\hat{F}\hat{A}'_{M/2,S/2}\hat{F}^\dagger &= \hat{A}_{-S/2,M/2} + \hat{A}_{-S/2,M/2+1/2} + \hat{A}_{-S/2-1/2,M/2} + \hat{A}_{-S/2-1/2,M/2+1/2} \\ \hat{F}\hat{A}'_{M/2,S/2}\hat{F}^\dagger &= \hat{A}_{-S/2-1,M/2} + \hat{A}_{-S/2-1,M/2+1/2} + \hat{A}_{-S/2-3/2,M/2} \\ &\quad + \hat{A}_{-S/2-3/2,M/2+1/2}\end{aligned} \tag{3.64}$$

for periodic and anti-periodic boundary conditions respectively. But $\hat{F}\hat{A}'_{M/2,S/2}\hat{F}^\dagger$ should also be equal to $\hat{A}'_{-S/2,M/2}$ or $\hat{A}'_{-S/2-1,M/2}$ for proper Fourier behavior with periodic and anti-periodic boundary conditions. From the definition, Equation 3.63, we have that

$$\begin{aligned}\hat{A}'_{-S/2,M/2} &= \hat{A}_{-S/2,M/2} + \hat{A}_{-S/2+1/2,M/2} + \hat{A}_{-S/2,M/2+1/2} + \\ &\quad \hat{A}_{-S/2+1/2,M/2+1/2} \\ \hat{F}\hat{A}'_{-S/2-1,M/2}\hat{F}^\dagger &= \hat{A}_{-S/2-1,M/2} + \hat{A}_{-S/2-1/2,M/2} + \hat{A}_{-S/2,M/2} + \\ &\quad \hat{A}_{-S/2-1/2,M/2+1/2}.\end{aligned} \tag{3.65}$$

A comparison between Equation 3.64 and Equation 3.65 reveals that these two different sets of operators are not equal; therefore, this "4-fold" Wigner function does not have proper symmetry behavior for either periodic or anti-periodic boundary conditions.

This problem is detailed graphically in Figures 3.5 and 3.6 for 2 dimensions with periodic and anti-periodic boundary conditions respectively. The operators used to create a D^2 Wigner function[10] A, B, C, and D, represented as boxes, are created by the linear combination of Equation 3.63 (the original operators are the large dots at the box vertices). The boxes in the middle represent the Fourier transform

[10]Obviously, there are 4 operators in this case.

of the linear combination, *i.e.* Equation 3.64. The boxes on the right show the proper transformation of states under Fourier transform for a D^2 Wigner function, Equation 3.65. We see that they do not agree. We need all $4D^2$ operators to have proper Fourier behavior.

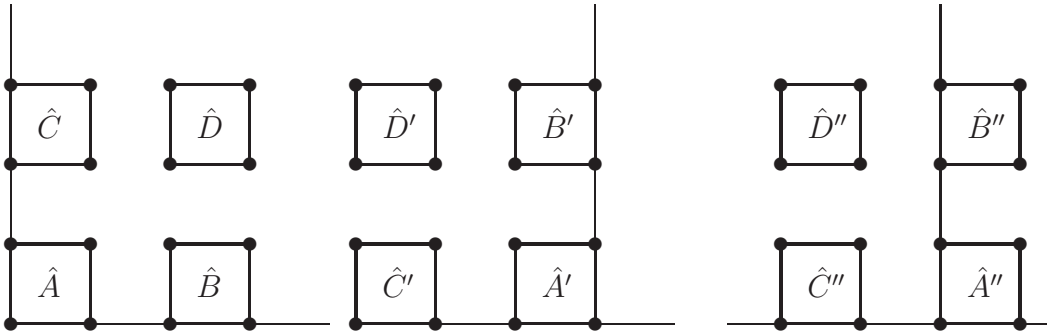

Figure 3.5: A D^2-valued Wigner function created by linear combinations of operators does not have proper behavior under Fourier transformation. In 2 dimensions four operators $\hat{A}$, $\hat{B}$, $\hat{C}$, and $\hat{D}$ (drawn as squares) can be created by taking a linear combination of the original operators (represented by the large dots in each of the pictures). Under Fourier transform, these operators become the new linear combinations labelled $\hat{A}'$, $\hat{B}'$, $\hat{C}'$, and $\hat{D}'$ (as shown in the middle picture). As the right hand picture portrays, however, the proper Fourier behavior of A, B, C, and D labelled $\hat{A}''$, $\hat{B}''$, $\hat{C}''$, and $\hat{D}''$ is different.

As a final note, Luis and Peřina [69] have shown for Hilbert spaces of dimension $D = 4, 8, 12 \ldots$ that it is possible to create a Wigner function that has proper Fourier symmetry (but not time reversal). While we question some of their mathematical techniques[11], we agree with the conclusion. It is possible to have Fourier symmetry in certain cases. However, it seems (to the author) that it is better to use a Wigner function which has all symmetry properties for all dimensions instead of one which only works in fraction of them.

[11]Especially the statement that for anti-periodic boundary conditions, the hermitian conjugate of the displacement operator raised to a power is the same as that operator raised to the negative of that power mod D

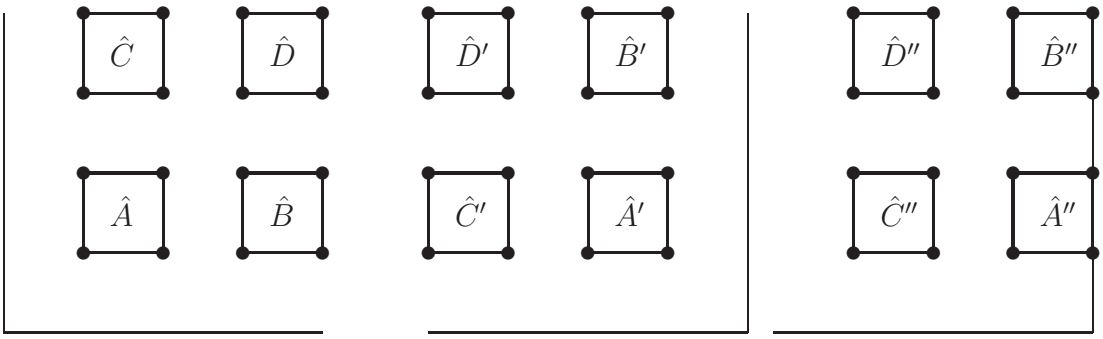

Figure 3.6: A D^2-valued Wigner function created by linear combinations of operators does not have proper Fourier behavior for anti-periodic boundary conditions either. Once again, the primed operators are the Fourier transform of the linear combinations while the double primed operators are the combination of states necessary for proper Fourier behavior.

Equation summary for section 3.5

$$\hat{F}\hat{A}_{M/2,S/2}\hat{F}^\dagger = \hat{A}_{-S/2-(\alpha+\beta),M/2}$$

$$\hat{T}^\dagger\hat{A}_{M/2,S/2}\hat{T} = \hat{A}_{M/2,-S/2-2\alpha}$$

Chapter 4

A Q-function for finite-dimensional Hilbert spaces

4.1 Coherent states for $\mathcal{H}_D$

We will now introduce coherent states for the finite-dimensional Hilbert space. These states[1] are infinite-dimensional coherent states that have been periodically continued in both position in momentum so as to be valid states in $\mathcal{H}_D$.

We begin with the expression for the standard Weyl group coherent states,

$$\langle x|a\rangle = (\pi\hbar)^{-1/4} \exp\left[-\frac{1}{2\hbar}(x-x_0)^2\right] \exp\left[\frac{i}{\hbar}xp_0\right] \exp\left[-\frac{i}{2\hbar}x_0p_0\right], \tag{4.1}$$

$a = x_0 + ip_0$. We then periodically continue these states using the isomorphism,

[1]First introduced by Shau-Jin and Shi [51] and used by among others Leboeuf [71] and Nonnenmacher [72].

Equation 3.15, from section 3.2,

$$\begin{aligned}\langle e_j|a\rangle = \sqrt{\frac{1}{\mathcal{N}}} \sum_{m=-\infty}^{\infty} \exp\left[-\frac{1}{2\hbar}\left(e_j - x_0 + mQ\right)^2\right] \exp\left[\frac{i}{\hbar}\left(e_j + mQ\right)p_0\right] \\ \times \exp\left[-\frac{i}{2\hbar}x_0 p_0\right] \exp\left[-2\pi i m\alpha\right].\end{aligned} \tag{4.2}$$

As usual e_j in equations is shorthand for $Q(j+\beta)/D$ and $\mathcal{N}$ is a constant to ensure normalization. Equation 4.2 reveals the states' periodicity,

$$\begin{aligned}\langle e_{j+D}|a\rangle &= \exp\left[2\pi i\alpha\right]\langle e_j|a\rangle, \\ |a+Q\rangle &= \exp\left[\pi i D\frac{p_0}{P}\right]\exp\left[-2\pi i\alpha\right]|a\rangle, \\ |a+iP\rangle &= \exp\left[-\pi i D\frac{x_0}{Q}\right]\exp\left[2\pi i\beta\right]|a\rangle.\end{aligned} \tag{4.3}$$

The first expression above is the important verification that these states obey the fundamental position boundary condition of $\mathcal{H}_D$. To verify the states' momentum boundary condition, we will need to find their momentum representation. We also find the states are periodic with respect to x_0 and p_0; thus, we can restrict our attention to those states centered within the fiducial rectangle[2]. We see that they are not strictly α or β-periodic due to the $\exp\left[-ix_0p_0/2\hbar\right]$ term in Equation 4.2. The reason for keeping this term will be discussed next when finding the momentum representation of the coherent states.

Figure 4.1 shows the Wigner function for the coherent state $a = 4/16 + i4/16$, *i.e.* $a = 1/4 + i/4$. We see a Gaussian peak at the coherent state's center. The remaining three peaks are realized as being a consequence of Equation 3.49 and create the proper marginals shown in Figure 4.2. These peaks can also be given a geometric interpretation as being interference terms. The Wigner function is periodic, $W_{M/2+D,S/2} = W_{M/2,S/2+D} = W_{M/2,S/2}$; therefore, we can imagine an infinite set of

[2]The rectangle of area QP such that $0 \le x_0 \le Q$, $0 \le p_0 \le P$.

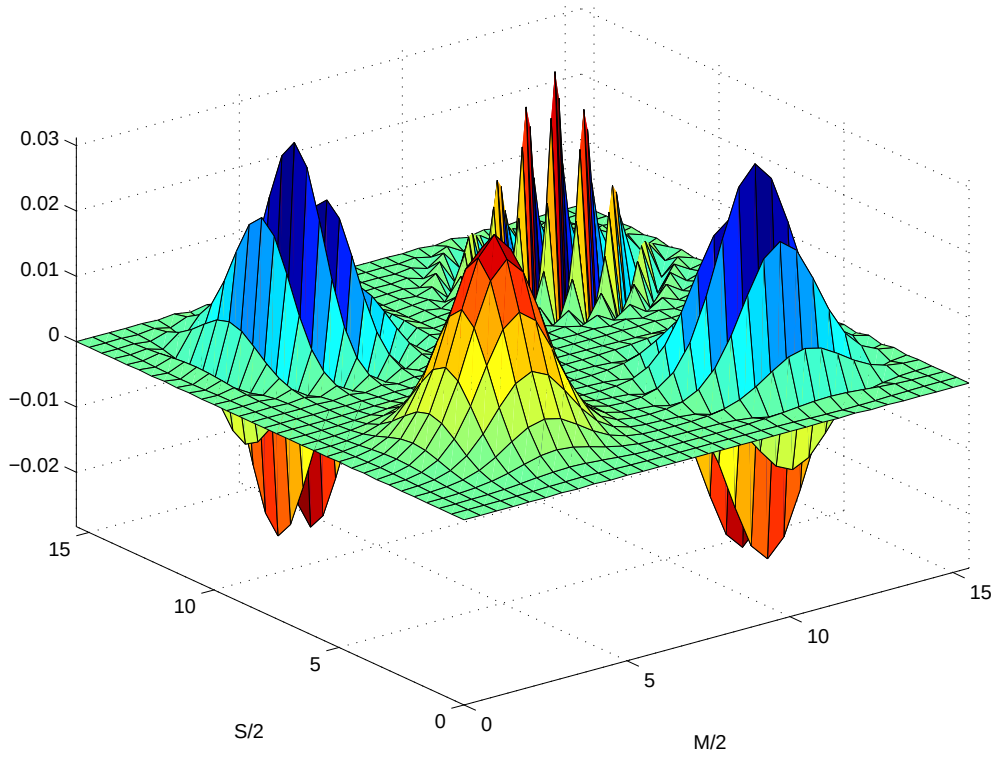

Figure 4.1: The Wigner function of the coherent state centered at $x_0 = 4/16$, $p_0 = 4/16$ in $D = 16$ dimensions.

repeated peaks in the unplotted, non-fiducial rectangles. As was discussed in section 3.4, there will be quantum mechanical interference between these peaks which manifests itself as these regions of rapid oscillation.

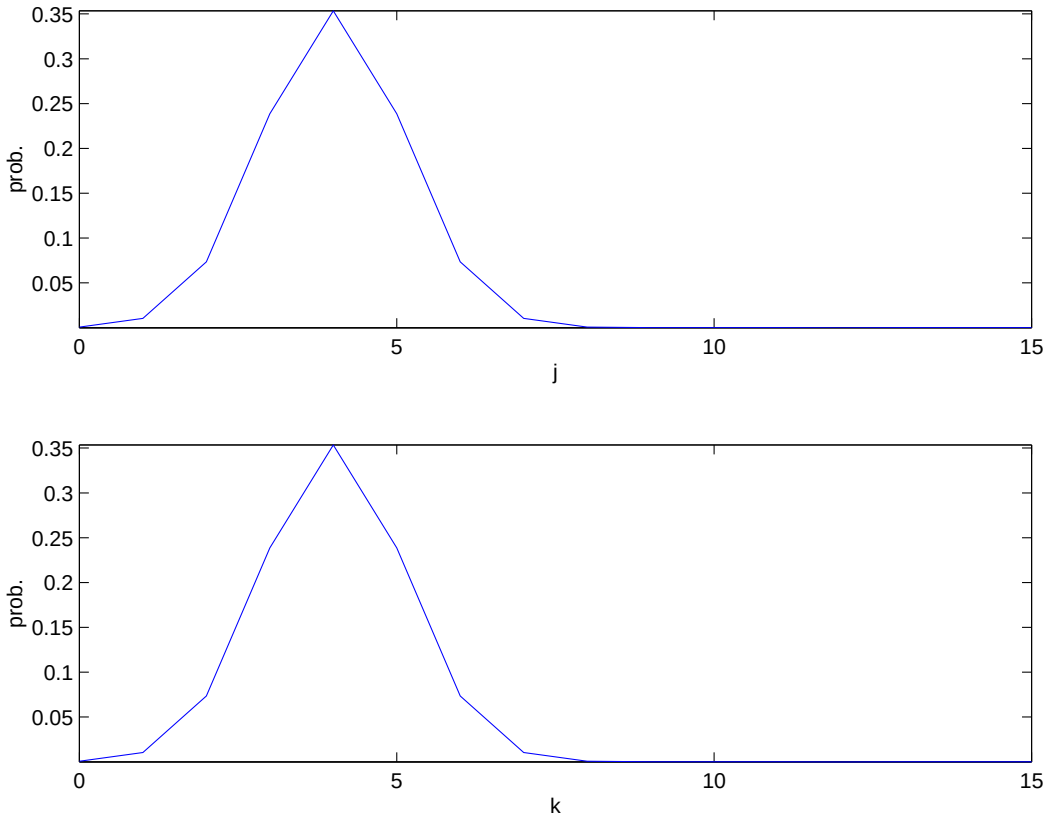

Figure 4.2: The position and momentum marginal distributions of the coherent state of Figure 4.1. We see symmetrical Gaussian like probabilities for $|\langle e_j|a\rangle|^2$ and $|\langle p_k|a\rangle|^2$.

Equation summary for section 4.1

$$\langle e_j|a\rangle = \sqrt{\frac{1}{\mathcal{N}}} \sum_{m=-\infty}^{\infty} \exp\left[-\frac{1}{2\hbar}\left(e_j - x_0 + mQ\right)^2\right] \exp\left[\frac{i}{\hbar}\left(e_j + mQ\right)p_0\right] \times \exp\left[-\frac{i}{2\hbar}x_0p_0\right] \exp\left[-2\pi i m\alpha\right]$$

$$|a+Q\rangle = \exp\left[\pi i D\frac{p_0}{P}\right] \exp\left[-2\pi i\alpha\right] |a\rangle$$

$$|a+iP\rangle = \exp\left[-\pi i D\frac{x_0}{Q}\right] \exp\left[2\pi i\beta\right] |a\rangle$$

4.2 The momentum representation of the coherent states

We find the momentum representation using the completeness of the position basis states,

$$\langle p_k|a\rangle = \sum_{j=0}^{D-1} \langle p_k|e_j\rangle\langle e_j|a\rangle, \tag{4.4}$$

and the discrete Fourier transform,

$$\langle p_k|e_j\rangle = \frac{1}{\sqrt{D}} \exp\left[-\frac{2\pi i}{D}(j+\beta)(k+\alpha)\right].$$

Using Equation 4.2, we have

$$\begin{aligned}\langle p_k|a\rangle = \sqrt{\frac{1}{\mathcal{N}D}} \exp\left[-\frac{1}{2\hbar}x_0p_0\right] \sum_{m=-\infty}^{\infty}\sum_{j=0}^{D-1} \exp\left[-\frac{1}{2\hbar}\left(e_j - x_0 + mQ\right)^2\right] \\ \times \exp\left[\frac{i}{\hbar}\left(e_j + mQ\right)p_0\right] \exp\left[-2\pi i m\alpha\right] \exp\left[-\frac{2\pi i}{D}(j+\beta)(k+\alpha)\right].\end{aligned} \tag{4.5}$$

To further the calculation, we shall introduce a mathematical technique which will be of great use in the rest of this chapter.

4.2.1 The Fourier representation of periodic functions

We begin by considering the function,

$$\begin{aligned}f(u) = \sum_{m=-\infty}^{\infty} \exp\left[-\frac{1}{2\hbar}\left(Qu/D - x_0' + mQ\right)^2\right] \exp\left[-2\pi i m\alpha\right] \\ \times \exp\left[\frac{i}{\hbar}\left(Qu/D + Q\beta/D + mQ\right)p_0\right] \exp\left[-\frac{2\pi i}{D}(u+\beta)(k+\alpha)\right],\end{aligned} \tag{4.6}$$

where $x_0' = x_0 - Q\beta/D$. With a little bit of work, it can be seen that this function is strictly periodic with period D, *i.e.* $f(u+D) = f(u)$; therefore, we can write it as a Fourier series,

$$f(u) = \sum_{r=-\infty}^{\infty} \exp\left[\frac{2\pi i}{D}ru\right] c_r. \tag{4.7}$$

The expansion coefficients are found in the usual way,

$$c_r = \frac{1}{D}\int_0^D du\, f(u) \exp\left[-\frac{2\pi i}{D} r u\right]. \tag{4.8}$$

To calculate the expansion coefficients in this case, we insert Equation 4.6 into the expression above, square out the Gaussian, collect terms, and then re-combine them by completing the square. The end result is

$$\begin{aligned} c_r = \frac{1}{D}\int_0^D du \sum_{m=-\infty}^{\infty} &\exp\left[-\frac{1}{2\hbar}\left(Qu/D + \xi\right)^2\right] \exp\left[-\frac{1}{2\hbar}\left(-\xi^2 - \left(mQ - x_0'\right)^2\right)\right] \\ &\times \exp\left[\frac{i}{\hbar} p_0 \left(Q\beta/D + mQ\right) - \frac{\beta(k+\alpha)}{D} - 2\pi i m\alpha\right], \end{aligned} \tag{4.9}$$

where

$$\xi = mQ - x_0' + i\left(\frac{P}{D}(r + k + \alpha) - p_0\right) = mQ - x_0' + i\left(\frac{P}{D} r + p_k - p_0\right).$$

After squaring the variable ξ and inserting the definition of x_0', we find that there are many cancellations. We are left with

$$\begin{aligned} c_r = \frac{1}{D}\int_0^D du \sum_{m=-\infty}^{\infty} &\exp\left[-\frac{1}{2\hbar}\Big(Qu/D + mQ - x_0' + i\Big(\frac{P}{D} r + p_k - p_0\Big)\Big)^2\right] \\ &\times \exp\left[-\frac{1}{2\hbar}\left(p_k - p_0 + Pr/D\right)^2\right] \exp\left[-\frac{i}{\hbar} x_0 \left(p_k + Pr/D\right)\right] \exp\left[\frac{i}{\hbar} x_0 p_0\right] \\ &\times \exp\left[\frac{2\pi i}{D}\beta r\right]. \end{aligned} \tag{4.10}$$

The remaining dependence on the variables m and u is found in the leading Gaussian term only; we can combine them into a continuous variable defined for the entire real

line,

$$\begin{aligned}
&\frac{1}{D}\int_0^D du \sum_{m=-\infty}^{\infty} \exp\left[-\frac{1}{2\hbar}\Big(Qu/D + mQ - x_0' + i\Big(\frac{P}{D}r + p_k - p_0\Big)\Big)^2\right] \\
= \;& \frac{1}{D}\int_{-\infty}^{\infty} dy \exp\left[-\frac{1}{2\hbar}\Big(Qy/D - x_0' + i\Big(\frac{P}{D}r + p_k - p_0\Big)\Big)^2\right] \\
= \;& \frac{\sqrt{2\pi\hbar}}{Q} = \sqrt{\frac{P}{QD}}
\end{aligned}$$

Our final expression for $f(u)$ is

$$\begin{aligned}
f(u) = \sqrt{\frac{P}{QD}} \sum_{r=-\infty}^{\infty} \exp\left[\frac{2\pi i}{D} ru\right] \exp\left[-\frac{1}{2\hbar}\left(p_k - p_0 + Pr/D\right)^2\right] \\
\times \exp\left[-\frac{i}{\hbar} x_0 \left(p_k + Pr/D\right)\right] \exp\left[\frac{i}{\hbar} x_0 p_0\right] \exp\left[2\pi i \beta r/D\right].
\end{aligned} \tag{4.11}$$

This equation is true for all real numbers u; therefore, it must hold when u is an integer.

Returning to the momentum representation for the coherent state, we use Equation 4.11 to write our inner product as

$$\begin{aligned}
\langle p_k|a\rangle = \sqrt{\frac{P}{Q\mathcal{N}}}\frac{1}{D} \sum_{r=-\infty}^{\infty}\sum_{j=0}^{D-1} \exp\left[\frac{2\pi i}{D} rj\right] \exp\left[-\frac{1}{2\hbar}\left(p_k - p_0 + Pr/D\right)^2\right] \\
\times \exp\left[-\frac{i}{\hbar} x_0 \left(p_k + Pr/D\right)\right] \exp\left[\frac{i}{2\hbar} x_0 p_0\right] \exp\left[\frac{2\pi i}{D}\beta r\right].
\end{aligned} \tag{4.12}$$

Using Equation 2.26 yet again, we know that

$$\sum_{j=0}^{D-1} \exp\left[\frac{2\pi i}{D} rj\right] = D \sum_{t=-\infty}^{\infty} \delta_{r,tD}. \tag{4.13}$$

Consequently, we have

$$\begin{aligned}
\langle p_k|a\rangle = \sqrt{\frac{P}{Q\mathcal{N}}} \sum_{t=-\infty}^{\infty} \exp\left[-\frac{1}{2\hbar}\left(p_k - p_0 + tP\right)^2\right] \exp\left[-\frac{i}{\hbar}\left(p_k + tP\right) x_0\right] \\
\times \exp\left[\frac{i}{2\hbar} x_0 p_0\right] \exp\left[2\pi i \beta t\right].
\end{aligned} \tag{4.14}$$

Comparing this expression with Equation 4.2, we see the expression one would expect for the Weyl coherent states. The momentum representation could easily have been found using the isomorphism of section 3.2; however, as the Fourier series technique will prove immensely useful in the upcoming chapter, this simple problem allowed its introduction in a natural, elegant way.

We find that our states have been periodically continued in the correct way,

$$\begin{aligned}
\langle p_{k+D}|a\rangle &= \exp\left[-2\pi i\beta\right]\langle p_k|a\rangle && (4.15)\\
|a+Q\rangle &= \exp\left[-\pi i D\frac{p_0}{P}\right]\exp\left[-2\pi i\alpha\right]|a\rangle && (4.16)\\
|a+iP\rangle &= \exp\left[-\pi i D\frac{x_0}{Q}\right]\exp\left[2\pi i\beta\right]|a\rangle. && (4.17)
\end{aligned}$$

They have the fundamental momentum boundary condition of $\mathcal{H}_D$ and necessarily have the same periodicity for x_0 and p_0.

There is another reason to be pleased with Equation 4.14. It can be interpreted[3] as showing that under Fourier transform, the state $a = x_0 + ip_0$ transforms to the state $a' = p_0 - ix_0$; we have ninety degree rotation in phase space. This interpretation is possible only with the $\exp\left[-ix_0p_0/2\hbar\right]$ term in Equation 4.2 hence its inclusion even though it alters the periodicity one might desire for these states.

[3]Assuming that $Q = P$.

Equation summary for section 4.2

$$\sum_{m=-\infty}^{\infty} \exp\left[-\frac{1}{2\hbar}\left(Qx/D - x_0' + mQ\right)^2\right] \exp\left[-2\pi i m\alpha\right]$$
$$\times \exp\left[\frac{i}{\hbar}\left(Qx/D + Q\beta/D + mQ\right)p_0\right] \exp\left[-\frac{2\pi i}{D}(x+\beta)(k+\alpha)\right]$$
$$= \sqrt{\frac{P}{QD}} \sum_{r=-\infty}^{\infty} \exp\left[\frac{2\pi i}{D} rx\right] \exp\left[-\frac{1}{2\hbar}\left(p_k - p_0 + Pr/D\right)^2\right]$$
$$\times \exp\left[-\frac{i}{\hbar} x_0\left(p_k + Pr/D\right)\right] \exp\left[\frac{i}{\hbar} x_0 p_0\right] \exp\left[2\pi i\beta r/D\right]$$

$$\langle p_k | a\rangle = \sqrt{\frac{P}{Q\mathcal{N}}} \sum_{t=-\infty}^{\infty} \exp\left[-\frac{1}{2\hbar}\left(p_k - p_0 + tP\right)^2\right] \exp\left[-\frac{i}{\hbar}\left(p_k + tP\right)x_0\right]$$
$$\times \exp\left[\frac{i}{2\hbar} x_0 p_0\right] \exp\left[2\pi i\beta t\right]$$

4.3 Normalization for a subset of the coherent states

From here, we will be considering a very special subset of the coherent states which in Equation 4.2 were defined for all x_0 and p_0. If we create a lattice of coherent states by taking the set

$$\begin{aligned} x_0 &= \frac{Q}{D}(l+\beta) \\ p_0 &= \frac{P}{D}(v+\alpha) \end{aligned} \tag{4.18}$$

with $l, v = 0, 1, \ldots, D-1$, then we can show that they have some very nice properties, the least of which is a simple form for normalization.

Substituting these definitions for x_0 and p_0 into Equation 4.2, we have a simple

coherent state form,

$$\begin{aligned}\langle e_j|a\rangle = \sqrt{\frac{1}{\mathcal{N}}}\sum_{m=-\infty}^{\infty}\exp\left[-\frac{1}{2\hbar}\big(Q(j-l)/D+mQ\big)^2\right] \\ \times\exp\left[\frac{2\pi i}{D}(j+\beta)(v+\alpha)\right]\exp\left[-\frac{\pi i}{D}(l+\beta)(v+\alpha)\right].\end{aligned} \tag{4.19}$$

We obviously find the normalizing constant by insisting that $\langle a|a\rangle = 1$. Inserting a resolution of the identity and using the expression for our coherent state gives

$$\mathcal{N} = \sum_{j=0}^{D-1}\sum_{m,n=-\infty}^{\infty}\exp\left[-\frac{1}{2\hbar}\big(Q(j-l)/D+mQ\big)^2\right]\exp\left[-\frac{1}{2\hbar}\big(Q(j-l)/D+nQ\big)^2\right]. \tag{4.20}$$

We can simplify this expression by showing that the sum over j is independent of the mean l. To see this, we redefine the summing variable to be $j' = j - l$. This simplifies the sum to be

$$\sum_{j'=-l}^{D-1-l}\sum_{m,n=-\infty}^{\infty}\exp\left[-\frac{1}{2\hbar}\big(Qj'/D+mQ\big)^2\right]\exp\left[-\frac{1}{2\hbar}\big(Qj'/D+nQ\big)^2\right]. \tag{4.21}$$

Split this new sum into two pieces:

$$\sum_{j'=-l}^{D-1-j} = \sum_{j'=-l}^{-1} + \sum_{j'=0}^{D-1-l}.$$

For the first term, define yet another summing variable, $j'' = j' + D$. This change of variable produces a simple output,

$$\sum_{j''=D-j}^{D-1}\exp\left[-\frac{1}{2\hbar}\big(Qj''/D+(m-1)Q\big)^2\right]\exp\left[-\frac{1}{2\hbar}(Qj''/D+(n-1)Q)^2\right].$$

We can redefine the summing variables m and n without affecting their infinite summing ranges.

The irrelevancy on the l variable reveals the normalizing expression to be

$$\mathcal{N} = \sum_{j=0}^{D-1}\sum_{m,n=-\infty}^{\infty}\exp\left[-\frac{1}{2\hbar}\left(Qj/D+mQ\right)^2\right]\exp\left[-\frac{1}{2\hbar}\left(Qj/D+nQ\right)^2\right]. \tag{4.22}$$

We now use the techniques from section 4.2.1 to re-write the Gaussians in a form that is easier to manipulate. The function

$$f(u) = \sum_{m=-\infty}^{\infty} \exp\left[-\frac{1}{2\hbar}(Qu/D + mQ)^2\right]$$

is periodic with period D; we can write it as a Fourier series,

$$\begin{aligned} &\sum_{m=-\infty}^{\infty} \exp\left[-\frac{1}{2\hbar}(Qj/D + mQ)^2\right] \\ &= \sqrt{\frac{P}{QD}} \sum_{r=-\infty}^{\infty} \exp\left[\frac{2\pi i}{D} jr\right] \exp\left[-\frac{1}{2\hbar}\left(\frac{Pr}{D}\right)^2\right]. \end{aligned} \tag{4.23}$$

Using this expression in Equation 4.22 gives

$$\mathcal{N} = \frac{P}{QD} \sum_{j=0}^{D-1} \sum_{r,t=-\infty}^{\infty} \exp\left[\frac{2\pi i}{D} j(r+t)\right] \exp\left[-\frac{1}{2\hbar}(Pr/D)^2\right] \exp\left[-\frac{1}{2\hbar}(Pt/D)^2\right]. \tag{4.24}$$

Using Equation 2.26 again tells us that

$$\sum_{j=0}^{D-1} \exp\left[\frac{2\pi i}{D} j(r+t)\right] = D \sum_{s=-\infty}^{\infty} \delta_{r+t,sD}.$$

Inserting this fact into our normalizing constant and making some slight algebraic simplifications , we arrive at

$$\mathcal{N} = \frac{P}{Q} \sum_{s=-\infty}^{\infty} \exp\left[-\frac{1}{4\hbar}(Ps)^2\right] \sum_{t=-\infty}^{\infty} \exp\left[-\frac{1}{\hbar}\left(\frac{Pt}{D} - \frac{Ps}{2}\right)^2\right]. \tag{4.25}$$

We see that the second term is periodic in the s variable, this time with period $2/D$. Its Fourier series is given by

$$\sum_{t=-\infty}^{\infty} \exp\left[-\frac{1}{\hbar}\left(\frac{Pt}{D} - \frac{Ps}{2}\right)^2\right] = \sqrt{\frac{QD}{2P}} \sum_{t'=-\infty}^{\infty} \exp\left[\pi i D t'\right] \exp\left[-\frac{1}{4\hbar}(Qt')^2\right]. \tag{4.26}$$

Our final expression is

$$\mathcal{N} = \sqrt{\frac{DP}{2Q}} \sum_{s,t=-\infty}^{\infty} \exp\left[\pi i D st\right] \exp\left[-\frac{1}{4\hbar}\Big((Ps)^2 + (Qt)^2\Big)\right]. \tag{4.27}$$

Dimension, D	$\sum_{s,t=-\infty}^{\infty} \exp\left[\pi i D s t\right] \exp\left[-\frac{1}{4\hbar}\left(s^2+t^2\right)\right]$
2	1.18034059901610
3	1.03561039253191
4	1.00748372034508
5	1.00155221000889
6	1.00032282411993
7	1.00006710200039
8	1.00001394941807
9	1.00000289978690
10	1.00000060280700
11	1.00000012531124
12	1.00000002604965
13	1.00000000541519
14	1.00000000112571
15	1.00000000023401

Table 4.1: The very precise values for the normalization sum of the coherent state as a function of dimension. Its value is seen to decrease rapidly enough to approximate as unity.

The scale of the normalizing constant is

$$\mathcal{N} \sim \sqrt{\frac{DP}{2Q}}, \tag{4.28}$$

but scanning Table 4.1 which gives the values for Equation 4.27 when $Q = P = 1$, shows that in practice the value of the sum decays rapidly to 1 as D increases. A very good approximation for a normalized coherent state is

$$\begin{aligned}\left\langle e_j \middle| a \right\rangle = \left(\frac{2Q}{DP}\right)^{1/4} \sum_{m=-\infty}^{\infty} \exp\left[-\frac{1}{2\hbar}\big(Q(j-l)/D + mQ\big)^2\right] \\ \times \exp\left[\frac{2\pi i}{D}(j+\beta)(v+\alpha)\right] \exp\left[-\frac{\pi i}{D}(l+\beta)(v+\alpha)\right].\end{aligned} \tag{4.29}$$

Inserting the value for $\mathcal{N}$ into Equation 4.14, we find that

$$\begin{aligned}\langle p_k|a\rangle = \left(\frac{2P}{DQ}\right)^{1/4} \sum_{t=-\infty}^{\infty} \exp\left[-\frac{1}{2\hbar}\big(P(k-v)/D + tP\big)^2\right] \\ \times \exp\left[-\frac{2\pi i}{D}(k+\alpha)(l+\beta)\right] \exp\left[\frac{\pi i}{D}(l+\beta)(v+\alpha)\right],\end{aligned} \tag{4.30}$$

which nicely mirrors the position representation.

Finally, when we perform our semi-classical analysis in Chapter 6, it will be more convenient to represent the coherent states in terms of the complex variable a. To this end, we can rewrite Equation 4.29 as

$$\langle e_j|a\rangle \equiv \left(\frac{2Q}{DP}\right)^{1/4} \sum_{\mu=-\infty}^{\infty} \exp\left[-\frac{\pi D}{2}\left(|a|^2 - a^2\right) - \pi D\left(e_j - a + \mu\right)^2 + i\pi\mu\right]. \tag{4.31}$$

Equation summary for section 4.3

$$\sum_{m=-\infty}^{\infty} \exp\left[-\frac{1}{2\hbar}(Qj/D + mQ)^2\right]$$
$$= \sqrt{\frac{P}{QD}} \sum_{r=-\infty}^{\infty} \exp\left[\frac{2\pi i}{D} jr\right] \exp\left[-\frac{1}{2\hbar}\left(\frac{Pr}{D}\right)^2\right]$$

$$\mathcal{N} = \sqrt{\frac{DP}{2Q}} \sum_{s,t=-\infty}^{\infty} \exp\left[\pi i D s t\right] \exp\left[-\frac{1}{4\hbar}\left((Ps)^2 + (Qt)^2\right)\right]$$

$$\mathcal{N} \sim \sqrt{\frac{DP}{2Q}}$$

$$\langle e_j | a \rangle = \left(\frac{2Q}{DP}\right)^{1/4} \sum_{m=-\infty}^{\infty} \exp\left[-\frac{1}{2\hbar}\big(Q(j-l)/D + mQ\big)^2\right]$$
$$\times \exp\left[\frac{2\pi i}{D}(j+\beta)(v+\alpha)\right] \exp\left[-\frac{\pi i}{D}(l+\beta)(v+\alpha)\right]$$

$$\langle p_k | a \rangle = \left(\frac{2P}{DQ}\right)^{1/4} \sum_{t=-\infty}^{\infty} \exp\left[-\frac{1}{2\hbar}\big(P(k-v)/D + tP\big)^2\right]$$
$$\times \exp\left[-\frac{2\pi i}{D}(k+\alpha)(l+\beta)\right] \exp\left[\frac{\pi i}{D}(l+\beta)(v+\alpha)\right]$$

$$\langle e_j | a \rangle \equiv \left(\frac{2Q}{DP}\right)^{1/4} \sum_{\mu=-\infty}^{\infty} \exp\left[-\frac{\pi D}{2}\left(|a|^2 - a^2\right) - \pi D\left(e_j - a + \mu\right)^2 + i\pi\mu\right]$$

4.4 Proof of completeness for the subset of coherent states

Finally, we shall define a Q-function for $\mathcal{H}_D$ using the subset of coherent states defined by Equation 4.29. The proof that this lattice of coherent states is complete is straight forward. One merely shows that,

$$\sum_{l=0}^{D-1}\sum_{v=0}^{D-1}\langle e_j|a\rangle\langle a|e_k\rangle \propto \delta_{j,k}, \tag{4.32}$$

and thus

$$\sum_{l=0}^{D-1}\sum_{v=0}^{D-1}|a\rangle\langle a| \propto \hat{1}. \tag{4.33}$$

We begin our proof by inserting the definition for the coherent state,

$$\sum_{l,v=0}^{D-1}\langle e_j|a\rangle\langle a|e_k\rangle = \frac{1}{\mathcal{N}}\sum_{l=0}^{D-1}\sum_{m=-\infty}^{\infty}\sum_{n=-\infty}^{\infty}\exp\left[-\frac{1}{2\hbar}\big(Q(j-l)/D+mQ\big)^2\right] \times\exp\left[-\frac{1}{2\hbar}\big(Q(k-l)/D+nQ\big)^2\right]\sum_{v=0}^{D-1}\exp\left[\frac{2\pi i}{D}(v+\alpha)(j-k)\right]. \tag{4.34}$$

The reason for taking a "step back" and not using the normalization factor found in the previous section will become apparent shortly.

Continuing our habit of using Equation 2.26 in every section, we have that

$$\sum_{v=0}^{D-1}\exp\left[\frac{2\pi i}{D}(v+\alpha)(j-k)\right] = D\sum_{r=-\infty}^{\infty}\exp\left[2\pi i r\alpha\right]\delta_{j-k,rD}. \tag{4.35}$$

In this case, we shall assume that $|e_j\rangle$ and $|e_k\rangle$ have been chosen in the fiducial $0,\ldots,D-1$ range such that we can set[4] $r=0$.

[4]The other values of r are a reminder of the periodicity of $\mathcal{H}_D$. We see from Equation 4.32 that choosing j or k outside the fiducial range would create an overall phase; the variable r keeps track of this phase.

This delta function simplifies the matrix element to

$$\sum_{l,v=0}^{D-1} \langle e_j|a\rangle\langle a|e_k\rangle = \delta_{j,k}\,\frac{D}{\mathcal{N}} \sum_{l=0}^{D-1}\sum_{m=-\infty}^{\infty}\sum_{n=-\infty}^{\infty} \exp\left[-\frac{1}{2\hbar}\big(Q(j-l)/D+mQ\big)^2\right] \times \exp\left[-\frac{1}{2\hbar}\big(Q(j-l)/D+nQ\big)^2\right]. \tag{4.36}$$

We see that the truly important part of the proof is finished. Equation 4.32 is true. The remaining task is to find the proportionality constant.

The first step in finding this constant is to remember that the sum

$$\sum_{l=0}^{D-1}\sum_{m=-\infty}^{\infty}\sum_{n=-\infty}^{\infty} \exp\left[-\frac{1}{2\hbar}\big(Q(j-l)/D+mQ\big)^2\right] \exp\left[-\frac{1}{2\hbar}\big(Q(j-l)/D+nQ\big)^2\right] \tag{4.37}$$

is independent of l, thus Equation 4.37 becomes

$$\sum_{l=0}^{D-1}\sum_{m=-\infty}^{\infty}\sum_{n=-\infty}^{\infty} \exp\left[-\frac{1}{2\hbar}\big(Ql/D+mQ\big)^2\right] \exp\left[-\frac{1}{2\hbar}\big(Ql/D+nQ\big)^2\right]. \tag{4.38}$$

A quick comparison with Equation 4.22 shows that this equation is equal[5] to $\mathcal{N}$. Our final expression is

$$\sum_{l=0}^{D-1}\sum_{v=0}^{D-1} \langle e_j|a\rangle\langle a|e_k\rangle = \delta_{j,k}\; D. \tag{4.39}$$

Our proof is complete (as are the coherent states).

[5]Hence the keeping of the normalization constant in Equation 4.34. No approximations are necessary to make these states complete.

Equation summary for section 4.4

$$x_0 = \frac{Q}{D}(l+\beta)$$

$$p_0 = \frac{P}{D}(v+\alpha)$$

$$\frac{1}{D}\sum_{l=0}^{D-1}\sum_{v=0}^{D-1}|a\rangle\langle a| = \hat{1}$$

4.5 A Q-function for $\mathcal{H}_D$

Now that we have shown that this subset of coherent states is complete, we may use them to define a quasi-distribution function. In analogy to the continuous case, we define a finite-dimensional Q-function for a system with a density operator $\hat{\rho}$ by

$$Q(a) \equiv \frac{1}{D}\langle a|\hat{\rho}|a\rangle, \quad a = \left(\frac{l+\beta}{D}\right) + i\left(\frac{v+\alpha}{D}\right) \tag{4.40}$$

$l, v = 0, 1, \ldots, D-1$. This function is discrete with D^2 values.

Due to the completeness relation, the Q-function is normalized,

$$\sum_{l=0}^{D-1}\sum_{v=0}^{D-1} Q(a) = 1,$$

but as with the continuous case, the Q-function does not give the proper marginals. If we substitute the position[6] expansion of the density matrix,

$$\hat{\rho} = \sum_{j,k=0}^{D-1} \rho_{j,k}|e_j\rangle\langle e_k|,$$

[6]The momentum expansion for the density matrix would give similar results for the momentum marginal.

into Equation 4.40 and use the expression for the coherent state, we find that

$$\begin{aligned} Q(a) = \frac{1}{D}\sqrt{\frac{2Q}{DP}} \sum_{j,k=0}^{D-1} \sum_{m,n=-\infty}^{\infty} \rho_{j,k} \exp\left[-\frac{1}{2\hbar}\big(Q(j-l)/D + mQ\big)^2\right] \\ \times \exp\left[-\frac{1}{2\hbar}\big(Q(k-l)/D + nQ\big)^2\right] \exp\left[\frac{2\pi i}{D}(k-j)(v+\alpha)\right]. \end{aligned} \tag{4.41}$$

If this quasi-distribution was like the Wigner function, summing over the variable v would create the position marginal probability distribution. Instead, we find after using[7] Equation 2.26,

$$\begin{aligned} \sum_{v=0}^{D-1} Q(a) = \sqrt{\frac{2Q}{DP}} \sum_{j=0}^{D-1} \sum_{m,n=-\infty}^{\infty} \rho_{j,j} \exp\left[-\frac{1}{2\hbar}\big(Q(j-l)/D + mQ\big)^2\right] \\ \times \exp\left[-\frac{1}{2\hbar}\big(Q(j-l)/D + nQ\big)^2\right]. \end{aligned} \tag{4.42}$$

No further simplifications are possible. We find the discrete analog of the continuous result that instead of the marginal, we have a Gaussian convolution of the density matrix.

Figures 4.3 and 4.4 show the Q-function for different systems. Its usefulness lies in it giving an idea of what the system "looks like." We see that the position and momentum states behave as expected: localized in one variable while completely delocalized in the other. The Q-function for a coherent state (Figure 4.5) is a Gaussian centered at the point $[x_0, p_0]$. Comparing the Q-function with the Wigner function for such states (Figure 4.1), we see that the Q-function lacks the interference terms found in the Wigner function, making interpretation easier.

As a final note, we see that even though the subset of D^2 coherent states is complete, it is possible to include more coherent states for the purpose of creating plots with greater detail. Figure 4.6 shows the two Q-functions for the squeezed

[7]Here, as before, the restricted values of j and k make the sum over Kronecker-delta functions unnecessary

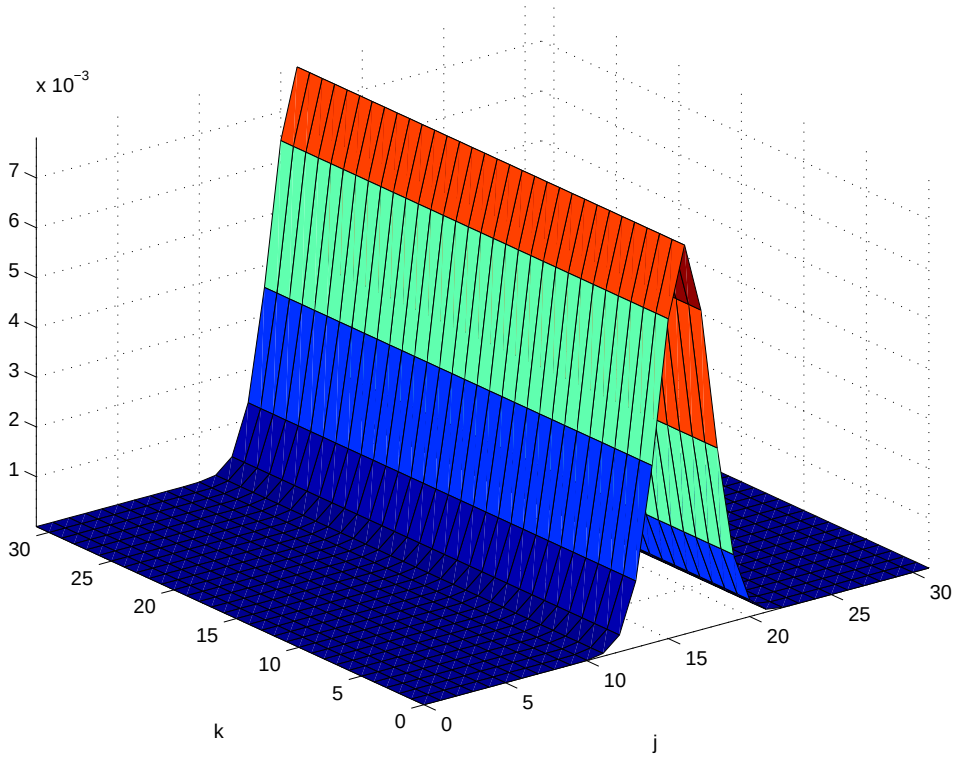

Figure 4.3: The Q-function of the $\left|e_{16}\right\rangle$ position eigenstate in $D = 32$ dimensions with periodic boundary conditions plotted as a function of $x_0 = j/D$, $p_0 = k/D$.

state[8] centered at $\sigma = 1/2 + i/2$ with squeezing parameters $r = 1$, $\phi = \pi/4$. The first plot has dimension $D \times D$, the other has $2D \times 2D$. The greater number of points helps fill in the shape of the squeezed state. Since Equation 4.27 is not applicable, care must be taken to normalize these extra coherent states and the resultant quasi-distribution numerically, but the increase in detail helps "round out" the squeezed state's features.

[8]These discrete analogs of the continuous squeezed states along with their parameters will be introduced in the next section.

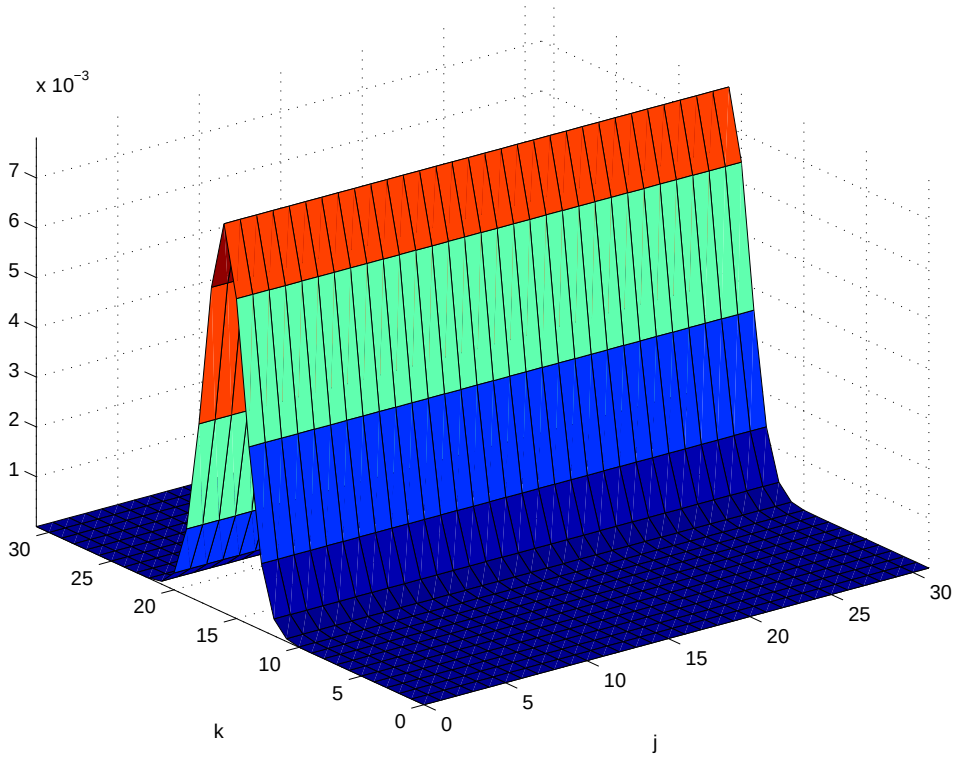

Figure 4.4: The Q-function of the $\left|p_{16}\right\rangle$ momentum eigenstate in $D = 32$ dimensions with periodic boundary conditions; $x_0 = j/D$, $p_0 = k/D$.

4.5.1 Symmetry properties of the Q-function

As was the case for the Wigner function, we would like the Q-function to have a geometrical interpretation in phase space. Writing Equation 4.40 as

$$Q(a) = \frac{1}{D}\mathrm{tr}\left(\hat{\rho}\left|a\right\rangle\left\langle a\right|\right), \tag{4.43}$$

we see the analogous relation between the Wigner function's $\hat{A}_{M/2,S/2}$ operator and the Q-function's $\left|a\right\rangle\left\langle a\right|$ operator.

For later comparison, we write the position representation of the operator $\left|a\right\rangle\left\langle a\right|$

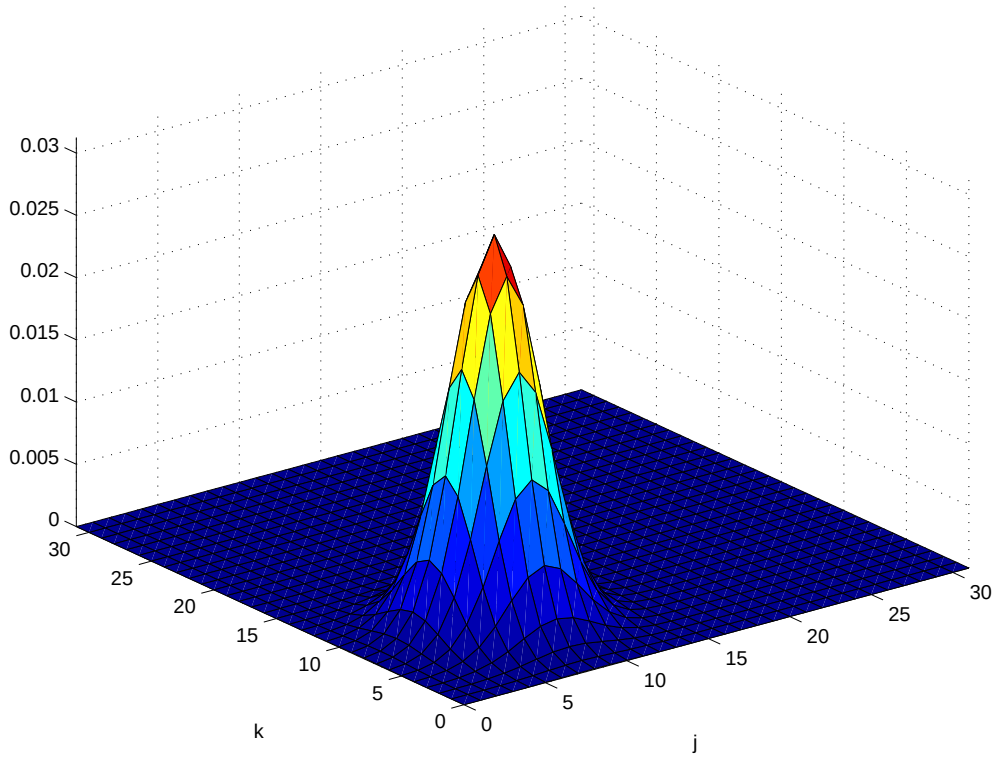

Figure 4.5: The Q-function of the coherent state centered at $a = 1/4 + i/4$ in $D = 32$ dimensions with periodic boundary conditions; $x_0 = j/D$, $p_0 = k/D$.

using Equation 4.2,

$$\langle e_j|a\rangle\langle a|e_k\rangle = \frac{1}{\mathcal{N}} \sum_{m,n=-\infty}^{\infty} \exp\left[-\frac{1}{2\hbar}\left(e_j - x_0 + mQ\right)^2\right] \exp\left[-\frac{1}{2\hbar}\left(e_k - x_0 + nQ\right)^2\right] \times \exp\left[\frac{i}{\hbar}\left(e_j - e_k + (m-n)Q\right)p_0\right] \exp\left[-2\pi i(m-n)\alpha\right]. \tag{4.44}$$

Here we have used the more general Equation 4.2 instead of Equation 4.29 to show that these symmetry properties hold for all x_0 and p_0 values.

Using Equation 4.3, we quickly see that the Q-function has displacement sym-

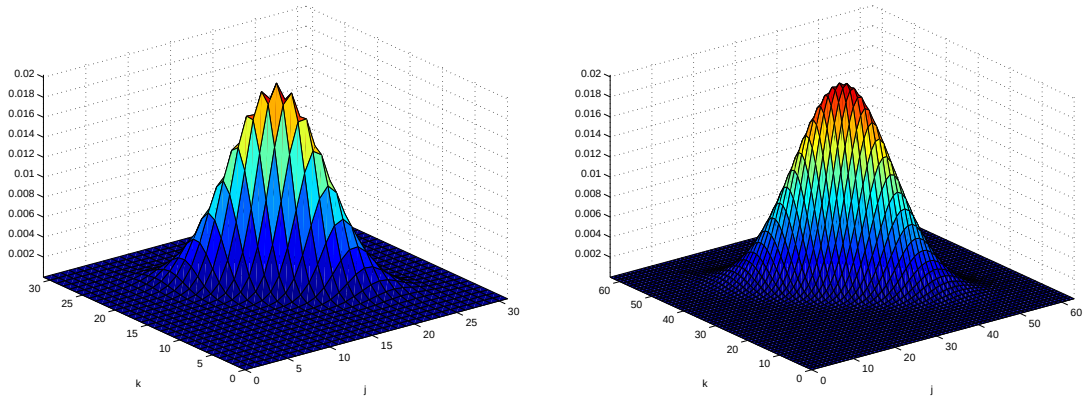

Figure 4.6: Two Q-functions of the $\sigma = 1/2 + i/2$ squeezed state with squeezing parameters $r = 1$, $\phi = \pi/4$. The second plot shows the increase of detail obtained by using more than the required D^2 points.

metry,

$$\begin{aligned} \big|a+Q\big\rangle\big\langle a+Q\big| &= \big|a\big\rangle\big\langle a\big| \\ \big|a+iP\big\rangle\big\langle a+iP\big| &= \big|a\big\rangle\big\langle a\big|. \end{aligned} \tag{4.45}$$

As was already mentioned when finding the momentum representation of the coherent state, this Q-function behaves correctly under Fourier transform when Q and P are equal. We see that

$$\big\langle e_j\big|\hat{F}^\dagger\big|a\big\rangle\big\langle a\big|\hat{F}\big|e_k\big\rangle = \big\langle p_j\big|a\big\rangle\big\langle a\big|p_k\big\rangle. \tag{4.46}$$

Using Equation 4.14, we have that

$$\begin{aligned} \big\langle p_j\big|a\big\rangle\big\langle a\big|p_k\big\rangle = \frac{1}{\mathcal{N}} \sum_{m,n=-\infty}^{\infty} &\exp\left[-\frac{1}{2\hbar}\left(p_j - p_0 + mP\right)^2\right] \exp\left[-\frac{1}{2\hbar}\left(p_k - p_0 + nP\right)^2\right] \\ &\times \exp\left[-\frac{i}{\hbar}\left(p_j - p_k + (m-n)P\right)x_0\right] \exp\left[2\pi i(m-n)\beta\right]. \end{aligned} \tag{4.47}$$

The Fourier transform operator has a 90° phase space rotation interpretation for

periodic, $\alpha = \beta = 0$ and anti-periodic, $\alpha = \beta = 1/2$ boundary conditions; thus,

$$\exp\left[2\pi i(m-n)\beta\right] = \exp\left[-2\pi i(m-n)\alpha\right].$$

Remembering that $Q = P$ implies that $p_k = e_k$, such that when we compare this expression with Equation 4.44, we see that our Q-function has the proper Fourier behavior,

$$x_0 \to p_0, \qquad p_0 \to -x_0.$$

Finally, we see that time reversal also behaves properly,

$$\begin{aligned}\left\langle e_j\middle|\hat{T}^\dagger\middle|a\right\rangle\left\langle a\middle|\hat{T}\middle|e_k\right\rangle = \frac{1}{\mathcal{N}}\sum_{m=-\infty}^{\infty}\sum_{n=-\infty}^{\infty}&\exp\left[-\frac{1}{2\hbar}\left(e_j - x_0 + mQ\right)^2\right]\\ &\times\exp\left[-\frac{1}{2\hbar}\left(e_k - x_0 + nQ\right)^2\right]\\ &\times\exp\left[-\frac{i}{\hbar}\left(e_j - e_k + (m-n)Q\right)p_0\right]\exp\left[2\pi i(m-n)\alpha\right].\end{aligned} \tag{4.48}$$

Time reversal has a phase space interpretation when 2α is an integer; therefore, we have that

$$\exp\left[2\pi i(m-n)\alpha\right] = \exp\left[-2\pi i(m-n)\alpha\right].$$

Hence, under time reversal the state center at $a = x_0 + ip_0$ goes to the state $a' = x_0 - ip_0$ which is the proper behavior.

Without much fuss, the Q-function defined through the use of the periodically continued coherent states obeys all symmetry properties[9]. This property alone makes these coherent states special. As we saw with the finite-dimensional Wigner function, it's not always easy to find such accommodating states.

[9]The reader is reminded that all symmetry operations can be written in terms of the displacement, Fourier transform, and time reversal operators. See Table 2.1 for details.

Equation summary for section 4.5

$$Q(a) \equiv \frac{1}{D}\left\langle a\middle|\hat{\rho}\middle|a\right\rangle, \quad a = \left(\frac{l+\beta}{D}\right) + i\left(\frac{v+\alpha}{D}\right)$$

$$Q(a) = \frac{1}{D}\mathrm{tr}\left(\hat{\rho}\left|a\right\rangle\left\langle a\right|\right)$$

$$\left|a+Q\right\rangle\left\langle a+Q\right| = \left|a\right\rangle\left\langle a\right|$$

$$\left|a+iP\right\rangle\left\langle a+iP\right| = \left|a\right\rangle\left\langle a\right|$$

$$\hat{F}\left|x_0+ip_0\right\rangle\left\langle x_0+ip_0\right|\hat{F}^\dagger = \left|p_0-ix_0\right\rangle\left\langle p_0-ix_0\right|$$

$$\hat{T}\left|x_0+ip_0\right\rangle\left\langle x_0+ip_0\right|\hat{T}^\dagger = \left|x_0-ip_0\right\rangle\left\langle x_0-ip_0\right|$$

4.6 Squeezed states for finite dimensions

Given the success of periodically continuing the standard Weyl coherent states, it seems natural to question whether there are other states which could be periodically continued to create finite-dimensional analogies.

An obvious choice would be the squeezed states. They have a position representation,

$$\left\langle x\middle|\sigma\right\rangle = \left(\frac{\gamma}{\pi\hbar}\right)^{1/4}\exp\left[-\frac{\gamma}{2\hbar}\left(x-x_0\right)^2\right]\exp\left[\frac{i}{\hbar}xp_0\right]\exp\left[-\frac{i}{2\hbar}x_0p_0\right], \tag{4.49}$$

where

$$\gamma = \frac{\cosh r + \exp\left[2i\phi\right]\sinh r}{\cosh r - \exp\left[2i\phi\right]\sinh r}$$

is a constant determined by the squeezing parameter $r \geq 0$ and rotation angle $0 \leq \phi \leq \pi$. To ensure a valid wave function, the constant γ is such that

$$\text{Re}\,(\gamma) = \frac{2}{(\cosh r + \sinh r)^2 - 4\cosh r \sinh r \cos^2\phi} \tag{4.50}$$

is always positive; the Gaussian never diverges.

The coherent states re-emerge when $r = 0$, *i.e.* when there is no squeezing. In the infinite squeezing limit,

$$\gamma \to \frac{i\cos\phi}{\sin\phi} = i\cot\phi. \tag{4.51}$$

An unrotated state with $\phi = 0$ causes the Gaussian to become a Dirac-delta function[10]. Our squeezed state becomes

$$\begin{aligned} \big|\sigma\big\rangle &= \int_{-\infty}^{\infty} dx\, \big|x\big\rangle \delta(x - x_0) \exp\left[\frac{i}{\hbar} x p_0\right] \exp\left[-\frac{i}{2\hbar} x_0 p_0\right] \\ &= \exp\left[\frac{i}{2\hbar} x_0 p_0\right] \big|x_0\big\rangle. \end{aligned} \tag{4.52}$$

We have a position eigenstate.

When $\phi = \pi/2$, $\gamma = 0$ thus causing the Gaussian to become unity. In this case, the squeezed state is

$$\begin{aligned} \big|\sigma\big\rangle &= (\pi\hbar)^{-1/4} \int_{-\infty}^{\infty} dx\, \big|x\big\rangle \exp\left[\frac{i}{\hbar} x p_0\right] \exp\left[-\frac{i}{2\hbar} x_0 p_0\right] \\ &= \exp\left[-\frac{i}{2\hbar} x_0 p_0\right] \big|p_0\big\rangle \end{aligned} \tag{4.53}$$

which is a momentum eigenstate.

[10]Technically, the square of the wavefunction has the correct Dirac-delta normalization, but the end result is the same.

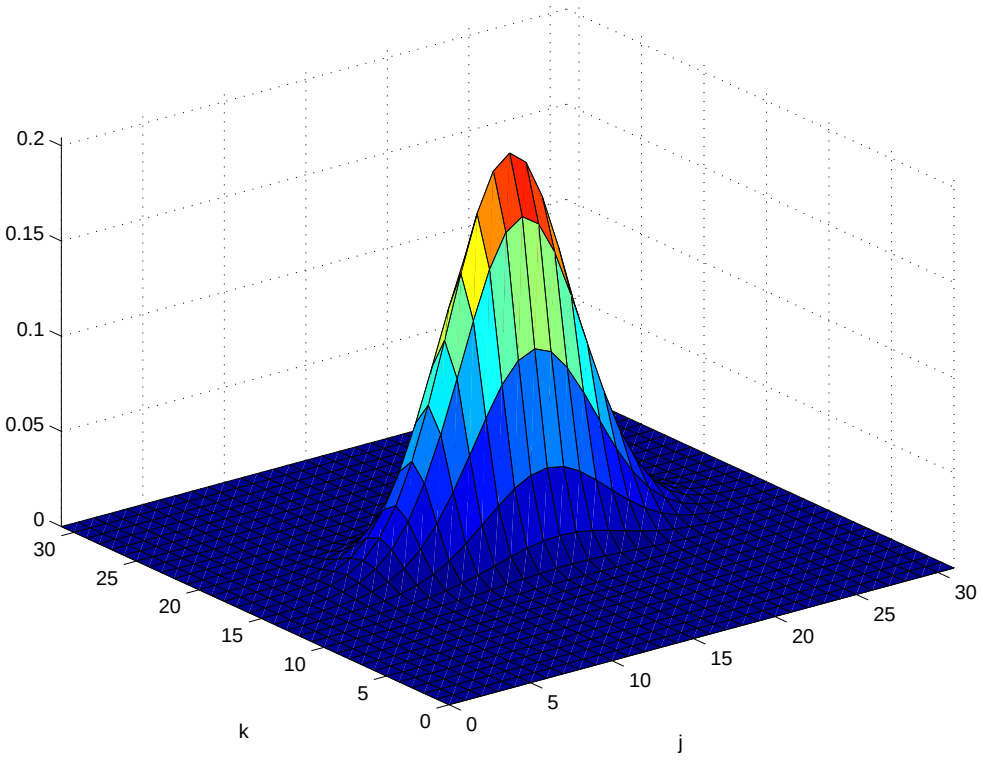

Figure 4.7: The Q-function of the $\sigma = 1/2 + i/2$ squeezed state with squeezing parameters $r = 0.75$, $\phi = \pi/2$ in $D = 32$ dimensions with periodic boundary conditions; $x_0 = j/D$, $p_0 = k/D$.

An analogous periodically continued squeezed state would be

$$\langle e_j|\sigma\rangle = \sqrt{\frac{1}{\mathcal{N}}} \sum_{m=-\infty}^{\infty} \exp\left[-\frac{\gamma}{2\hbar}\left(e_j - x_0 + mQ\right)^2\right] \exp\left[\frac{i}{\hbar}\left(e_j + mQ\right)p_0\right] \times \exp\left[-\frac{i}{2\hbar}x_0 p_0\right] \exp\left[-2\pi i m\alpha\right] \tag{4.54}$$

where γ has the same definition as in the continuous case and $\sigma = x_0 + ip_0$. As would

be expected, these states have the same periodicity as the coherent states

$$\begin{aligned}\langle e_{j+D}|\sigma\rangle &= \exp\left[2\pi i\alpha\right]\langle e_j|\sigma\rangle,\\ |\sigma+Q\rangle &= \exp\left[\pi i D\frac{p_0}{P}\right]\exp\left[-2\pi i\alpha\right]|\sigma\rangle,\\ |\sigma+iP\rangle &= \exp\left[-\pi i D\frac{x_0}{Q}\right]\exp\left[2\pi i\beta\right]|\sigma\rangle.\end{aligned} \tag{4.55}$$

As with the continuous case, our periodically continued coherent states are recovered when $r = 0$. In the large squeezing limit, we find that not all analogies with the continuous case survive. When $\phi = \pi/2$ such that $\gamma = 0$, we, in some cases, can still recover a momentum eigenstate. We have that

$$|\sigma\rangle = \sqrt{\frac{1}{\mathcal{N}'}}\sum_{j=0}^{D-1}\sum_{m=-\infty}^{\infty}|e_j\rangle\exp\left[\frac{i}{\hbar}\left(e_j+mQ\right)p_0\right]\exp\left[-\frac{i}{2\hbar}x_0p_0\right]\exp\left[-2\pi im\alpha\right]. \tag{4.56}$$

If we make an obvious guess and take $p_0 = P(v+\alpha)/D$, we have[11]

$$\begin{aligned}|\sigma\rangle &= \sqrt{\frac{1}{D}}\sum_{j=0}^{D-1}|e_j\rangle\exp\left[\frac{2\pi i}{D}(v+\alpha)(j+\beta)\right]\exp\left[-\frac{i}{2\hbar}x_0p_0\right]\\ &= \exp\left[-\frac{i}{2\hbar}x_0p_0\right]|p_0\rangle.\end{aligned} \tag{4.57}$$

Other choices for p_0 lead to states that are not momentum eigenstates.

For $\phi = 0$ in the large squeezing limit, *i.e.* when γ approaches infinity, our Gaussian becomes zero unless[12] $e_j = x_0$ and $m = 0$. The only way for e_j and x_0 to be equal is for $x_0 = (l+\beta)/D$. In which case,

$$|\sigma\rangle = \exp\left[\frac{i}{2\hbar}x_0p_0\right]|x_0\rangle. \tag{4.58}$$

[11] It has not been shown, but one can easily derive that $\mathcal{N}' = D$ for this choice of p_0.

[12] Given that we have a periodically continued Gaussian, anytime $x_0 = e_j + nQ$ for any integer n will produce a non-zero result as well, but let's stick to the fiducial rectangle.

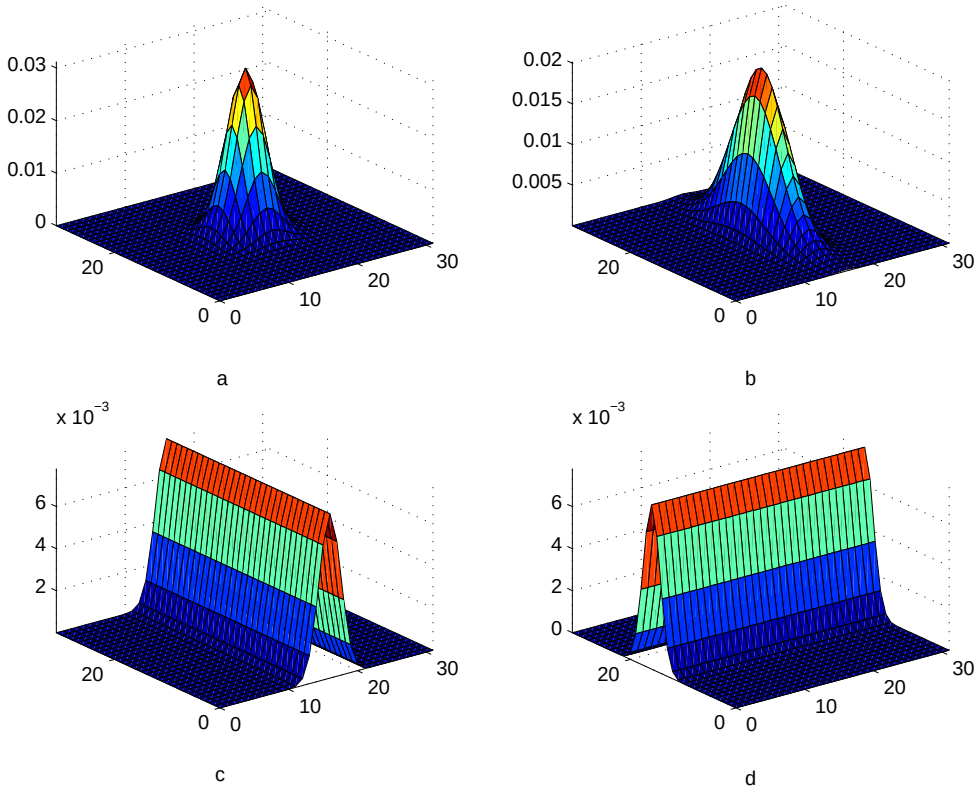

Figure 4.8: The Q-functions for the state $\sigma = 1/2 + i/2$ for increasing squeezing parameter. For large squeezing and specially chosen σ, we recover (c) position and (d) momentum eigenstates.

In summary, we find that for large squeezing, we can recover position and momentum eigenstates, but only for the special subset of Equation 4.18. Figure 4.8 demonstrates the eigenstate recovery, Plot a: the Q-function for an initially unsqueezed, $r = 0$ coherent state centered at one of the special points, $a = 1/2 + i/2$. Plot b: with the increase of the parameter r to $r = 1$ $\phi = 0$, the Q-function demonstrates the characteristic elongation of a squeezed state. Plot c: setting $r = 10$, $\phi = 0$, provides enough squeezing to create a position eigenstate thus verifying our position eigenstate recovery statement. Plot d: Setting $\phi = \pi/2$ with $r = 10$ rotates the position eigenstate to a momentum eigenstate. Figure 4.9 shows the periodic boundary condition

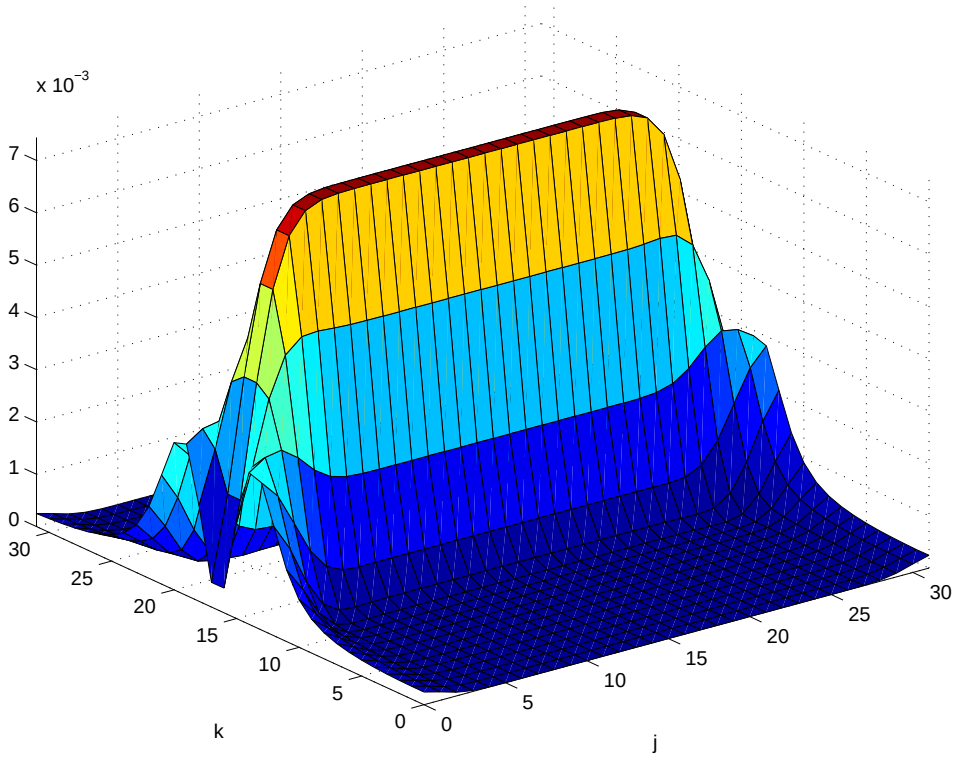

Figure 4.9: The Q-function for a $\phi = \pi/2$ squeezed state centered at a point not in the special subset of Equation 4.18; it is not a momentum eigenstate.

Q-function of the non-special subset $\phi = \pi/2$ squeezed state $\sigma = 1/2 + i/2 + i/(2D)$. While having characteristics similar to a momentum eigenstate, this function is not a momentum eigenstate. The Q-function for a state centered at a non-special position value in the large squeezing limit is not shown since given the argument above, it is trivially zero valued everywhere.

The various Figures 4.6, 4.7, and 4.8 have shown the Q-function for these squeezed states. As desired, these states have the same characteristics as their continuous counterparts. As the squeezing parameter increases, the states' variance changes. We also see that as the angle ϕ is changed, the states have a corresponding rotation.

Even more exciting than these states behaving "correctly" is the fact that they also can be used to define a quasi-distribution function. If one uses the subset defined in Equation 4.18,

$$\begin{aligned} x_0 &= \frac{Q}{D}(l+\beta) \\ p_0 &= \frac{P}{D}(v+\beta), \end{aligned} \tag{4.59}$$

and substitutes it into Equation 4.55, then

$$\begin{aligned} \langle e_j|\sigma\rangle = \sum_{m=-\infty}^{\infty} \sqrt{\frac{1}{\mathcal{N}}} \exp\left[-\frac{\gamma}{2\hbar}\left(\frac{Q}{D}(j-l)+mQ\right)^2\right] \exp\left[\frac{2\pi i}{D}(v+\alpha)(j+\beta)\right] \\ \times \exp\left[-\frac{\pi i}{D}(l+\beta)(v+\alpha)\right]. \end{aligned} \tag{4.60}$$

It can be shown that

$$\frac{1}{D}\sum_{l,v=0}^{D-1} |\sigma\rangle\langle\sigma| = \hat{1}. \tag{4.61}$$

One way of proving this fact follows the coherent state case exactly. We look at the position representation matrix element

$$\begin{aligned} \sum_{l,v=0}^{D-1} \langle e_j|\sigma\rangle\langle\sigma|e_k\rangle = \sum_{j=0}^{D-1}\sum_{m,n=-\infty}^{\infty} \frac{1}{\mathcal{N}} \exp\left[-\frac{\gamma}{2\hbar}\left(\frac{Q}{D}(j-l)+mQ\right)^2\right] \\ \times \exp\left[-\frac{\gamma}{2\hbar}\left(\frac{Q}{D}(k-l)+mQ\right)^2\right] \sum_{v=0}^{D-1} \exp\left[\frac{2\pi i}{D}(v+\alpha)(j-k)\right]. \end{aligned} \tag{4.62}$$

As was the case previously, Equation 2.26 gives that the sum over v is $D\delta_{j,k}$; therefore,

$$\begin{aligned} \sum_{l,v=0}^{D-1} \langle e_j|\sigma\rangle\langle\sigma|e_k\rangle &= \delta_{j,k}\sum_{j=0}^{D-1}\sum_{m,n=-\infty}^{\infty} \frac{D}{\mathcal{N}} \exp\left[-\frac{\gamma}{2\hbar}\left(\frac{Q}{D}(j-l)+mQ\right)^2\right] \\ &\quad \times \exp\left[-\frac{\gamma}{2\hbar}\left(\frac{Q}{D}(j-l)+mQ\right)^2\right] \\ &= D\,\frac{\mathcal{N}}{\mathcal{N}}\,\delta_{j,k}. \end{aligned} \tag{4.63}$$

Alternatively, one could look deeper into the states' creation for a proof of their completeness. In the continuous phase space, Perelomov has generalized the coherent states definition to ones created by the displacement of a fiducial state about phase space [35]. The Weyl coherent states' fiducial function is a Gaussian. Likewise, our grid of D^2 coherent or squeezed states can be created by a displacement operator,[13]

$$\hat{D}_{l,v} = \exp\left[\frac{\pi i}{D} lv\right] \exp\left[\frac{\pi i}{D}\left(l\alpha - v\beta\right)\right] \hat{V}^l \hat{U}^v, \tag{4.64}$$

acting upon the fiducial state $\big|0\big\rangle$ whose definition is

$$\big\langle e_j\big|0\big\rangle = \frac{1}{\mathcal{N}} \sum_{m=-\infty}^{\infty} \exp\left[-\frac{\gamma}{2\hbar}\left(\frac{Q}{D} j + mQ\right)^2\right] \exp\left[\frac{2\pi i}{D}\left(j+\beta\right)\alpha\right] \exp\left[-\frac{\pi i}{D}\alpha\beta\right]. \tag{4.65}$$

This operator is a slightly modified version of Equation 2.19, the symmetric displacement operator $\hat{B}_{l,v} = \exp\left[-\pi i \left(l\alpha - v\beta\right)/D\right] \hat{D}_{l,v}$ of section 2.1.2. The modification is necessary to create the $\exp\left[-ix_0 p_0/2\hbar\right]$ term in our coherent ($\gamma = 1$) or squeezed state. It is easily seen that for any normalized fiducial state, the operator $\sum_{l,v=0}^{D-1} \hat{D}_{l,v}\big|0\big\rangle\big\langle 0\big|\hat{D}_{l,v}^{\dagger}$ always resolves the identity,

$$\begin{aligned}
\sum_{l,v=0}^{D-1} \big\langle e_j\big|\hat{D}_{l,v}\big|0\big\rangle\big\langle 0\big|\hat{D}_{l,v}^{\dagger}\big|e_k\big\rangle &= \sum_{v=0}^{D-1} \exp\left[\frac{2\pi i}{D} v\left(j-k\right)\right] \sum_{l=0}^{D-1} \big\langle e_{j-l}\big|0\big\rangle\big\langle 0\big|e_{k-l}\big\rangle \\
&= D\,\delta_{j,k} \sum_{l=0}^{D-1} \big\langle 0\big|e_{j-l}\big\rangle\big\langle e_{j-l}\big|0\big\rangle \\
&= D\,\delta_{j,k}\,\big\langle 0\big|0\big\rangle = D\,\delta_{j,k}.
\end{aligned} \tag{4.66}$$

It is neither mysterious nor surprising that both the coherent and squeezed states can define a quasi-distribution function.

In the continuous case, the squeezed states can also be used to define a probability distribution. For that case, the distribution corresponds to a true probability.

[13] Please see the equation summary of section 2.1.2 for the action of the displacement operators $\hat{U}$ and $\hat{V}$.

It corresponds to a simultaneous position and momentum measurement taken in the Arthurs-Kelly measurement model [73, 74, 75]. The ability of the discrete squeezed states to also define a Q-function may be a remnant of the continuous form used in their definition. Alternatively, it may be that there is a discrete analog to the Arthurs-Kelly measurement model which enables them to define a Q-function. Obviously, one could use these operators to define a POVM and therefore a measurement model; however, given that position and momentum are not defined in $\mathcal{H}_D$, it is uncertain if an interpretation of a discrete Arthurs-Kelly model could be rigorously upheld.

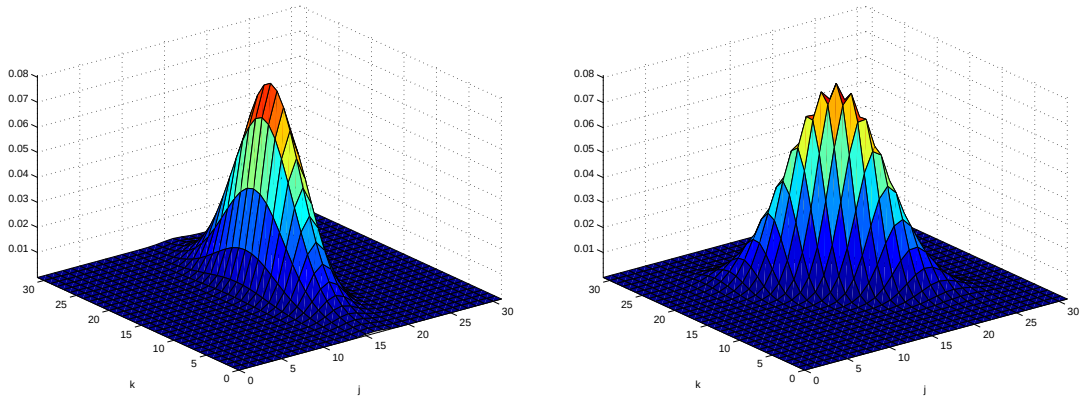

Figure 4.10: Two "squeezed" Q-functions, *i.e.* Q-functions defined using squeezed instead of coherent states, for the $a = 1/2+i/2$ **coherent** state. In this representation coherent states appear squeezed.

Figure 4.10 shows the "squeezed" Q-function representation of a coherent state using the squeezed states with parameters $r = 1$, $\phi = 0$ and $r = 1$, $\phi = \pi/4$ respectively. In this representation, coherent states appear squeezed. However, as Figure 4.11 shows, this characteristic is not reversible; the squeezed Q-function for a squeezed states is not symmetric even, as shown in the right hand side of Figure 4.11, when the same squeezed state is used for system and basis.

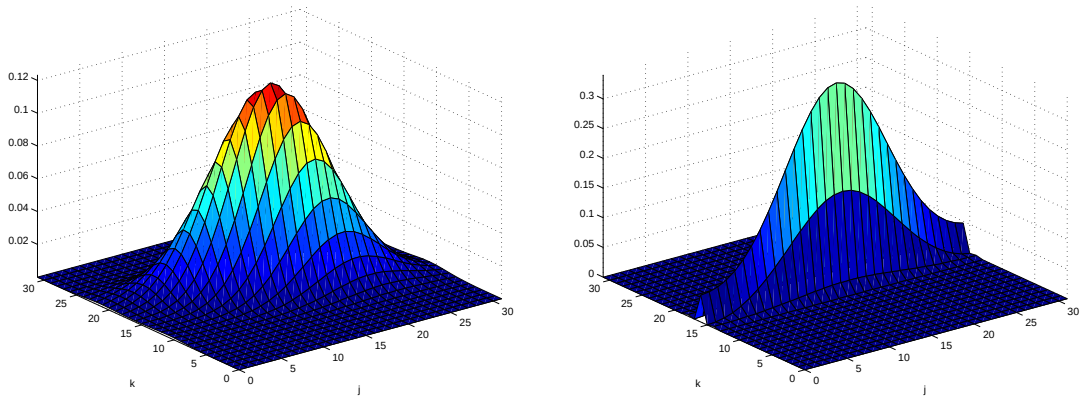

Figure 4.11: Two "squeezed" Q-functions for the $\sigma = 1/2 + i/2$ **squeezed** state $r = 1$, $\phi = \pi/2$ using basis states $r = 1$, $\phi = \pi/4$ and $r = 1$, $\phi = \pi/2$.

As with the coherent states, we can find a normalizing expression[14] analogous to Equation 4.27 for our squeezed states. Following the derivation for the coherent states, we find the obvious analogs for Equation 4.23

$$\begin{aligned} &\sum_{m=-\infty}^{\infty} \exp\left[-\frac{\gamma}{2\hbar}(Qj/D + mQ)^2\right] \\ &= \sqrt{\frac{P}{\gamma QD}} \sum_{r=-\infty}^{\infty} \exp\left[\frac{2\pi i}{D} jr\right] \exp\left[-\frac{1}{2\gamma\hbar}\left(\frac{Pr}{D}\right)^2\right] \end{aligned} \tag{4.67}$$

and Equation 4.26

$$\sum_{t=-\infty}^{\infty} \exp\left[-\frac{1}{\gamma\hbar}\left(\frac{Pt}{D} - \frac{Ps}{2}\right)^2\right] = \sqrt{\frac{QD\gamma}{2P}} \sum_{t'=-\infty}^{\infty} \exp\left[\pi i D t'\right] \exp\left[-\frac{1}{4\gamma\hbar}\left(Qt'\right)^2\right]. \tag{4.68}$$

We are left with a normalizing expression of

$$\mathcal{N} = \sqrt{\frac{DP}{2Q\gamma}} \sum_{s,t=-\infty}^{\infty} \exp\left[\pi i D s t\right] \exp\left[-\frac{1}{4\hbar}\left(\frac{1}{\gamma}(Ps)^2 + \gamma(Qt)^2\right)\right]. \tag{4.69}$$

Given that γ is continuously defined, it would be unwise try an approximation like the one used previously when finding $\mathcal{N}$ for the coherent states. We will note, however,

[14] Once again, we deal only with the special subset of states.

that a starting approximation to normalize the squeezed states would be

$$\mathcal{N} \sim \sqrt{\frac{DP}{2Q\gamma}}.$$

Equation summary for section 4.6

$$\gamma = \frac{\cosh r + \exp\left[2i\phi\right]\sinh r}{\cosh r - \exp\left[2i\phi\right]\sinh r}$$

$$\langle e_j|\sigma\rangle = \sqrt{\frac{1}{\mathcal{N}}}\sum_{m=-\infty}^{\infty}\exp\left[-\frac{\gamma}{2\hbar}\left(e_j - x_0 + mQ\right)^2\right]\exp\left[\frac{i}{\hbar}\left(e_j + mQ\right)p_0\right] \times \exp\left[-\frac{i}{2\hbar}x_0p_0\right]\exp\left[-2\pi i m\alpha\right]$$

$$\frac{1}{D}\sum_{l,v=0}^{D-1}|\sigma\rangle\langle\sigma| = 1$$

4.7 The relation between the Q and Wigner functions for finite dimensions

In this final section of this chapter, we shall find how the finite-dimensional Q-function and Wigner function are related. Along the way, we shall find how to express the density matrix in terms of the Wigner function. In the end, we shall find the amazing fact that the Q-function is a Gaussian convolution of the continuous Wigner function for a periodically continued state[15].

[15]It appears that this fact has been proven in Nonnenmacher [72]. Given this author's inaptitude with *la langue française*, it remains unverified.

We begin with the expression for the finite-dimensional Wigner function, Equation 3.45,

$$W_{M/2,S/2} = \frac{1}{2D}\sum_{j=0}^{D-1} \rho_{j,M-j}\ \exp\left[\frac{2\pi i}{D}(M-2j)(S/2+\alpha)\right] \tag{4.70}$$

where the reader is reminded that the indices, M and S, range from 0 to $2D-1$. We then find the following

$$\begin{aligned}\sum_{S=0}^{2D-1} W_{M/2,S/2} \exp\left[\frac{2\pi i}{D}\left(\frac{S}{2}+\alpha\right)k\right] = \frac{1}{2D}\sum_{j=0}^{D-1}\rho_{j,M-j}\exp\left[\frac{2\pi i}{D}\left(M-2j+k\right)\alpha\right] \\ \times \sum_{S=0}^{2D-1}\exp\left[\frac{2\pi i}{D}\left(\frac{M+k}{2}-j\right)S\right].\end{aligned} \tag{4.71}$$

The sum over S is similar to the one performed when finding the marginals of the Wigner function. We find that

$$\begin{aligned}&\sum_{S=0}^{2D-1}\exp\left[\frac{2\pi i}{D}\left(\frac{M+k}{2}-j\right)S\right] = \\ &\quad\begin{cases} 2\sum_{S=0}^{D-1}\exp\left[\frac{2\pi i}{D}\left(\frac{M+k}{2}-j\right)S\right], & \text{when } M+k \text{ is even,} \\ 0, & \text{when } M+k \text{ is odd.}\end{cases}\end{aligned} \tag{4.72}$$

When $M+k$ is even, we can apply Equation 2.26 to get a Kronecker-delta function[16] which simplifies our expression to

$$\sum_{S=0}^{2D-1} W_{M/2,S/2}\exp\left[\frac{2\pi i}{D}\left(\frac{S}{2}+\alpha\right)k\right] = \rho_{M/2+k/2,M/2-k/2}. \tag{4.73}$$

Given that

$$\hat{\rho} = \sum_{j,k}\rho_{j,k}\big|e_j\big\rangle\big\langle e_k\big|,$$

[16]Yet again, the sum over delta functions in Equation 2.26 is unimportant here. The sum creates terms which cancel each other.

we find that a density matrix can be written as

$$\hat{\rho} = \sum_{M,k} \sum_{S=0}^{2D-1} W_{M/2,S/2} \exp\left[\frac{2\pi i}{D}\left(\frac{S}{2}+\alpha\right)k\right] \left|e_{M/2+k/2}\right\rangle\!\left\langle e_{M/2-k/2}\right| \tag{4.74}$$

where the sums over M and k are performed such that the $M+k$ is even.

To simplify these sums, we shall introduce two new variables

$$\mu = \frac{M+k}{2}, \quad \nu = \frac{M-k}{2}$$

which range from 0 to $D-1$. Substituting them yields our final expression for the Wigner function expansion of the density matrix,

$$\hat{\rho} = \sum_{\mu,\nu=0}^{D-1} \sum_{S=0}^{2D-1} W_{(\mu+\nu)/2,S/2} \exp\left[\frac{2\pi i}{D}\left(\frac{S}{2}+\alpha\right)(\mu-\nu)\right] \left|e_{\mu}\right\rangle\!\left\langle e_{\nu}\right|. \tag{4.75}$$

Using Equations 4.40 and 4.75, we can now write our Q-function in terms of our Wigner function,

$$Q(a) = \frac{1}{D} \sum_{\mu,\nu=0}^{D-1} \sum_{S=0}^{2D-1} W_{(\mu+\nu)/2,S/2} \exp\left[\frac{2\pi i}{D}\left(\frac{S}{2}+\alpha\right)(\mu-\nu)\right] \left\langle a\middle|e_{\mu}\right\rangle\!\left\langle e_{\nu}\middle|a\right\rangle. \tag{4.76}$$

We shall use Equation 4.29 to find the inner products[17]. After a tiny bit of algebra, we find that

$$\begin{aligned} Q(a) = \sqrt{\frac{2Q}{DP}}\frac{1}{D} \sum_{\mu,\nu=0}^{D-1} \sum_{S=0}^{2D-1} \sum_{m,n=-\infty}^{\infty} W_{(\mu+\nu)/2,S/2} \exp\left[-\frac{1}{2\hbar}\big(Q(\mu-l)/D+mQ\big)^2\right] \\ \times \exp\left[-\frac{1}{2\hbar}\big(Q(\nu-l)/D+nQ\big)^2\right] \exp\left[\frac{2\pi i}{D}(\mu-\nu)(S/2-v)\right]. \end{aligned} \tag{4.77}$$

To further the calculation, we introduce another set of variables

$$\mu' = \mu+\nu, \quad \nu' = \mu-\nu$$

[17]The reader is reminded that our coherent states are centered at $x_0 = \frac{Q}{D}(l+\beta)$, $p_0 = \frac{P}{D}(v+\alpha)$.

which have values $0, 1, \ldots, 2D-1$. Substituting these new variables into the above Gaussians, we find, after many pages of algebraic simplification, a remarkable fact

$$\begin{aligned}
&\exp\left[-\frac{1}{2\hbar}\left(\frac{Q}{D}\Big(\mu-l\Big)+mQ\right)^2\right]\exp\left[-\frac{1}{2\hbar}\left(\frac{Q}{D}\Big(\nu-l\Big)+nQ\right)^2\right]\\
&=\exp\left[-\frac{1}{\hbar}\left(\frac{Q}{D}\Big(\frac{\mu'}{2}-l\Big)+Q\Big(\frac{m+n}{2}\Big)\right)^2\right]\exp\left[-\frac{1}{\hbar}\left(\frac{Q}{D}\frac{\nu'}{2}+Q\Big(\frac{m-n}{2}\Big)\right)^2\right].
\end{aligned} \tag{4.78}$$

Hence, we have

$$\begin{aligned}
Q(a)=\sqrt{\frac{2Q}{DP}}\frac{1}{D}\sum_{\mu',\nu'=0}^{2D-1}\sum_{S=0}^{2D-1}\sum_{m,n=-\infty}^{\infty}W_{\mu'/2,S/2}\,\exp\left[\frac{2\pi i}{D}\nu'(S/2-v)\right]\\
\times\exp\left[-\frac{1}{\hbar}\left(\frac{Q}{D}\frac{\nu'}{2}+Q\Big(\frac{m-n}{2}\Big)\right)^2-\frac{1}{\hbar}\left(\frac{Q}{D}\Big(\frac{\mu'}{2}-l\Big)+Q\Big(\frac{m+n}{2}\Big)\right)^2\right].
\end{aligned} \tag{4.79}$$

We now wish to define new variables for m and n, such that

$$m'=m+n,\quad n'=m-n.$$

We remember from the characteristic function calculation that such variables are parity related. When m' is even, n' must necessarily be even and *vice versa*. When m' is even, we write it as $m'=2\Upsilon$, $\Upsilon\in\mathcal{Z}$; likewise, $n'=2\Xi$, $\Xi\in\mathcal{Z}$. In this case, our Q-function is

$$\begin{aligned}
\sum_{\mu',\nu'=0}^{2D-1}\sum_{S=0}^{2D-1}\sum_{\Upsilon,\Xi=-\infty}^{\infty}W_{\mu'/2,S/2}\exp\left[-\frac{1}{\hbar}\left(\frac{Q}{D}\Big(\frac{\mu'}{2}-l\Big)+Q\Upsilon\right)^2\right]\\
\times\exp\left[-\frac{1}{\hbar}\left(\frac{Q}{D}\frac{\nu'}{2}+Q\Xi\right)^2\right]\exp\left[\frac{2\pi i}{D}\nu'(S/2-v)\right].
\end{aligned} \tag{4.80}$$

When m' and n' are odd, we write them as $m' = 2\Upsilon + 1$, $n' = 2\Xi + 1$ to give

$$\begin{aligned}\sum_{\mu',\nu'=0}^{2D-1}\sum_{S=0}^{2D-1}\sum_{\Upsilon,\Xi=-\infty}^{\infty} W_{\mu'/2,S/2}\exp\left[-\frac{1}{\hbar}\left(\frac{Q}{D}\left(\frac{\mu'+D}{2}-l\right)+Q\Upsilon\right)^2\right] \\ \times\exp\left[-\frac{1}{\hbar}\left(\frac{Q}{D}\left(\frac{\nu'+D}{2}\right)+Q\Xi\right)^2\right]\exp\left[\frac{2\pi i}{D}\nu'(S/2-v)\right]\end{aligned} \tag{4.81}$$

where we have combined the extra terms with μ' and ν'.

Here we consider making yet another variable change

$$\mu'' = \mu' + D, \quad \nu'' = \mu' + D$$

to simplify the Gaussians above. Inserting these variables makes three important changes. First, the summation limits change

$$\sum_{\mu',\nu'}^{2D-1} f(\mu',\nu') = \sum_{\mu'',\nu''=D}^{3D-1} f(\mu'',\nu'');$$

second, the Wigner function index changes

$$W_{\mu'/2,S/2} = W_{\mu''/2-D/2,S/2} = (-1)^S W_{\mu''/2,S/2};$$

and third, the Fourier component changes

$$\begin{aligned}\exp\left[\frac{2\pi i}{D}\nu'(S/2-v)\right] &= \exp\left[\frac{2\pi i}{D}(\nu''-D)(S/2-v)\right] \\ &= (-1)^S\exp\left[\frac{2\pi i}{D}\nu''(S/2-v)\right].\end{aligned}$$

Obviously, the two factors $(-1)^S$ cancel; we are left with

$$\begin{aligned}\sum_{\mu'',\nu''=D}^{3D-1}\sum_{S=0}^{2D-1}\sum_{\Upsilon,\Xi=-\infty}^{\infty} W_{\mu''/2,S/2}\exp\left[-\frac{1}{\hbar}\left(\frac{Q}{D}\left(\frac{\mu''}{2}-l\right)+Q\Upsilon\right)^2\right] \\ \times\exp\left[-\frac{1}{\hbar}\left(\frac{Q}{D}\frac{\nu''}{2}+Q\Xi\right)^2\right]\exp\left[\frac{2\pi i}{D}\nu''(S/2-v)\right].\end{aligned} \tag{4.82}$$

Next, we realize that the sums over μ'' and ν'' can be renumbered with impunity. We see that

$$\sum_{\mu''=D}^{3D-1} = \sum_{\mu''=D}^{2D-1} + \sum_{\mu''=2D}^{3D-1}.$$

For the second term, we set $\mu''' = \mu'' - 2D$. The periodicity of the Wigner function and the periodic continuation of the first Gaussian ensures that our expression remains unchanged. A similar treatment for the sum over ν'' gives similar results; therefore, when m' and n' are odd, we have

$$\begin{aligned}\sum_{\mu',\nu'=0}^{2D-1}\sum_{S=0}^{2D-1}\sum_{\Upsilon,\Xi=-\infty}^{\infty} W_{\mu'/2,S/2}\exp\left[-\frac{1}{\hbar}\left(\frac{Q}{D}\left(\frac{\mu'}{2}-l\right)+Q\Upsilon\right)^2\right] \\ \times\exp\left[-\frac{1}{\hbar}\left(\frac{Q}{D}\frac{\nu'}{2}+Q\Xi\right)^2\right]\exp\left[\frac{2\pi i}{D}\nu'(S/2-v)\right].\end{aligned} \tag{4.83}$$

This is exactly what we had when m' and n' were even, so the sums can be recombined. Our Q-function is

$$\begin{aligned}Q(a) = \sqrt{\frac{2Q}{DP}}\frac{1}{D}\sum_{\mu',\nu'=0}^{2D-1}\sum_{S=0}^{2D-1}\sum_{\Upsilon,\Xi=-\infty}^{\infty} W_{\mu'/2,S/2}\exp\left[-\frac{1}{\hbar}\left(\frac{Q}{D}\left(\frac{\mu'}{2}-l\right)+Q\Upsilon\right)^2\right] \\ \times\exp\left[-\frac{1}{\hbar}\left(\frac{Q}{D}\frac{\nu'}{2}+Q\Xi\right)^2\right]\exp\left[\frac{2\pi i}{D}\nu'(S/2-v)\right].\end{aligned} \tag{4.84}$$

Finally, we use the same technique for finding Equation 4.23 to rewrite the second Gaussian as

$$\begin{aligned}\sum_{\Xi=-\infty}^{\infty}\exp\left[-\frac{1}{\hbar}\left(\frac{Q}{D}\frac{\nu'}{2}+Q\Xi\right)^2\right] \\ = \sqrt{\frac{P}{2QD}}\sum_{r=-\infty}^{\infty}\exp\left[\frac{2\pi i}{D}r\frac{\nu'}{2}\right]\exp\left[-\frac{1}{4\hbar}(Pr/D)^2\right].\end{aligned} \tag{4.85}$$

Combining this expression with the Fourier term from Equation 4.84, we have

the sum

$$\sum_{\nu'=0}^{2D-1} \exp\left[\frac{2\pi i}{D}\nu'\Big(\frac{r+S}{2}-v\Big)\right] = \begin{cases} 2D\sum_{t=-\infty}^{\infty}\delta_{r/2+S/2-v,tD}, & \text{when } r+S \text{ is even,} \\ 0, & \text{when } r+S \text{ is odd.} \end{cases} \tag{4.86}$$

Substituting for r into the above expression[18], we get our final expression

$$\begin{aligned} Q(a) = \frac{2}{D}\sum_{\mu',S=0}^{2D-1}\sum_{\Upsilon,t=-\infty}^{\infty} W_{\mu'/2,S/2}\exp\left[-\frac{1}{\hbar}\Big(\frac{Q}{D}\Big(\frac{\mu'}{2}-l\Big)+\Upsilon Q\Big)^2\right] \\ \times\exp\left[-\frac{1}{\hbar}\Big(\frac{P}{D}\Big(\frac{S}{2}-v\Big)+tP\Big)^2\right]. \end{aligned} \tag{4.87}$$

Rewriting it slightly, we have

$$\begin{aligned} Q(a) = \frac{2}{D}\sum_{M,S=0}^{2D-1}\sum_{m,n=-\infty}^{\infty} W_{M/2,S/2}\exp\left[-\frac{1}{\hbar}\big(e_{M/2}-x_0+mQ\big)^2\right] \\ \times\exp\left[-\frac{1}{\hbar}\big(p_{S/2}-p_0+nP\big)^2\right] \end{aligned} \tag{4.88}$$

which is the discrete analog of the fact the Q-function is the Gaussian convolution of the Wigner function.

Even more remarkable is the relation between Equation 4.88 and the Wigner function for a doubly periodic state. As stated before, the continuous Q and Wigner function are related by the Gaussian convolution,

$$Q(x_0,p_0) = \frac{1}{\pi\hbar}\int_{-\infty}^{\infty} dqdp\, W(q,p)\exp\left[-\frac{1}{\hbar}(q-x_0)^2\right]\exp\left[-\frac{1}{\hbar}(p-p_0)^2\right]. \tag{4.89}$$

To derive our expression for the discrete Wigner function, we used the natural relationship between the discrete Hilbert space $\mathcal{H}_D$ and the space of doubly-periodic

[18]Actually, to enforce the $r+S$ even restriction, we have to break the sums into their two non-zero pieces: $\sum_{r=even}\sum_{S=even}+\sum_{r=odd}\sum_{S=odd}$. For each piece, we substitute for r; the net result is a straight substitution for r.

wavefunctions. During the course of our derivation, we found the expression for the Wigner function of a state that is doubly-periodic. It is given by Equation 3.44,

$$W(q,p) = \sum_{S,M=-\infty}^{\infty} W_{M/2,S/2}\, \delta\left(q - \frac{Q}{D}\left(M/2+\beta\right)\right) \delta\left(p - \frac{P}{D}\left(S/2+\alpha\right)\right) \tag{4.90}$$

where $W_{M/2,S/2}$ is the expression used for the finite-dimensional Wigner function.

Using the periodicity of the finite Wigner function, we can write this as

$$W(q,p) = \sum_{M,S=0}^{2D-1} \sum_{m,n=-\infty}^{\infty} W_{M/2,S/2} \delta\left(q - e_{M/2} + mQ\right) \delta\left(p - p_{S/2} + nP\right). \tag{4.91}$$

Inserting this Wigner function into the Gaussian convolution expression, we find the expression for a doubly periodic state's Q-function,

$$\begin{aligned} Q(x_0,p_0) = \frac{1}{\pi\hbar} \sum_{M,S=0}^{2D-1} \sum_{m,n=-\infty}^{\infty} W_{M/2,S/2} \exp\left[-\frac{1}{\hbar}\left(e_{M/2} - x_0 + mQ\right)^2\right] \\ \times \exp\left[-\frac{1}{\hbar}\left(e_{S/2} - p_0 + nP\right)^2\right] \end{aligned} \tag{4.92}$$

which[19] is Equation 4.88.

We see that our choice of using the coherent states of Equation 4.29, which at first may have seemed a bit arbitrary, is instead the most natural ones to use. The coherent states give us a direct connection between the discrete and continuous Hilbert spaces.

[19] Aside from some normalization problems due to the difference between discrete and continuous spaces.

Equation summary for section 4.7

$$\hat{\rho} = \sum_{\mu,\nu=0}^{D-1} \sum_{S=0}^{2D-1} W_{\frac{\mu+\nu}{2},\frac{S}{2}} \exp\left[\frac{2\pi i}{D}\left(\frac{S}{2}+\alpha\right)(\mu-\nu)\right] \big|e_\mu\big\rangle\big\langle e_\nu\big|$$

$$Q(a) = \frac{2}{D} \sum_{M,S=0}^{2D-1} \sum_{m,n=-\infty}^{\infty} W_{\frac{M}{2},\frac{S}{2}} \exp\left[-\frac{1}{\hbar}\big(e_{M/2} - x_0 + mQ\big)^2\right] \times \exp\left[-\frac{1}{\hbar}\big(p_{S/2} - p_0 + nP\big)^2\right]$$

Chapter 5

Quantization of the baker's map

5.1 The classical baker's map

The baker's map [19] is a standard example in chaotic dynamics. It is a mapping of the unit square onto itself in the form

$$\Big(q_{n+1}, p_{n+1}\Big) = \begin{cases} \Big(2q_n, \dfrac{p_n}{2}\Big), & 0 < q_n < 1/2 \\ \Big(2q_n - 1, \dfrac{(p_n+1)}{2}\Big), & 1/2 < q_n < 1 \end{cases} \tag{5.1}$$

where $q, p \in [0, 1)$ and n denotes the n-th iteration of the map. Geometrically, the map acts like a baker kneading bread, stretching the unit square by a factor of two in the q direction, squeezing by a factor of two in the p direction, and then stacking the right half onto the left[1].

The map's action may be rewritten in terms of the complex variable $a \equiv q + ip$,

$$a_{n+1} = \frac{5}{4}a_n + \frac{3}{4}a_n^* + \left(\frac{i}{2} - 1\right)\lfloor a_n + a_n^* \rfloor \equiv b_n(a_n, a_n^*) \tag{5.2}$$

[1]See Figure 1.2.

where $\lfloor a_n \rfloor$ denotes the integer part of a_n. A generating function for this mapping[2] is

$$W(b^*, a) = \frac{1}{10}\left(3b^{*2} + 8ab^* - 3a^2\right) + \frac{4}{5}\left(1 + \frac{i}{2}\right)\left(a + ib^* - \frac{1}{2}\right)\lfloor a + a^* \rfloor \qquad (5.3)$$

assuming $a + a^*$ is non-integer. The classical baker's map may then be rederived *via* the relations

$$\frac{\partial W}{\partial b^*} = b, \qquad \frac{\partial W}{\partial a} = a^*. \qquad (5.4)$$

Interest in the baker's map is due mainly to the simplicity of its *symbolic dynamics*. Each point of the unit square can be identified through its binary representation,

$$q = 0 \cdot s_1 s_2 \ldots = \sum_{k=1}^{\infty} s_k 2^{-k}$$

and

$$p = 0 \cdot s_0 s_{-1} \ldots = \sum_{k=0}^{\infty} s_{-k} 2^{-k-1}$$

with a bi-infinite symbolic string

$$s = \ldots s_{-2} s_{-1} s_0 \bullet s_1 s_2 s_3 \ldots \qquad (5.5)$$

$s_i \in \{0, 1\}$. If the point is in the region $0 \leq q < 1/2$, then its binary representation must necessarily have $s_1 = 0$. Likewise when $1/2 \leq q < 1$, $s_1 = 1$; therefore, using mod 1 arithmetic, we can rewrite Equation 5.1 in the simple form

$$\begin{aligned} q' &= 2\,(q - s_1) = 0 \cdot s_2 s_3 \ldots \\ p' &= \frac{(p + s_1)}{2} = 0 \cdot s_1 s_0 s_{-1} \ldots \end{aligned} \qquad (5.6)$$

where (q', p') is the mapped point. The action of the baker's map is to shift the position of the dot

$$s \to s' = \ldots s_{-2} s_{-1} s_0 s_1 \bullet s_2 s_3 \ldots \qquad (5.7)$$

by one point to the right.

[2]Generating functions are necessarily defined up to an arbitrary constant.

Equation summary for section 5.1

$$W(b^*, a) = \frac{1}{10}\left(3b^{*2} + 8ab^* - 3a^2\right) + \frac{4}{5}\left(1 + \frac{i}{2}\right)\left(a + ib^* - \frac{1}{2}\right)\lfloor a + a^* \rfloor$$

$$\ldots s_{-2}s_{-1}s_0 \bullet s_1 s_2 s_3 \ldots \rightarrow \ldots s_{-2}s_{-1}s_0 s_1 \bullet s_2 s_3 \ldots$$

5.2 The quantum baker's map of Balazs, Voros, and Saraceno

The first work on a quantum baker's map was done by Balazs and Voros [20]. Their expression for the map was given in the form

$$\hat{B} = \hat{F}_D^{-1} \begin{pmatrix} \hat{F}_{D/2} & 0 \\ 0 & \hat{F}_{D/2} \end{pmatrix} \tag{5.8}$$

where $\hat{F}_{D/2}$ is the finite Fourier transform acting on half of the Hilbert space. Later Saraceno [21] improved certain symmetry characteristics of the map using anti-periodic boundary conditions ($\alpha = \beta = 1/2$).

This expression can be rather cryptic unless one knows how to express it in a more active form. Figure 5.1 shows two Q-functions. Obviously, the second one is a momentum eigenstate. In fact, it is the Q-function for the $\left|p_{11}\right\rangle$ momentum eigenstate when $D = 30$. The first is the Q-function for the state $\left|\psi\right\rangle$ created by the inverse of Equation 5.8 acting on $\left|p_{11}\right\rangle$; therefore, the net result of this quantum baker's map is

$$\hat{B}\left|\psi\right\rangle = \left|p_{11}\right\rangle. \tag{5.9}$$

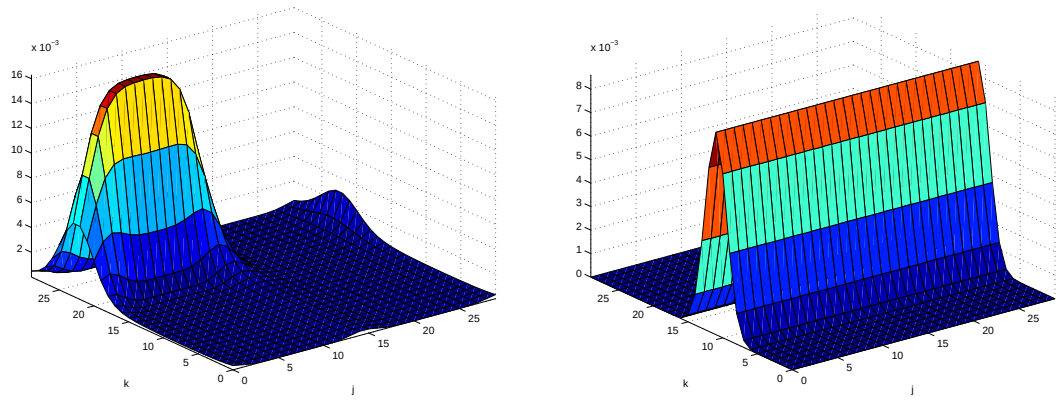

Figure 5.1: Two Q-functions in $D = 30$ dimensions with anti-periodic boundary conditions. The Balazs-Voros-Saraceno quantum baker's map acting on the left hand state produces the momentum eigenstate on the right.

Figure 5.2 shows the action of this quantum baker's map on the state $\left|\psi'\right\rangle$ which results in the $\left|p_{19}\right\rangle$ momentum eigenstate. Studying the states $\left|\psi\right\rangle$ and $\left|\psi'\right\rangle$, we find that they are localized in either the left or right hand side in position and well reasonably localized in momentum. Figure 5.3 shows for $D = 8$ dimensions the peak contours of the states which map to momentum eigenstates[3]. We see that indeed all of these states are localized either in the region $0 < x < 1/2$ or $1/2 < x < 1$, and they are well localized in momentum. The action of the Balazs-Voros-Saraceno baker's map is to take these states to momentum states, which as we know are completely localized in momentum and delocalized in position. This is the essence of their quantization: the mapped states are such that their position spread is twice that of the original state while the momentum spread is halved. In this way, their quantum map mimics the classical baker's map.

[3]For higher dimensions, the essential characteristics are the same. The main difference is that there are more circles.

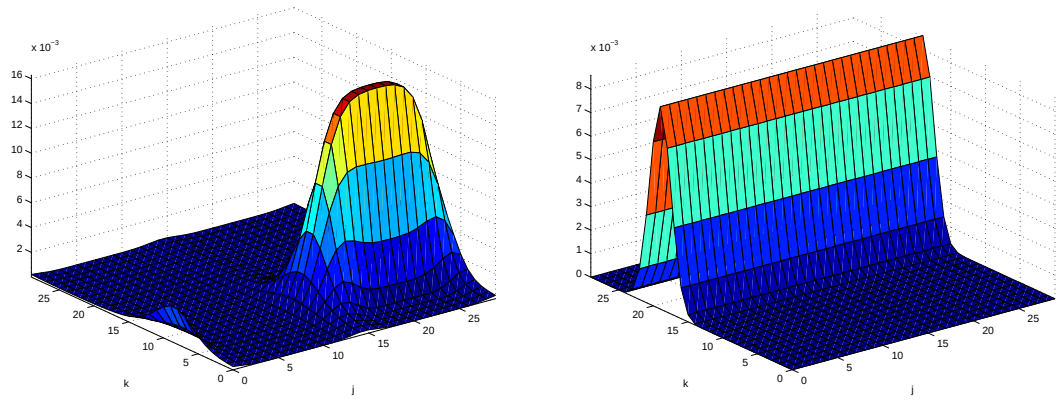

Figure 5.2: Another example of the action of the Balazs-Voros-Saraceno quantum baker's map in $D = 30$ dimensions.

5.3 A class of baker's maps

Inspired by the active interpretation of the Balazs-Voros-Saraceno quantum baker's map espoused in the previous section, Schack and Caves formulated a set of quantized maps [28] by creating different types of "localized" states using the partial Fourier transform operator, which we will define below. These maps will be the focus of the next chapter, where we will use a semi-classical treatment to find their classical limit.

The Schack-Caves quantum baker's maps are defined for anti-periodic Hilbert spaces in which $D = 2^N$. In this case, we can model our system as the outer product of N qubits, *i.e.* N two-level systems. We write our position basis vectors[4] as

$$\left|e_j\right\rangle = \left|x_1\right\rangle \otimes \left|x_2\right\rangle \otimes \cdots \otimes \left|x_N\right\rangle, \qquad x_l \in \{0, 1\}, \tag{5.10}$$

[4]Since the classical baker's map is defined on the unit square, we shall from now on be setting our characteristic position and momentum scales Q and P equal to one.

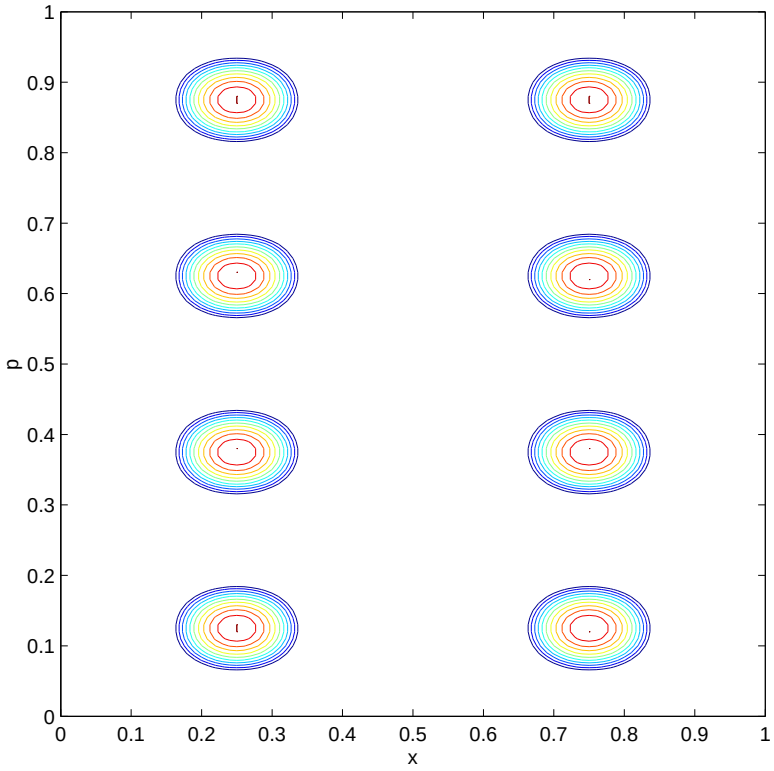

Figure 5.3: The Q-function's contour plots for the peaks of the 8 states which map to the momentum eigenstates under the Balazs-Voros-Saraceno quantum baker's map in $D = 8$ dimensions.

where j has the binary expansion[5]

$$j = x_1 \dots x_N.0 = \sum_{l=1}^{N} x_l 2^{N-l} \qquad \text{and} \qquad e_j = \frac{j + 1/2}{D} = \frac{x_1 \dots x_N.1}{D}, \tag{5.11}$$

where the use of ".1" is binary shorthand for $1/2$. Next we rewrite the quantum Fourier transform as

$$\big|p_k\big\rangle = \hat{F}_D \big|e_k\big\rangle = \frac{1}{\sqrt{2^N}} \sum_{x_1,\dots,x_N} \big|x_1\big\rangle \otimes \big|x_2\big\rangle \otimes \cdots \otimes \big|x_N\big\rangle \, \exp\left[\frac{2\pi i}{2^N}(y + 1/2)(x + 1/2)\right] \tag{5.12}$$

[5]All strings ending with either ".0" or ".1" denote a binary number.

where

$$y + 1/2 = y_1 \dots y_N.1 = k + 1/2 \qquad \text{and} \qquad p_k = \frac{k+1/2}{D} = \frac{y_1 \dots y_N.1}{D}.$$

The connection with the classical baker's map comes from its symbolic dynamics. In the quantum case, a set of states localized in position and momentum is created through the partial Fourier transform, $\hat{G}_n$, which is an operator that Fourier transforms the $N-n$ least significant qubits, *i.e.*,

$$\begin{aligned}
&\hat{G}_n\Big(\big|x_1\big\rangle \otimes \cdots \otimes \big|x_n\big\rangle \otimes \big|a_1\big\rangle \otimes \cdots \otimes \big|a_{N-n}\big\rangle\Big) \\
&\equiv \big|x_1\big\rangle \otimes \cdots \otimes \big|x_n\big\rangle \\
&\quad \otimes \frac{1}{\sqrt{2^{N-n}}} \sum_{x_{n+1},\dots,x_N} \big|x_{n+1}\big\rangle \otimes \cdots \otimes \big|x_N\big\rangle \exp\left[\frac{2\pi i}{2^{N-n}}(a+1/2)(x+1/2)\right]
\end{aligned} \tag{5.13}$$

where a and x are defined through the binary expansions $a = a_1 \dots a_{N-n}.0$ and $x = x_{n+1} \dots x_N.0$. In the limiting cases, we have $\hat{G}_0 = \hat{F}_D$ and $\hat{G}_N = i\hat{1}$. The analogy to the classical case is made clear through the definition

$$\big|a_{N-n} \dots a_1 \bullet x_1 \dots x_n\big\rangle \equiv \hat{G}_n\Big(\big|x_1\big\rangle \otimes \cdots \otimes \big|x_n\big\rangle \otimes \big|a_1\big\rangle \otimes \cdots \otimes \big|a_{N-n}\big\rangle\Big). \tag{5.14}$$

Notice that

$$\big|\bullet x_1 \dots x_N\big\rangle = i\,\big|x_1\big\rangle \otimes \dots \otimes \big|x_N\big\rangle.$$

These states form an orthonormal basis since

$$\begin{aligned}
&\big\langle b_{N-n} \dots b_1 \bullet y_1 \dots y_n \big| a_{N-n} \dots a_1 \bullet x_1 \dots x_n\big\rangle \\
&= \delta_{y_1,x_1} \dots \delta_{y_n,x_n} \frac{1}{2^{N-n}} \sum_{x=0}^{2^{N-n}-1} \exp\left[\frac{2\pi i}{2^{N-n}}(x+1/2)(a-b)\right] \\
&= \delta_{y_1,x_1} \dots \delta_{y_n,x_n} \delta_{b_1,a_1} \dots \delta_{b_{N-n},a_{N-n}},
\end{aligned} \tag{5.15}$$

and they are localized in both position and momentum. They are quantum analogies of localized classical phase space regions. Looking at Equation 5.13, we see that they are strictly localized in a position region of width $1/2^n$ centered at

$$0.x_1 \dots x_n 1 = \frac{x_1 \dots x_n.1}{2^n}. \tag{5.16}$$

To find the momentum representation, we begin with

$$\begin{aligned}&\big\langle p_k\big|a_{N-n}\dots a_1\bullet x_1\dots x_n\big\rangle\\&=\frac{\sqrt{2^n}}{2^N}\sum_{x_{n+1},\dots,x_N}\exp\left[-\frac{2\pi i}{D}(y+1/2)\big(x_1x_2\dots x_nx_{n+1}\dots x_N.1\big)\right]\\&\quad\times\exp\left[\frac{2\pi i}{2^{N-n}}(a+1/2)(x+1/2)\right].\end{aligned}\tag{5.17}$$

To combine the two Fourier terms, we expand the variable

$$\begin{aligned}x_1x_2\dots x_nx_{n+1}\dots x_N.1&=2^{N-n}x_1x_2\dots x_n.0+x_{n+1}\dots x_N.1\\&=2^{N-n}x_1x_2\dots x_n.0+x+1/2,\end{aligned}\tag{5.18}$$

using the fundamental definition of a binary number. This leaves us with

$$\begin{aligned}&\big\langle p_k\big|a_{N-n}\dots a_1\bullet x_1\dots x_n\big\rangle\\&=\frac{\sqrt{2^n}}{2^N}\exp\left[-\frac{2\pi i}{2^n}(x_1\dots x_n.0)(y+1/2)\right]\\&\quad\times\sum_{x=0}^{2^{N-n}-1}\exp\left[\frac{2\pi i}{2^{N-n}}(x+1/2)\left(a+1/2-\frac{y+1/2}{2^n}\right)\right].\end{aligned}\tag{5.19}$$

Unfortunately, $a+1/2-(y+1/2)/2^n$ is not an integer; therefore, we cannot apply Equation 2.26. We can instead perform the geometric sum over x. After a little bit of algebra, we find that

$$\begin{aligned}\big\langle p_k\big|a_{N-n}\dots a_1\bullet x_1\dots x_n\big\rangle=\frac{\sqrt{2^n}}{2^N}\exp\left[-\frac{2\pi i}{2^n}(x_1\dots x_n.1)(y+1/2)\right]\\\times\frac{\cos\Big(\pi(y+1/2)/2^n\Big)}{\sin\Big(\pi\xi/2^{N-n}\Big)}\end{aligned}\tag{5.20}$$

where $\xi=a+1/2-(y+1/2)/2^n$. Consequently, the momentum probability distribution is given by

$$\Big|\big\langle p_k\big|a_{N-n}\dots a_1\bullet x_1\dots x_n\big\rangle\Big|^2=\frac{2^n}{D^2}\frac{\cos^2\Big(\pi(y+1/2)/2^n\Big)}{\sin^2\Big(\pi\xi/2^{N-n}\Big)}=\frac{2^n}{D^2}\frac{\cos^2\big(\pi2^{N-n}p_k\big)}{\sin^2\left(\pi2^np_a-\pi p_k\right)}\tag{5.21}$$

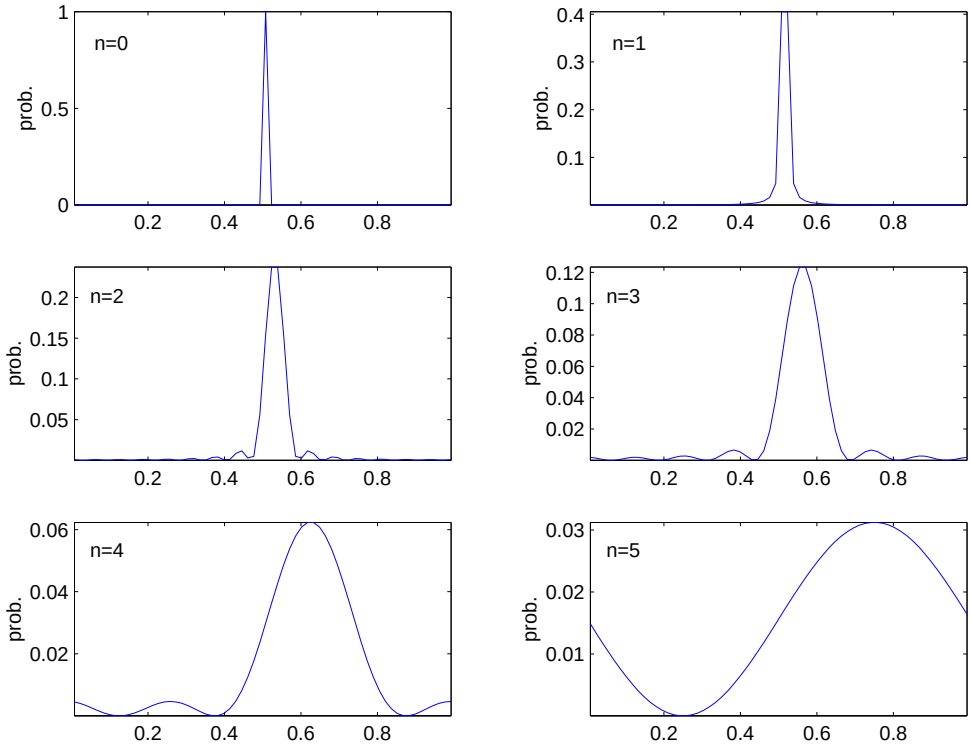

Figure 5.4: The momentum distributions, $\left|\langle p_k | a_{N-n} \dots a_1 \bullet x_1 \dots x_n \rangle\right|^2$, for $D = 2^6$. For each plot, $a_1 \dots a_{N-n} = 2^{N-n-1}$.

where $p_a = (a + 1/2)/2^N$.

This form is not very illuminating, but we can use numerical calculation to interpret it. Figure 5.4 shows the plots of $\left|\langle p_k | a_{N-n} \dots a_1 \bullet x_1 \dots x_n \rangle\right|^2$ as function of $p = (k + 1/2)/D$ for $n = 0, 1, 2, \dots, 5$ and $D = 2^6$. Here a has been chosen to be half of its maximum value[6] 2^{N-n}. We see that the states are roughly localized in a momentum region of width $1/2^{N-n}$ centered at $p = 0.a_1 \dots a_{N-n}1$. The scale at which the momentum is localized increases, as expected, as n increases. More importantly, the sharpness of the momentum localization is best for small n and gets progressively worse as n increases.

[6]Other choices of a shift the center of the plots.

Using the notation of Equation 5.14, Schack and Caves defined a whole class of quantum baker's maps $\hat{B}_n$ $(n = 1, \ldots, N)$

$$\hat{B}_n \equiv \sum_{\substack{x_1,\ldots,x_n \\ a_1,\ldots,a_{N-n}}} \big|a_{N-n}\ldots a_1 x_1 \bullet x_2 \ldots x_n\big\rangle\big\langle a_{N-n}\ldots a_1 \bullet x_1 x_2 \ldots x_n\big|. \tag{5.22}$$

The Balazs-Voros-Saraceno quantum baker's map is recovered when $n = 1$. In the language of Equation 5.5, we see that each quantum baker's map takes a state localized at $1a_{N-n}\ldots a_1 \bullet x_1 \ldots x_n 1$ to a state localized at $1a_{N-n}\ldots a_1 x_1 \bullet x_2 \ldots x_n 1$. The decrease in the number of position bits and increase in momentum bits enforces a stretching and squeezing of phase space in a manner resembling the classical baker's map. As n increases, the progressively poorer momentum localization might be expected to have important consequences on the map's behavior. When considering the classical limit in the next chapter, we find this to be true.

It will be useful to rewrite our baker's map in the position basis. To do this, we first use Equations 5.13 and 5.14 to rewrite Equation 5.22 as

$$\begin{aligned}\hat{B}_n = \frac{\sqrt{2}}{2^{N-n+1}} \sum_{\substack{x_1,\ldots,x_n \\ a_1,\ldots,a_{N-n}}} \sum_{\substack{z_1,\ldots,z_{N-n+1} \\ y_1,\ldots,y_{N-n}}} \big|\bullet x_2 \ldots x_n z_1 \ldots z_{N-n+1}\big\rangle\big\langle \bullet\ x_1 \ldots x_n y_1 \ldots y_{N-n}\big| \\ \times \exp\left[\frac{\pi i}{2^{N-n}}\Big((j+1/2)(l+1/2) + 2^{N-n}x_1(l+1/2) - 2(j+1/2)(k+1/2)\Big)\right]\end{aligned} \tag{5.23}$$

where

$$j = \sum_{k=1}^{N-n} a_k 2^{N-n-k}, \quad k = \sum_{k=1}^{N-n} y_k 2^{N-n-k} \quad \text{and} \quad l = \sum_{k=1}^{N-n+1} z_k 2^{N-n+1-k}.$$

Next, using Equations 5.10, 5.14, and the notation $e_j = (j + 1/2)/D$, $e_k = (k + 1/2)/D$, *etc.*, we arrive at the quantum baker's map in the position basis

$$\begin{aligned}\hat{B}_n = \frac{\sqrt{2}}{2^{N-n+1}} \sum_{x_1=0}^{1} \sum_{j,k=0}^{2^{N-n}-1} \sum_{l=0}^{2^{N-n+1}-1} \sum_{m=0}^{2^{n-1}-1} \\ \times \Big|e_l + e_m 2^{N-n+1} - 2^{-n}\Big\rangle\Big\langle e_k + x_1/2 + e_m 2^{N-n} - 2^{-n-1}\Big| \\ \times \exp\left[2\pi i D 2^{n-1}\left(e_j e_l + 2^{-n}x_1 e_l - 2e_j e_k\right)\right].\end{aligned} \tag{5.24}$$

Notice that it is possible to sum over the index j at this point; however the representation above proves to be most convenient when performing our semi-classical analysis.

Equation summary for section 5.3

$$\hat{G}_n\Big(\big|x_1\big\rangle \otimes \cdots \otimes \big|x_n\big\rangle \otimes \big|a_1\big\rangle \otimes \cdots \otimes \big|a_{N-n}\big\rangle\Big)$$
$$\equiv \big|x_1\big\rangle \otimes \cdots \otimes \big|x_n\big\rangle \otimes \frac{1}{\sqrt{2^{N-n}}} \sum_{x=0}^{2^{N-n}-1} \big|x_{n+1}\big\rangle \otimes \cdots \otimes \big|x_N\big\rangle \exp\left[\frac{2\pi i}{2^{N-n}}(a.1)(x.1)\right]$$

$$\big|a_{N-n}\ldots a_1 \bullet x_1 \ldots x_n\big\rangle \equiv \hat{G}_n\Big(\big|x_1\big\rangle \otimes \cdots \otimes \big|x_n\big\rangle \otimes \big|a_1\big\rangle \otimes \cdots \otimes \big|a_{N-n}\big\rangle\Big)$$

$$\hat{B}_n = \sum_{\substack{x_1,\ldots,x_n \\ a_1,\ldots,a_{N-n}}} \big|a_{N-n}\ldots a_1 x_1 \bullet x_2 \ldots x_n\big\rangle\big\langle a_{N-n}\ldots a_1 \bullet x_1 x_2 \ldots x_n\big|$$

$$\hat{B}_n = \frac{\sqrt{2}}{2^{N-n+1}} \sum_{x_1=0}^{1} \sum_{j,k=0}^{2^{N-n}-1} \sum_{l=0}^{2^{N-n+1}-1} \sum_{m=0}^{2^{n-1}-1}$$
$$\times \Big|e_l + e_m 2^{N-n+1} - 2^{-n}\Big\rangle\Big\langle e_k + x_1/2 + e_m 2^{N-n} - 2^{-n-1}\Big|$$
$$\times \exp\left[2\pi i D 2^{n-1}\left(e_j e_l + 2^{-n} x_1 e_l - 2 e_j e_k\right)\right]$$

5.3.1 The importance of anti-periodic boundary conditions

When Saraceno introduced the anti-periodic boundary conditions for the quantum baker's map, he was mostly interested in giving his map the proper phase space symmetry of inversion through the center of the square [21], *i.e.* the phase space operation of

$$q \to 1 - q, \quad p \to 1 - p.$$

While this symmetry is very important, we shall see that the choice of boundary conditions has a profound impact upon the fundamental "correctness" of the Schack-Caves quantum baker's maps.

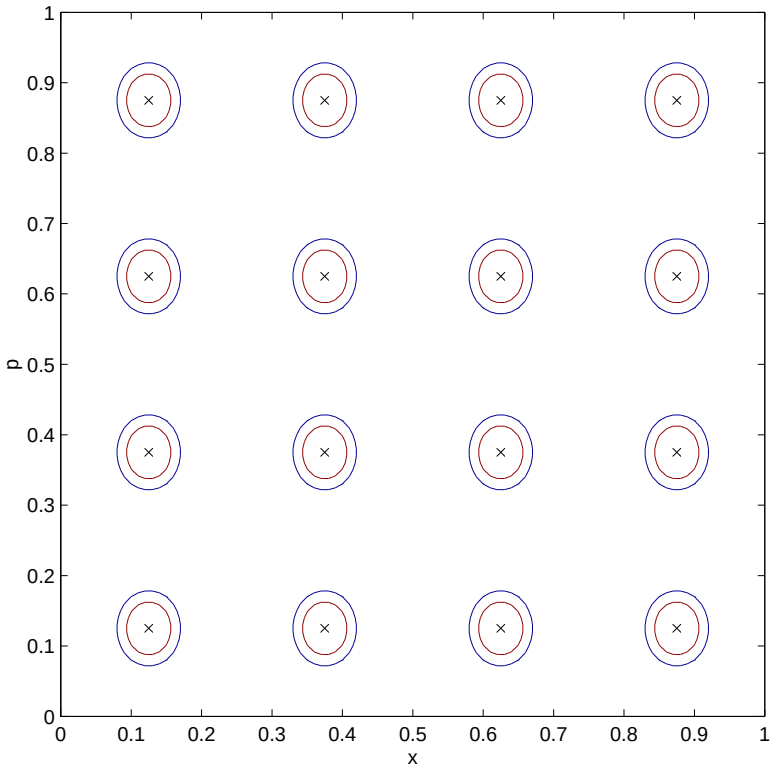

Figure 5.5: The peak contours for the states $\left|a_2 a_1 \bullet x_1 x_2\right\rangle$ with anti-periodic boundary conditions. The expected centers are plotted with an 'X'.

Figure 5.5 shows the Q-function contours for the peak of the states $\left|a_2 a_1 \bullet x_1 x_2\right\rangle$ plotted as a function of continuous variables x and p. These states are correctly centered at the points $x = 0.x_1 x_2 1$ and $p = 0.a_1 a_2 1$ as shown by the 'X' plotted in the center of each contour. One could have defined the Schack-Caves maps using periodic boundary conditions. In this case, the states $\left|a_2 a_1 \bullet x_1 x_2\right\rangle$ would be expected to be centered at $x = 0.x_1 x_2$ and $p = 0.a_1 a_2$, but as Figure 5.6 shows, this is clearly not the case. These states are correctly centered in momentum, but not in position.

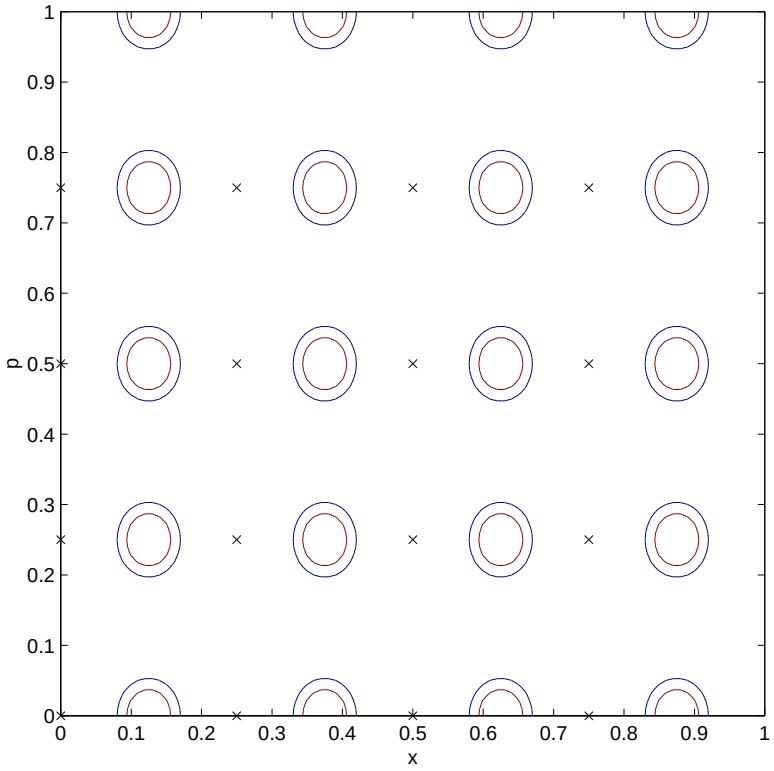

Figure 5.6: The peak contours for the states $\left|a_2 a_1 \bullet x_1 x_2\right\rangle$ with periodic boundary conditions. The expected centers are plotted with an 'X'.

The reason for this lack of position centering is not mysterious and helps give insight into the nature of these partially Fourier transformed states. As stated before, the state $\left|a_{N-n} \ldots a_1 \bullet x_1 \ldots x_n\right\rangle$ is strictly localized in position. The distribution $\left\langle e_j \middle| a_{N-n} \ldots a_1 \bullet x_1 \ldots x_n \right\rangle$ is a step function with non-zero values only in the region where the first n bits of j are equal to $x_1 x_2 \ldots x_n$. Using the definition of a binary number, we see that there are non-zero values when j ranges from

$$j = x_1 x_2 \ldots x_n 000 \ldots 0.0 = 2^{N-n} x_1 x_2 \ldots x_n .0 + 0$$

to

$$j = x_1 x_2 \ldots x_n 111 \ldots 1.0 = 2^{N-n} x_1 x_2 \ldots x_n .0 + 2^{N-n} - 1.$$

Hence there are 2^{N-n} values of j which yield non-zero probability. Obviously, the partially Fourier transformed state will have position extent uniformly in this region; therefore, they will be centered at j_m, the midpoint of this region. This midpoint is given by

$$j_m = 2^{N-n} x_1 x_2 \dots x_n.0 + \frac{2^{N-n}}{2} = 2^{N-n} \left(x_1 x_2 \dots x_n.0 + 1/2 \right). \tag{5.25}$$

Expressing this point in terms of the continuous variable $x = j/D = j/2^N$, we find that the partially Fourier transformed states are centered at

$$x_m = \frac{x_1 x_2 \dots x_n.0 + 1/2}{2^n} = 0.x_1 x_2 \dots x_n 1. \tag{5.26}$$

This is exactly the point specified by the anti-periodic version of the Schack-Caves quantum baker's map. Moreover, we see that this midpoint's value is unaffected by the choice of boundary condition; hence, the position centering for the states is unchanged in Figures 5.5 and 5.6.

5.4 Eigenvalue statistics

In quantum chaos, there has been much research done into the area of eigenvalue statistics [17, 76, 77, 78, 79, 80]. The idea is based upon Wigner's random matrix theory and predicts that if one makes a histogram of the spacing between a quantum map's nearest neighbor eigenvalues, then this histogram will have a characteristic shape [11]. If the system is not chaotic then the shape will be Poissonian; otherwise, it will have one of a variety of shapes predicted by random matrix theory[7]. While the subject of eigenvalue statistics is too peripheral to be discussed in detail here, we will show that the Schack-Caves B_{N-1} quantum baker's map has eigenvalues whose spacing is completely regular; a trait not shared by the rest of the maps.

[7]See the introduction of [81] for a brief but thorough description of the possible histogram shapes.

In this case, Equation 5.22 becomes

$$\begin{aligned} B_{N-1} &= \sum_{x_1,\ldots,x_N} \left|x_1 \bullet x_2 \ldots x_N\right\rangle\!\left\langle \bullet\, x_1 x_2 \ldots x_N\right| \\ &= \frac{1}{\sqrt{2}} \sum_{x_1\ldots,x_N} \sum_{y_1=0}^{1} \exp\left[\pi i (y_1+1/2)(x_1+1/2)\right] \left|x_2 \ldots x_N y_1\right\rangle\!\left\langle x_1 x_2 \ldots x_N\right| \end{aligned} \tag{5.27}$$

where we used Equation 5.13 to rewrite the expression in the position basis.

We see that the action of B_{N-1} is very simple. It is to shift all the qubits by one position to the left, the leading qubit is moved to the end of the string and is then subjected to a Fourier transform. Realizing this pattern, we can quickly calculate the action of N iterations of the map,

$$\begin{aligned} \left(B_{N-1}\right)^N = \frac{1}{\sqrt{2^N}} \sum_{x_1\ldots,x_N} \sum_{y_1,\ldots y_N} &\exp\left[\pi i (y_1+1/2)(x_1+1/2)\right] \cdots \\ &\times \exp\left[\pi i (y_N+1/2)(x_N+1/2)\right] \left|y_N \ldots y_1\right\rangle\!\left\langle x_1 \ldots x_N\right|. \end{aligned} \tag{5.28}$$

Operating the map once again, we get

$$\begin{aligned} \left(B_{N-1}\right)^{N+1} = \frac{1}{\sqrt{2^{N+1}}} \sum_{x_1\ldots,x_N} \sum_{y_1,\ldots y_{N-1}} \sum_{z_1=0}^{1} &\exp\left[\pi i (y_1+1/2)(x_1+1/2)\right] \cdots \\ &\times \sum_{y_N=0}^{1} \exp\left[\pi i (y_N+1/2)(x_N+z_1+1)\right] \left|y_{N-1} \ldots y_1 z_1\right\rangle\!\left\langle x_1 \ldots x_N\right|. \end{aligned} \tag{5.29}$$

This last sum can be done; we find that

$$\begin{aligned} \sum_{y_N=0}^{1} \exp\left[\pi i (y_N+1/2)(x_N+z_1+1)\right] &= \exp\left[\frac{\pi i}{2}(x_N+z_1+1)\right]\left(1-(-1)^{x_N+z_1}\right) \\ &= \begin{cases} -2, & \text{if } x_N = 0 \text{ and } z_1 = 1, \\ -2, & \text{if } x_N = 1 \text{ and } z_1 = 0, \\ 0, & \text{else.} \end{cases} \end{aligned} \tag{5.30}$$

Equation 5.30 gives the values of the sum for the possible values of x_N and z_1. In the language of binary numbers, z_1 has to be the "not" of x_N which is represented by $z_1 = \bar{x}_N$. This negating will occur for each successive variable as we continue to operate B_{N-1}; therefore, we see that

$$\left(\hat{B}_{N-1}\right)^{2N} = (-1)^N \sum_{x_1,\ldots x_N} \left|\bar{x}_1 \ldots \bar{x}_N\right\rangle\left\langle x_1 \ldots x_N\right|. \tag{5.31}$$

Of course, the "not" of a "not" is identity, so we find that if we continue to operate the $\hat{B}_{N-1}$ quantum baker's map enough times, we will get the identity operator,

$$\left(\hat{B}_{N-1}\right)^{4N} = (-1)^{2N} \sum_{x_1,\ldots x_N} \left|x_1 \ldots x_N\right\rangle\left\langle x_1 \ldots x_N\right| = \hat{1}. \tag{5.32}$$

Equation 5.32 has a profound effect upon the eigenvalues of the map $\hat{B}_{N-1}$. It implies that all of the eigenvalues are roots of unity. In fact, they will be given by

$$\exp\left[\frac{2\pi i}{4N} j\right],$$

where j is an integer. For large values of N, this map will have highly degenerate eigenvalues, and the nearest neighbor spacing will either be zero or $2\pi/4N$. The eigenvalue statistics will be completely regular.

Chapter 6

The classical limit for a class of quantum baker's maps

6.1 Introduction

This chapter details the author's work published in the *Journal of Physics A: Mathematics and General* [82].

The inspiration for this classical limit program begins with Saraceno and Voros [39] and their semi-classical "Van Vleck" [1] ansatz. It states that in the limit $\hbar \to 0$ a quantum propagator $\hat{U}$ has the position representation

$$\langle x' | \hat{U} | x \rangle \approx (2\pi\hbar)^{-1/2} \sqrt{\frac{\partial^2 W}{\partial x' \partial x}} \exp\left[-\frac{i}{\hbar} W(x, x') \right],$$

where $W(x, x')$ is the generating function for the classical map. The square root in the expression acts as a Jacobian since in effect we are performing a change of variable. Inspired by the spin coherent state work of Kuś [49] and Scott [50], this ansatz has been modified for use with our coherent states,

$$\langle b | \hat{U} | a \rangle \approx \sqrt{\frac{\partial^2 W}{\partial a \partial b^*}} \exp\Big[W(b^*, a)/2\hbar \Big] \exp\Big[-\frac{1}{4\hbar}(|a|^2 + |b|^2) \Big]. \qquad (6.1)$$

In this work, we use the Schack-Caves quantum baker's map from Chapter 5 and the coherent states of Chapter 4. To the best of the author's knowledge, this is the first time this technique has been applied to a map on this space.

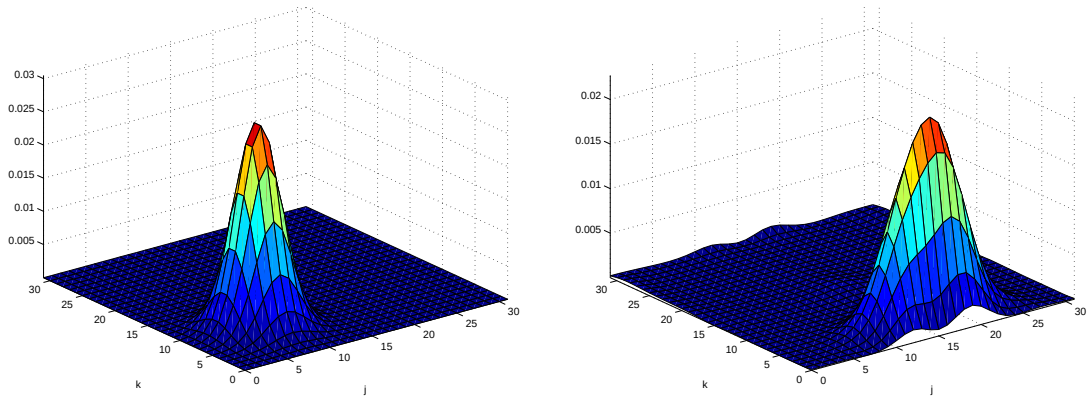

Figure 6.1: The Q-function, in $D = 32$ dimensions, for the $a = 1/4 + i/4$ coherent state and the state created when the $\hat{B}_2$ quantum baker's map acts upon it.

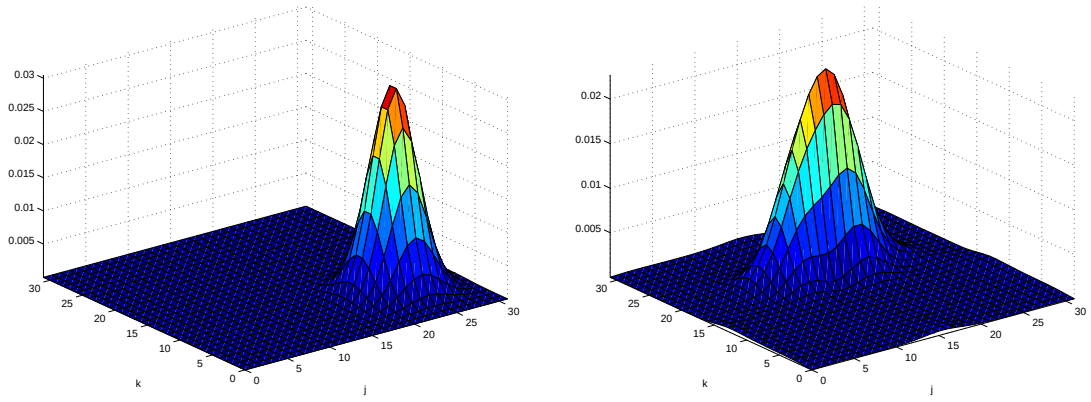

Figure 6.2: The Q-function, in $D = 32$ dimensions, for the $a = 3/4 + i/4$ coherent state and the state created when the $\hat{B}_2$ quantum baker's map acts upon it.

The Q-function has been of great importance in helping motivate the theoretical work of this section. Figure 6.1 shows the Q-function for the $a = 1/4 + i/4$ coherent state and the Q-function for the state, $\hat{B}_2|a\rangle$ in $D = 32$ dimensions. Although it

may not be apparent from the figure, the mapped state is centered at the point $1/2 + i/8$ which is the mapped point of the classical baker's map. Figure 6.2 repeats the procedure for the $a = 3/4 + i/4$ coherent state. It is mapped to a state correctly centered at $1/2 + 5i/8$. Of course, two examples are not sufficient to entail a proof that all points are mapped correctly, hence the rest of this chapter.

It is interesting to note that the quantum baker's map not only takes the center of the states to the classically directed point, but that it recreates the map's action in another way. The classical map stretches the unit square in position and squeezes in momentum. In the same fashion, the quantum baker's map takes a symmetrical coherent state and squeezes it along its momentum axis, thus necessarily stretching it along position.

Our goal for the rest of this chapter is to calculate explicitly the quantum baker's map representation in the coherent state basis and find its semi-classical form, *i.e.* we wish to obtain the leading term in an asymptotic expansion of the matrix element $\langle b|\hat{B}_n|a\rangle$ as $D = 2^N \to \infty$. We see that in this limit the total number of position and momentum bits, N, necessarily become infinite. As Figure 6.3 illustrates, however, there is considerable freedom of choice on how this may occur. We wish to consider cases where the relative number of position and momentum bits approaches infinity at different rates. To this end, we take the number of position bits to be $n = n(N) \equiv \theta N + s$, where $0 \leq \theta \leq 1$ is rational and s takes integer values. For ease of reading, we also introduce the constant $\phi = 1 - \theta$ such that the number of momentum bits $N - n = \phi N - s$. We will now identify the different Schack-Caves quantum baker's maps, Equation 5.24, through the new parameters, $\hat{B}_{\theta,s} \equiv \hat{B}_n$. In the analysis which follows, we must consider the two extreme cases of $\theta = 0$ and $\theta = 1$ separately. We find that for all cases except when $\theta = 1$ the semi-classical propagator has the Van Vleck form, *i.e.* Equation 6.1; hence, we claim they have the correct classical limit. The $\theta = 0$ interpretation will be discussed below.

We consider first the $\theta = 0$ case where the number of position bits is fixed at s as $N \to \infty$; the Balazs, Voros, and Saraceno quantum baker's map is the special case where $s = 1$.

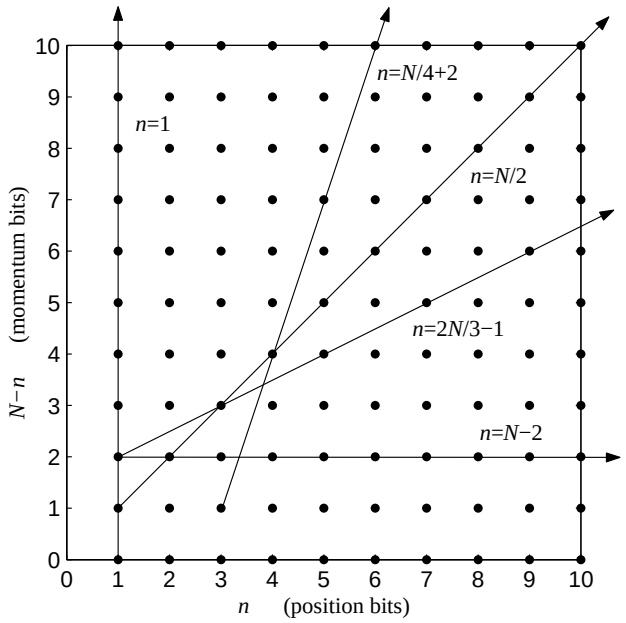

Figure 6.3: Different possible ways of taking the classical limit for the quantum baker's map.

6.2 The limit of the Balazs-Voros-Saraceno quantum baker's map

In the $\theta = 0$ case, the number of position bits remains constant at $n = s \geq 1$ as we let $D \to \infty$. Using Equations 5.24 and 4.31, our matrix element becomes

$$\begin{aligned}\langle b|\hat{B}_{0,s}|a\rangle = SD^{-3/2} \sum_{\mu,\nu=-\infty}^{\infty} \sum_{x_1=0}^{1} \sum_{j,k=0}^{D/S-1} \sum_{l=0}^{2D/S-1} \sum_{m=0}^{S/2-1} \\ \exp\Bigg[-\frac{\pi D}{2}\Big(|a|^2 + |b|^2 - a^2 - b^{*2}\Big) + i\pi(\mu - \nu) \\ - \pi D\Big(e_k + x_1/2 + (De_m - 1/2)/S - a + \mu\Big)^2 \\ - \ \pi D\Big(e_l + 2(De_m - 1/2)/S - b^* + \nu\Big)^2 \\ + i\pi SD\Big(e_j e_l + x_1 e_l/S - 2e_j e_k\Big)\Bigg]\end{aligned} \tag{6.2}$$

where $S \equiv 2^s$. To further the calculation, we now use the Poisson formula to replace each sum by an integral, *e.g.*

$$\begin{aligned}\sum_{\zeta=-\infty}^{\infty} \int_0^{1/S} \exp\Big[2\pi i(Dx - 1/2)\zeta\Big] f(x)dx &= \frac{1}{D} \int_0^{1/S} \sum_{j=-\infty}^{\infty} \delta\Big(x - (j + 1/2)/D\Big) f(x)dx \\ &= \frac{1}{D} \sum_{j=0}^{D/S-1} f(e_j).\end{aligned} \tag{6.3}$$

The result is

$$\begin{aligned}\langle b|\hat{B}_{0,s}|a\rangle = SD^{3/2} \sum_{\substack{\mu,\nu,\zeta \\ \tau,\gamma=-\infty}}^{\infty} \sum_{x_1=0}^{1} \sum_{m=0}^{S/2-1} \int_0^{1/S} dx \int_0^{1/S} dy \int_0^{2/S} dz \\ \exp\Big[-\frac{\pi D}{2}\Big(|a|^2+|b|^2-a^2-b^{*2}\Big) + i\pi(\mu-\nu-\zeta-\tau-\gamma) \\ -\ \pi D\Big(y+x_1/2+m/S-a+\mu\Big)^2 - \pi D\Big(z+2m/S-b^*+\nu\Big)^2 \\ +\ i\pi SD\Big(xz+x_1z/S-2xy\Big) + 2i\pi D\left(x\zeta+y\tau+z\gamma\right)\Big].\end{aligned} \tag{6.4}$$

We are now ready to make a semi-classical approximation to our matrix element. More precisely, we will make a saddle-point approximation to the triple integral above[1]. Only near a saddle-point will contributions from such an integral cancel the prefactor $D^{3/2}$ and lead to an $O(1)$ contribution for the matrix element. The saddle-point approximation, Equation A.3, can be written down immediately using well-known formulae found in any standard text [83]. The limits in the above integrals are finite; therefore, the saddle point will not make a contribution in all cases. We need to consider this possibility carefully if we are to recover the classical baker's map.

Consider first the y integration[2] by defining

$$I_1 \equiv \int_0^{1/S} dy\ \exp\big[-\pi D f(y)\big] \tag{6.5}$$

where

$$f(y) \equiv (y-A)^2 + 2i(Sx-\tau)y \tag{6.6}$$

$$A \equiv a - x_1/2 - m/S - \mu. \tag{6.7}$$

An asymptotic calculation of this integral is done by deforming the integration path,

[1]See Appendix A for a brief introduction to the saddle-point approximation.

[2]The variable x is a fixed parameter for this calculation.

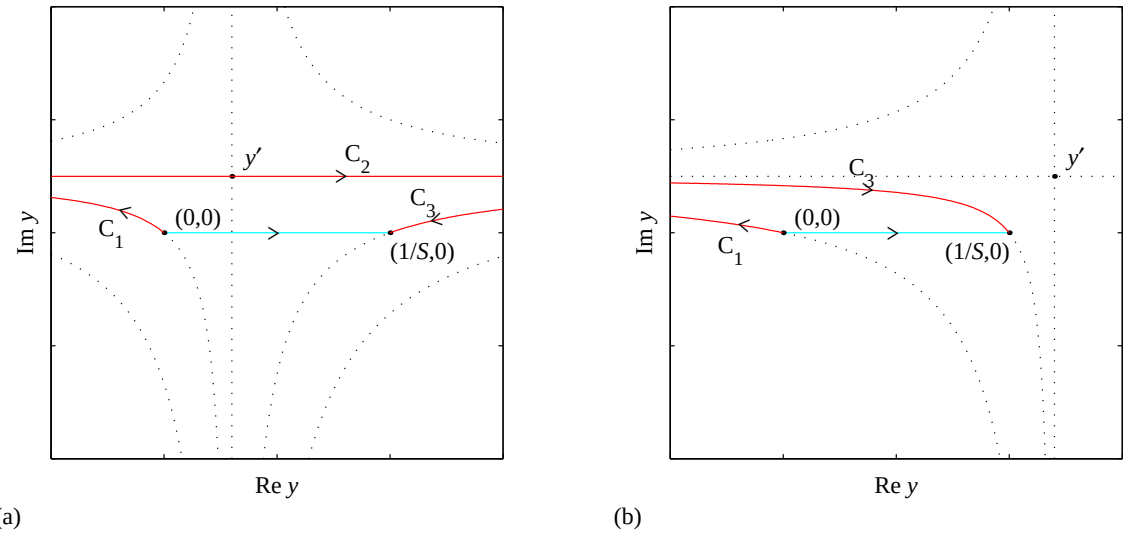

Figure 6.4: Steepest descent paths for $f(y)$. The original integration path along the real line (blue) is deformed to one where $\mathrm{Im}\, f(y) =$ constant (red). Only the first path allows for inclusion of the saddle point, y'.

initially along the real line, to one in the complex plane where $\mathrm{Im}\, f(y) =$ constant. Two important cases are drawn in Figure 6.4. The first (a) occurs when the saddle point[3]

$$y' = A - iSx + i\tau \tag{6.8}$$

satisfies $0 < \mathrm{Re}\,(y') < 1/S$. In this case, the steepest descent path is one which first travels along the hyperbola C_1 from 0 to $-\infty + i\,\mathrm{Im}\, y'$, then along the hyperbolic asymptote C_2 to $\infty + i\,\mathrm{Im}\, y'$, and finally back to $1/S$ *via* another hyperbola C_3. Consequently, an asymptotic expansion for the integral I_1 will be the sum of three parts, each associated with a different contour, C_1, C_2 or C_3, in the complex plane. Note that along the contours C_1 and C_3, the kernel attains its maximum at the end points 0 and $1/S$, respectively; therefore, the leading term in an asymptotic expansion takes the form

$$\frac{\mp 1}{\pi D f'(c)} \exp\big[-\pi D f(c)\big]\big[1 + O(1/D)\big] \tag{6.9}$$

[3]The saddle point is defined through $f'(y') = 0$

with $c = 0$ or $1/S$ with the sign of this leading term being $+1$ for $c = 1/S$ and *vice versa*. The prefactor of $1/D$ in the above expression inhibits such terms from playing a role in the leading order approximation of our matrix element. As remarked before, we need prefactors of $D^{-1/2}$ in each approximation of the three integrals in (6.4) in order to obtain an $O(1)$ overall contribution for the matrix element. Hence we will simply discard the integration along contours C_1 and C_3, and make the approximation

$$\begin{aligned} I_1 &\approx \int_{-\infty+i\,\mathrm{Im}\,y'}^{\infty+i\,\mathrm{Im}\,y'} dy\ \exp\big[-\pi D f(y)\big] \qquad \text{if} \qquad 0 < \mathrm{Re}\,(y') < 1/S \\ &= D^{-1/2} \exp\big[-\pi D f(y')\big]. \end{aligned} \tag{6.10}$$

As Figure 6.4 shows, when $\mathrm{Re}\,(y') < 0$ or $\mathrm{Re}\,(y') > 1/S$ the path of steepest descent no longer passes through the saddle point. In this case, there will be no leading order contributions to the matrix element, *i.e.* we may set $I_1 = 0$. The third and final case occurs when $\mathrm{Re}\,(y') = 0$ or $1/S$. One may investigate these possibilities by taking exactly one half of Equation 6.10 as the approximation for I_1. For simplicity, we will not deal with this case, except to make the odd casual remark when needed. In summary, we use Equation 6.10 as our approximation for I_1 when $0 < \mathrm{Re}\,(y') < 1/S$, and otherwise we set I_1 to zero.

Similarly, for the z integration,

$$\begin{aligned} I_2 &\equiv \int_0^{2/S} dz\ \exp\big[-\pi D g(z)\big] \\ &\approx D^{-1/2} \exp\big[-\pi D g(z')\big] \qquad \text{if} \qquad 0 < \mathrm{Re}\,(z') < 2/S, \end{aligned} \tag{6.11}$$

with

$$g(z) \equiv (z-B)^2 - 2i(Sx/2 + x_1/2 + \gamma)z, \tag{6.12}$$

$$B \equiv b^* - 2m/S - \nu, \tag{6.13}$$

and the saddle point is

$$z' = B + iSx/2 + ix_1/2 + i\gamma. \tag{6.14}$$

Now letting x vary again and setting

$$\begin{aligned} h(x) &\equiv f(y') + g(z') - 2i\zeta x \\ &= \frac{5}{4}S^2x^2 + S\Big(2iA - iB + x_1/2 - 2\tau + \gamma - 2i\zeta/S\Big)x - 2iA\tau \\ &\quad - iB(x_1 + 2\gamma) + \tau^2 + (x_1/2 + \gamma)^2, \end{aligned} \tag{6.15}$$

we have the final integral

$$\begin{aligned} I_3 &\equiv \int_0^{1/S} dx\ \exp\big[-\pi D h(x)\big] \\ &\approx \sqrt{\frac{4}{5S^2D}}\exp\big[-\pi D h(x')\big] \qquad \text{if} \qquad 0 < \mathrm{Re}\,(x') < 1/S, \end{aligned} \tag{6.16}$$

with the saddle point at

$$x' = -\frac{2}{5S}\Big(2iA - iB + x_1/2 - 2\tau + \gamma - 2i\zeta/S\Big). \tag{6.17}$$

Inserting our saddle-point approximations back into Equation 6.4 and setting $a \equiv a_1 + ia_2$ and $b \equiv b_1 + ib_2$, with a little algebra we obtain

$$\begin{aligned} \big\langle b\big|\hat{B}_{0,s}\big|a\big\rangle \approx \sqrt{\frac{4}{5}} \sum_{\substack{\mu,\nu,\zeta \\ \tau,\gamma=-\infty}}^{\infty} \sum_{x_1=0}^{1} \sum_{m=0}^{S/2-1} \exp\Bigg[&-\frac{\pi D}{5}\Big\{(2a_1 - b_1 - x_1 - 2\mu + \nu - 2\zeta/S)^2 \\ &+\ (a_2 - 2b_2 + x_1 + \tau + 2\gamma)^2\Big\} + i\pi(\mu - \nu - \zeta - \tau - \gamma) \\ &+\ i\pi D(a_1a_2 - b_1b_2) - \frac{2i\pi D}{5}\Big\{(2a_1 - b_1 - x_1 - 2\mu + \nu - 2\zeta/S)(2a_2 + b_2) \\ &-\ (a_1 + 2b_1 - x_1/2 - \mu - 2\nu)(x_1 + \tau + 2\gamma) + \zeta(x_1 - 4\tau + 2\gamma)/S\Big\}\Bigg] \end{aligned} \tag{6.18}$$

provided that all three of the inequalities

$$0 < \mathrm{Re}\,(x') = \frac{2}{5S}\Big(2a_2 + b_2 - x_1/2 + 2\tau - \gamma\Big) < \frac{1}{S} \tag{6.19}$$

$$0 < \mathrm{Re}\,(y') = \frac{1}{5}\Big(a_1 + 2b_1 - x_1/2 - \mu - 2\nu\Big) + \frac{1}{5S}\Big(4\zeta - 5m\Big) < \frac{1}{S} \tag{6.20}$$

$$0 < \frac{1}{2}\,\mathrm{Re}\,(z)' = \frac{1}{5}\Big(a_1 + 2b_1 - x_1/2 - \mu - 2\nu\Big) - \frac{1}{5S}\Big(\zeta + 5m\Big) < \frac{1}{S} \tag{6.21}$$

are satisfied. Otherwise the matrix element is taken to be zero.

Note that although m no longer appears in the exponent, we cannot trivially evaluate the sum since not all values of m will satisfy Equations 6.20 and 6.21. Consider the cases when the approximation in Equation 6.18 becomes $O(1)$, *i.e.*,

$$2a_1 - b_1 - x_1 - 2\mu + \nu - 2\zeta/S = 0, \tag{6.22}$$

$$a_2 - 2b_2 + x_1 + \tau + 2\gamma = 0. \tag{6.23}$$

Substituting (6.23) into (6.19) we obtain

$$0 < a_2 + \tau < 1 \qquad \text{or} \qquad 0 < b_2 - x_1/2 - \gamma < 1/2. \tag{6.24}$$

The integers τ and γ give the periodicity in the momentum direction. If we assume $0 < a_2, b_2 < 1$ then we may set $\tau = \gamma = 0$ in Equation 6.18, making a note that we are discarding exponentially small Gaussian tails. Also notice from Equation 6.24 that we must have $x_1 = \lfloor 2b_2 \rfloor$.

Now, negating Equation 6.21 and adding it to Equation 6.20, we immediately arrive at the inequality $-1 < \zeta < 1$; we must set $\zeta = 0$. Substituting this into Equations 6.20 and 6.21 implies that

$$\frac{2m}{S} < \frac{2}{5}\Big(a_1 + 2b_1 - x_1/2 - \mu - 2\nu\Big) < \frac{2(m+1)}{S}. \tag{6.25}$$

If we drop the sum over m in Equation 6.18, we have

$$0 < \frac{2}{5}\Big(a_1 + 2b_1 - x_1/2 - \mu - 2\nu\Big) < 1. \tag{6.26}$$

Following a similar procedure to the one above, we can substitute Equation 6.22 into Equation 6.26 and deduce that under the assumption $0 < a_1, b_1 < 1$, our matrix element, Equation 6.18, becomes $O(1)$ only when $\mu = \nu = 0$. Furthermore, we will have $x_1 = \lfloor 2a_1 \rfloor$.

The surviving term of the summation is our semi-classical approximation for the propagator,

$$\begin{aligned}\langle b|\hat{B}_{0,s}|a\rangle = \sqrt{\frac{4}{5}}\exp\Big[-\frac{\pi D}{5}\Big\{ \big(2a_1 - b_1 - \lfloor 2a_1 \rfloor\big)^2 + \big(a_2 - 2b_2 + \lfloor 2a_1 \rfloor\big)^2 \\ + \; i\big(3a_1a_2 + 3b_1b_2 + 4a_1b_2 - 4a_2b_1\big) \\ - 2i\lfloor 2a_1 \rfloor\big(a_1 + 2b_1 + 2a_2 + b_2 - \lfloor 2a_1 \rfloor/2\big)\Big\}\Big],\end{aligned} \tag{6.27}$$

where we have chosen $x_1 = \lfloor 2a_1 \rfloor$ and implicitly assumed $a_1 \neq 1/2$ and $b_2 \neq 1/2$ by ignoring cases of equality in Equations 6.19-6.21. All other terms in Equation 6.18, being exponentially small, are discarded.

Note that the above approximation is $O(1)$ only when b is the iterate of a under the classical baker's map. Furthermore, a little algebra reveals that our semi-classical propagator may be rewritten in the Van Vleck form

$$\begin{aligned}\langle b|\hat{B}_{0,s}|a\rangle &= \sqrt{\frac{4}{5}}\exp\Big[\pi D\Big(\frac{1}{10}\left(3b^{*2} + 8ab^* - 3a^2\right) \\ &\qquad + \frac{4}{5}\big(1 + \frac{i}{2}\big)\big(a + ib^* - \frac{1}{2}\big)\lfloor a + a^* \rfloor\Big)\Big]\exp\Big[-\frac{\pi D}{2}\left(|a|^2 + |b|^2\right)\Big] \\ &= \sqrt{\frac{\partial^2 W}{\partial a \partial b^*}}\exp\Big[\pi D W(b^*, a)\Big]\exp\Big[-\frac{\pi D}{2}\left(|a|^2 + |b|^2\right)\Big],\end{aligned} \tag{6.28}$$

where $W(b^*, a)$ is Equation 5.3, the classical generating function. Hence we have shown that the class of quantum baker's map with $\theta = 0$ will approach the classical baker's map in the limit $D \to \infty$.

6.3 The classical limit of the $0 < \theta < 1$ Schack-Caves quantum baker's maps

We will now consider the case when $0 < \theta < 1$, $n = N\theta + s$. Here we define

$$2^n = 2^{N\theta}2^s = D^\theta 2^s \equiv D_\theta, \qquad 2^{N-n} = D^\phi 2^{-s} \equiv D_\phi.$$

The quantum baker's map, Equation 5.24, becomes

$$\begin{aligned}\hat{B}_{\theta,s} = \frac{1}{\sqrt{2}D_\phi} \sum_{x_1=0}^{1} \sum_{j,k=0}^{D_\phi-1} \sum_{l=0}^{2D_\phi-1} \sum_{m=0}^{D_\theta/2-1} \\ \times \left|e_l + e_m 2D_\phi - \frac{1}{D_\theta}\right\rangle\!\left\langle e_k + x_1/2 + e_m D_\phi - \frac{1}{2D_\theta}\right| \\ \times \exp\left[\pi i D D_\theta \left(e_j e_l + \frac{x_1 e_l}{D_\theta} - 2e_j e_k\right)\right].\end{aligned} \tag{6.29}$$

To clear things up a bit, we introduce new variables

$$q_l = e_l D/D_\phi, \quad q_j = e_j D/D_\phi, \quad q_k = e_k D/D_\phi, \quad q_m = e_m D/D_\theta. \tag{6.30}$$

This replacement smartens up Equation 6.29 to the form

$$\begin{aligned}\hat{B}_{\theta,s} = \frac{1}{\sqrt{2}D_\phi} \sum_{x_1=0}^{1} \sum_{j,k=0}^{D_\phi-1} \sum_{l=0}^{2D_\phi-1} \sum_{m=0}^{D_\theta/2-1} \left|\frac{q_l - 1}{D_\theta} + 2q_m\right\rangle\!\left\langle \frac{q_k - 1/2}{D_\theta} + q_m + \frac{x_1}{2}\right| \\ \times \exp\left[\pi i D_\phi \left(q_j q_l + x_1 q_l - 2q_j q_k\right)\right].\end{aligned}$$

Equation 4.31 then yields a rather long expression for the coherent state matrix element,

$$\begin{aligned}\left\langle b\middle|\hat{B}_{\theta,s}\middle|a\right\rangle = \frac{1}{\sqrt{D}D_\phi} \sum_{\mu,\nu=-\infty}^{\infty} \sum_{x_1=0}^{1} \sum_{j,k=0}^{D_\phi-1} \sum_{l=0}^{2D_\phi-1} \sum_{m=0}^{D_\theta/2-1} \\ \exp\Big[-\frac{\pi D}{2}\left(|a|^2 + |b|^2 - a^2 - b^{*2}\right) + i\pi(\mu - \nu) \\ - \pi D\left(D_\theta^{-1}(q_k - 1/2) + q_m + x_1/2 - a + \mu\right)^2 \\ - \pi D\left(D_\theta^{-1}(q_l - 1) + 2q_m - b^* + \nu\right)^2 \\ + \pi i D_\phi \left(q_j q_l + x_1 q_l - 2q_j q_k\right)\Big].\end{aligned} \tag{6.31}$$

To further the calculation, we again use the Poisson formula to replace the finite sums over q_j, q_k, q_l, q_m with integrals over the variables x, y, z, and t, respectively. This trick turns our matrix element expression into a bit of a monster,

$$\begin{aligned}\left\langle b\middle|\hat{B}_{\theta,s}\middle|a\right\rangle = \sqrt{D}D_\phi \sum_{\substack{\mu,\nu,\zeta,\tau \\ \gamma,\kappa=-\infty}}^{\infty} \sum_{x_1=0}^{1} \int_0^1 dx \int_0^1 dy \int_0^2 dz \int_0^{1/2} dt \\ \exp\Big[-\frac{\pi D}{2}\left(|a|^2+|b|^2-a^2-b^{*2}\right) + i\pi(\mu-\nu) \\ -\pi D\left(t+x_1/2-a+\mu\right)^2 - \pi D\left(2t-b^*+\nu\right)^2 \\ -2\pi D_\phi(y-1/2)(t+x_1/2-a+\mu) - 2\pi D_\phi(z-1)(2t-b^*+\nu) \\ -\pi D_\phi(y-1/2)^2/D_\theta - \pi D_\phi(z-1)^2/D_\theta \\ +\pi i D_\phi(xz+x_1z-2xy) \\ +\pi i(2D_\phi x-1)\zeta + \pi i(2D_\phi y-1)\tau + \pi i(2D_\phi z-1)\gamma + \pi i(2D_\phi t-1)\kappa\Big].\end{aligned} \tag{6.32}$$

The terms with highest power of D are those containing t. We can write them as

$$I_4 \equiv \int_0^{1/2} dt\, \exp\left[-\pi D\left(t+A\right)^2 - \pi D\left(2t+B\right)^2 - 2\pi D_\phi t C + 2\pi D_\theta t E\right], \tag{6.33}$$

where

$$\begin{aligned} A &= x_1/2 - a + \mu, \qquad & B &= -b^* + \nu, \\ C &= y - 1/2 + 2(z-1), \qquad & E &= i\kappa. \end{aligned} \tag{6.34}$$

We now approximate this integral using a variation on the method of steepest descents[4]. The third and fourth terms in I_4, with their lower dependence on D, alters this expression from that usually found in standard steepest descent formulae; however, we need to keep them to ensure that the entirety of the matrix element is

[4]When $\phi = 1$, the third term of the exponent in Equation 6.33 also becomes dominant and must be incorporated. Hence the need to consider this case separately in the previous section.

calculated[5]. The technique for approximating this integral will be the same as that shown in Figure 6.4. We deform the integration along the real line to steepest descent paths in the complex plane. The integrals along the contours C_1 and C_3 are again set to zero, thereby leaving us with

$$I_4 \approx \int_{-\infty+it'}^{\infty+it'} dt\, \exp\left[-\pi D\left(t+A\right)^2 - \pi D\left(2t+B\right)^2 - 2\pi D_\phi tC + 2\pi D_\theta tE\right], \quad (6.35)$$

which is a standard Gaussian integral. The condition for making this approximation is

$$0 < a_1 + 2b_1 - x_1/2 - \mu - 2\nu < \frac{5}{2}. \quad (6.36)$$

We shall return to this inequality later.

Using the Gaussian integration of Equation 6.35, we have

$$\begin{aligned}\left\langle b\middle|\hat{B}_{\theta,s}\middle|a\right\rangle \approx \frac{D_\phi}{\sqrt{5}} \sum_{\substack{\mu,\nu,\zeta,\tau \\ \gamma,\kappa=-\infty}}^{\infty} \sum_{x_1=0}^{1} \int_0^1 dx \int_0^1 dy \int_0^2 dz \\ \exp\Big[-\frac{\pi D}{2}\left(|a|^2+|b|^2-a^2-b^{*2}\right) + i\pi(\mu-\nu) - \frac{\pi D}{5}(2A-B)^2 \\ - \frac{\pi D_\phi}{5D_\theta}(2y-z)^2 - \frac{2\pi D_\phi}{5}(2y-z) + \pi i D_\phi(xz+x_1z-2xy) \\ - \frac{2\pi i}{5}(y+2z)\kappa - \frac{2\pi i D_\theta}{5}(A+2B)\kappa - \frac{\pi D_\theta}{5D_\phi}\kappa^2 \\ + 2\pi i D_\phi(x\zeta+y\tau+z\gamma)\Big].\end{aligned} \quad (6.37)$$

The repeated appearance of terms with the expression $2y - z$ suggests a change of variable may be advantageous. After some trial-and-error, the following change of variables is found to be best,

$$\begin{bmatrix} u \\ v \\ w \end{bmatrix} = \begin{bmatrix} 1 & -2 & 1 \\ 1 & 2 & -1 \\ 0 & 1 & 2 \end{bmatrix} \begin{bmatrix} x \\ y \\ z \end{bmatrix}. \quad (6.38)$$

[5]Ironically, these terms will be set to zero in the final analysis. A fact that could not be known *a priori*.

Here the fairly simple integration region of $(x, y, z) \in [0,1] \times [0,1] \times [0,2]$ must be replaced by the parallel-piped Ω.

After changing to these variables and making some simplifications, we write Equation 6.37 in a form useful for the method of steepest descent,

$$\begin{aligned}\left\langle b\middle|\hat{B}_{\theta,s}\middle|a\right\rangle = \frac{D_\phi}{10\sqrt{5}} \sum_{\substack{\mu,\nu,\zeta,\tau \\ \gamma,\kappa=-\infty}}^{\infty} \sum_{x_1=0}^{1} \iiint_{\Omega} du\, dv\, dw\, \exp\Big[-\pi D_\phi f(v) \\ - \pi D_\phi g(u) - \frac{\pi D_\phi}{20 D_\theta}(v-u)^2\Big] F(w),\end{aligned} \tag{6.39}$$

where

$$\begin{aligned} f(v) &= \frac{i}{4}v^2 + (C - i\zeta)v, \\ g(u) &= -\frac{i}{4}u^2 - (C + i\zeta)u, \\ C &= \frac{1}{5}(2A - B) + \frac{ix_1}{10} - \frac{2i}{5}(\tau - \gamma/2) \equiv C_1 + iC_2, \\ F(w) &= \exp\left[\frac{2\pi i}{5} w \left(D_\phi(x_1 + \tau + 2\gamma) - \kappa\right)\right]. \end{aligned} \tag{6.40}$$

We'll start our steepest descent program by looking at the function $g(u)$. If we write u as $u_1 + iu_2$, we see that

$$g(u) = \frac{1}{2}u_1u_2 - C_1u_1 + (\zeta + C_2)u_2 + i\left(-\frac{1}{4}u_1^2 + \frac{1}{4}u_2^2 - (C_2 + \zeta)u_1 - C_1u_2\right). \tag{6.41}$$

The contours on which the imaginary part of g is constant are hyperbolae. We wish to find those contours which pass through its saddle point. A trivial calculation shows that the saddle point, u', is located at

$$u' \equiv u_1 + iu_2 = -2(\zeta + C_2) + i2C_1, \tag{6.42}$$

and that the saddle point contours are given by

$$u_1 - u_1' = \pm(u_2 - u_2'), \tag{6.43}$$

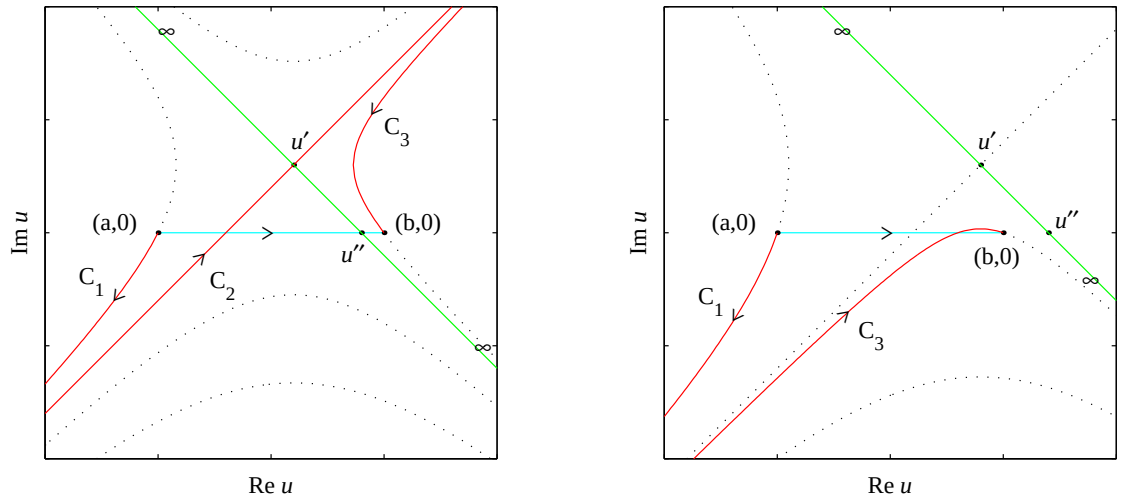

Figure 6.5: Two possible steepest descent paths. Only the first allows for inclusion of the saddle point.

which are the asymptotes of our steepest descent hyperbolae.

Looking at the real part of Equation 6.41, we see that along the line $u_1 - u_1' = -u_2 + u_2'$,

$$\mathrm{Re}\left(g(u)\right) = -1/2u_1^2 + \ldots \Rightarrow \exp\left[-\pi D_\phi \,\mathrm{Re}\left(g(u)\right)\right] \to \infty.$$

We shall refer to this contour as the ∞-asymptote[6]. Along the other line, $u_1 - u_1' = u_2 - u_2'$, we have

$$\exp\left[-\pi D_\phi \,\mathrm{Re}\left(g(u)\right)\right] \to 0.$$

To have a finite valued integration, we must integrate along this line.

The ∞-asymptote is not useless. As Figure 6.5 shows, this asymptote determines when the contribution from the saddle point is included. Whenever the ∞-asymptote passes through the real line integration region $[a, b]$, our steepest descent contours

[6]In figure 6.5, the ∞-asymptote is depicted in green.

include the saddle point. This occurs at the point $(u_1'', 0)$ where

$$u_1'' - u_1' = 0 + u_2' \Rightarrow u_1'' = u_1' + u_2'.$$

This last statement implies

$$a < u_1' + u_2' = 2(C_1 - C_2 - \zeta) < b. \tag{6.44}$$

The importance of the inequality is not clear yet. We shall return to it shortly.

Looking at Equation 6.40, we see that the function $f(v)$ is very similar to $g(u)$. It therefore should come as no surprise that the analysis is the same; the only differences are the position of the saddle point, $v' = 2(\zeta - C_2) + i2C_1$, and the equation for the saddle point asymptotes. In this case, the saddle point will be included provided that the ∞-asymptote, $v_1 - v_1' = v_2 - v_2'$ in this case, passes through the real line segment $[c, d]$; thus,

$$c < v_1' - v_2' = 2(\zeta - C_1 - C_2) < d. \tag{6.45}$$

But what are these mysterious points a, b, c, d? Unfortunately given the nature of the variable change, their values differ as one integrates over the volume element Ω. We must convert back to our original variables x, y, z. We do this by inverting the matrix in Equation 6.38. We see the following,

$$\begin{array}{rclcrcl} u'' & = & 2(C_1 - C_2 - \zeta) & & x'' & = & -2C_2 \\ v'' & = & 2(\zeta - C_2 - C_1) & \Rightarrow & y'' & = & \frac{4}{5}(\zeta - C_1) + \frac{1}{5}w \\ w'' & = & w & & z'' & = & -\frac{2}{5}(\zeta - C_1) + \frac{2}{5}w \end{array} , \tag{6.46}$$

where we have left the for now unrestricted variable w unchanged.

Given the independent integration ranges for x, y, z, the restrictions of Equations 6.44 and 6.45 become

$$0 < x'' < 1$$

$$0 < y'' < 1$$

$$0 < z'' < 2.$$

Using Equations 6.46 and 6.40, we can rewrite this as

$$\begin{aligned} 0 &< \frac{2}{5}(2a_2 + b_2) - \frac{1}{5}x_1 + \frac{4}{5}(\tau - \frac{1}{2}\gamma) < 1, \\ 0 &< \frac{4}{5}(\zeta - C_1) + \frac{1}{5}w < 1, \\ 0 &< -\frac{2}{5}(\zeta - C_1) + \frac{2}{5}w < 2. \end{aligned} \tag{6.47}$$

These last two expression restrict the values of w. Simply rewriting them gives

$$\begin{aligned} \zeta - C_1 < w < 5 + \zeta - C_1, \\ -4(\zeta - C_1) < w < 5 - 4(\zeta - C_1). \end{aligned}$$

This means that w is restricted to values $w_b < w < 5 + w_s$ where

$$w_b \equiv \max\Big(\zeta - C_1, -4(\zeta - C_1)\Big).$$

Similarly, w_s is the min of the previous expression. If $\zeta - C_1$ is positive, then it is necessarily true that $w_b = \zeta - C_1$; therefore,

$$\zeta - C_1 < w < 5 - 4(\zeta - C_1) \Rightarrow \zeta - C_1 < 1.$$

Similarly, if $\zeta - C_1$ is negative, then $w_b = -4(\zeta - C_1)$, such that

$$-4(\zeta - C_1) < w < 5 + (\zeta - C_1) \Rightarrow \zeta - C_1 > -1.$$

Combining these two conditions together gives another restriction,

$$-1 < \zeta - C_1 < 1. \tag{6.48}$$

Having learned all we can about the restrictions placed upon our variables by the finiteness of their integration, we can now proceed to finding the asymptotic form of the integrals over u and v. Given the form of Equation 6.39, we again use the variation of the steepest descent technique employed when integrating over t. After

much algebraic simplification, we find the following

$$\begin{aligned}\langle b|\hat{B}_{\theta,s}|a\rangle \approx \frac{1}{5}\sqrt{\frac{4}{5}} \sum_{\substack{\mu,\nu,\zeta,\tau \\ \gamma,\kappa=-\infty}}^{\infty} \sum_{x_1=0}^{1} \int_{w_b}^{5+w_s} dw \, \exp\Big[\big(|a|^2+|b|^2-a^2-b^2\big) \\ - i\pi\left(\zeta+\tau+\gamma-\mu+\nu\right) - \frac{\pi D}{5}\left(2A-B\right)^2 - \frac{\pi D_\theta}{5D_\phi}\kappa^2 \\ - \frac{2\pi i D_\theta}{5}\left((A+2B)\kappa\right) - \frac{2\pi i}{5}w\left(\kappa - D_\phi(x_1+\tau+2\gamma)\right) - \frac{4D_\phi}{5D_\theta}\pi\zeta^2 \\ - 4\pi D_\phi \zeta C\Big].\end{aligned} \tag{6.49}$$

Looking at Equations 6.36, 6.47, and 6.48, we see that currently there are no restrictions placed on the sum over κ. However, by doing the integration over w it is revealed that there are only certain values of κ that yield non-zero matrix elements,

$$\begin{aligned}&\int_{w_b}^{5+w_s} dw \, \exp\Big[-\frac{2\pi i}{5}w\left(\kappa - D_\phi(x_1+\tau+2\gamma)\right)\Big] \\ &= \frac{5i}{2\pi\left(\kappa - D_\phi(x_1+\tau+2\gamma)\right)}\Big[\exp[-\frac{2\pi i}{5}w\left(\kappa - D_\phi(x_1+\tau+2\gamma)\right)]\Big]_{w_b}^{5+w_s}.\end{aligned} \tag{6.50}$$

This expression goes to zero like $1/D_\phi$ unless

$$\kappa = D_\phi(x_1+\tau+2\gamma);$$

therefore, we have

$$\begin{aligned}\langle b|\hat{B}_{\theta,s}|a\rangle \approx \frac{1}{5}\sqrt{\frac{4}{5}} \sum_{\substack{\mu,\nu,\zeta,\tau \\ \gamma=-\infty}}^{\infty} \sum_{x_1=0}^{1} (5+w_s-w_b) \exp\Big[-\frac{\pi D}{2}\big(|a|^2+|b|^2-a^2-b^2\big) \\ - i\pi\left(\zeta+\tau+\gamma-\mu+\nu\right) - \frac{\pi D}{5}\left(2A-B\right)^2 - \frac{\pi D}{5}\left(x_1+\tau+2\gamma\right)^2 \\ - \frac{2\pi i D}{5}(A+2B)(x_1+\tau+2\gamma) - \frac{4D_\phi}{5D_\theta}\pi\zeta^2 - 4\pi D_\phi\zeta C\Big].\end{aligned} \tag{6.51}$$

Using the definitions of A and B from Equation 6.34, we see that

$$2A - B = x_1 - 2a + 2\mu + b^* - \nu,$$

$$A + 2B = \frac{1}{2}x_1 - a + \mu - 2b^* = 2\nu.$$

Writing the real and imaginary parts of our variables $a = a_1 + ia_2$, $b = b_1 + ib_2$, we can gather all terms which have leading power D and write them as

$$\begin{aligned}
&\frac{1}{5}\left(2a_1 - b_1 - x_1 - 2\mu + \nu\right)^2 + \frac{1}{5}\left(a_2 - 2b_2 + x_1 + \tau + 2\gamma\right)^2 \\
&+ \frac{i}{5}\left(3a_1a_2 + 3b_1b_2 + 4a_1b_2 - 4a_2b_1\right) \\
&+ \frac{2i}{5}\left(x_1/2 - a_1 + \mu - 2b_1 + 2\nu\right)\left(x_1 + \tau + 2\gamma\right) - \frac{2i}{5}\left(b_2 + 2a_2\right)\left(x_1 + 2\mu - \nu\right).
\end{aligned} \tag{6.52}$$

Both of these Gaussians decay rapidly. The matrix element will be $O(1)$ when

$$b_1 = 2a_1 - x_1 - 2\mu + \nu, \tag{6.53}$$

$$b_2 = a_2/2 - x_1/2 + \tau/2 + \gamma. \tag{6.54}$$

In this case, our restriction from the first integration, Equation 6.36, becomes

$$0 < a_1 - x_1/2 - \mu < \frac{1}{2}. \tag{6.55}$$

Given that a_1 is defined on the interval $[0, 1]$, this inequality implies that $\mu = 0$. We also know that b_1 is restricted to the same interval; therefore, Equation 6.53 implies

$$0 \leq 2a_1 - x_1 + \nu \leq 1, \tag{6.56}$$

so that $\nu = 0$ as well.

Combining Equation 6.54 with the inequality from Equation 6.47 gives

$$0 < a_2 + \tau < 1 \Rightarrow \tau = 0. \tag{6.57}$$

A similar argument with $0 \leq b_2 \leq 1$ gives

$$0 \leq a_2/2 + x_1/2 + \gamma \leq 1, \tag{6.58}$$

implying that $\gamma = 0$. Finally, Equation 6.48 gives[7]

$$-5 < 5\zeta + 2a_1 - b_1 - x_1 < 5. \tag{6.59}$$

Using Equation 6.53, we see that $\zeta = 0$ as well.

When all of the summing variables have been set to zero, we get the conditions

$$\begin{aligned} \frac{1}{2}x_1 < \quad a_1 \quad &< \frac{1}{2} + \frac{1}{2}x_1, \\ 0 < \quad a_2 \quad &< 1. \end{aligned}$$

The first of those means that $x_1 = \lfloor 2a_1 \rfloor$.

As a final note, we see that $w_b - w_s = 5|C_1| = b_1 - 2a_1 + x_1$ which we shall set to 0 given Equation 6.53. Using all of these facts in Equation 6.51, we arrive at our final answer,

$$\begin{aligned} \langle b|\hat{B}_{\theta,s}|a\rangle &= \sqrt{\frac{4}{5}} \exp\Big[-\frac{\pi D}{5}\Big((2a_1 - b_1 - \lfloor 2a_1 \rfloor)^2 + (a_2 - 2b_2 + \lfloor 2a_1 \rfloor)^2 \\ &\qquad + i(3a_1a_2 + 3b_1b_2 + 4a_1b_2 - 4a_2b_1) \\ &\qquad - 2i\lfloor 2a_1 \rfloor \big(a_1 + 2b_1 + 2a_2 + b_2 - \lfloor 2a_1 \rfloor/2\big)\Big)\Big] \\ &= \sqrt{\frac{4}{5}} \exp\Big[-\frac{\pi D}{2}\left(|a|^2 + |b|^2\right) + \pi D W(b^*, a)\Big], \end{aligned} \tag{6.60}$$

where once again $W(b^*, a)$ is Equation 5.3, the generating function for the classical baker's map. We see that for $0 < \theta < 1$, the semi-classical propagator also takes the Van Vleck form; thus, the classical baker's map will be recovered in the limit $D \to \infty$.

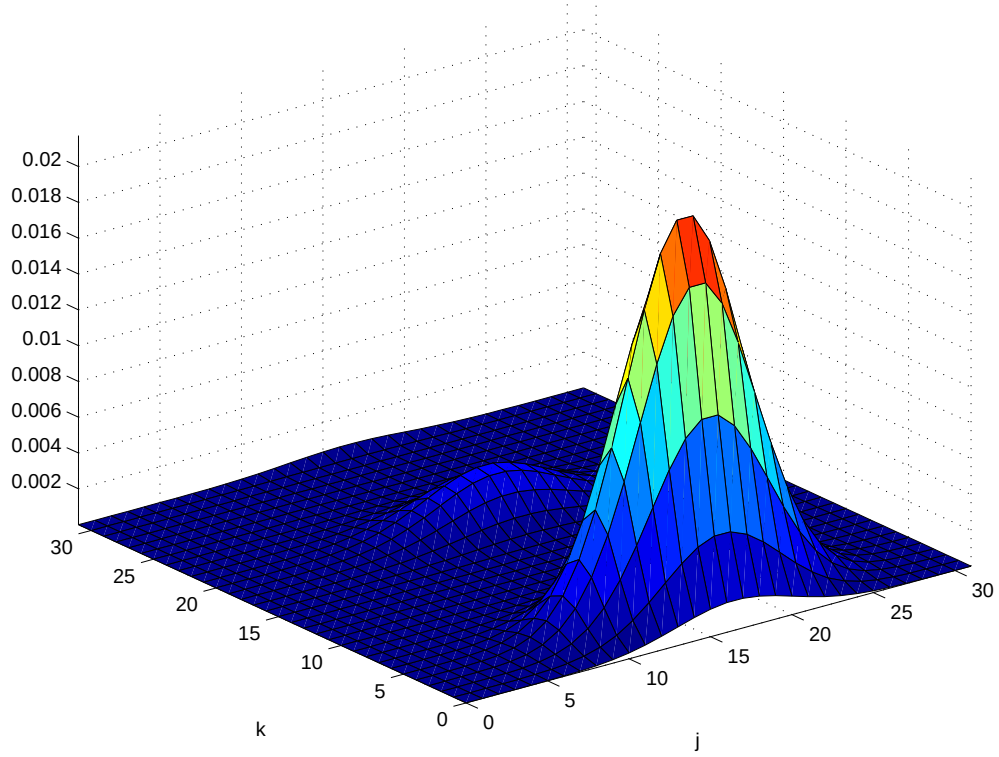

Figure 6.6: The Q-function in 32 dimensions of the $\hat{B}_5$ operator acting upon the $a = 1/4 + i/4$ coherent state.

6.4 The classical limit of the $\theta = 1$ Schack-Caves quantum baker's map

In Chapter 5, it was seen that the eigenvalues of the $\hat{B}_N$ Schack-Caves baker's map are significantly different from those of the rest of the maps. It should come as no surprise that the classical limit of this map is different as well. Figures 6.6 and 6.7 show the Q-function for the $\hat{B}_5$ map acting on the $a = 1/4 + i/4$ and $a = 3/4 + i/4$ coherent states respectively. Unlike Figures 6.1 and 6.2, these Q-functions for the

[7] After using the fact that $C_1 = 1/5(b_1 - 2a_1 + x_1)$.

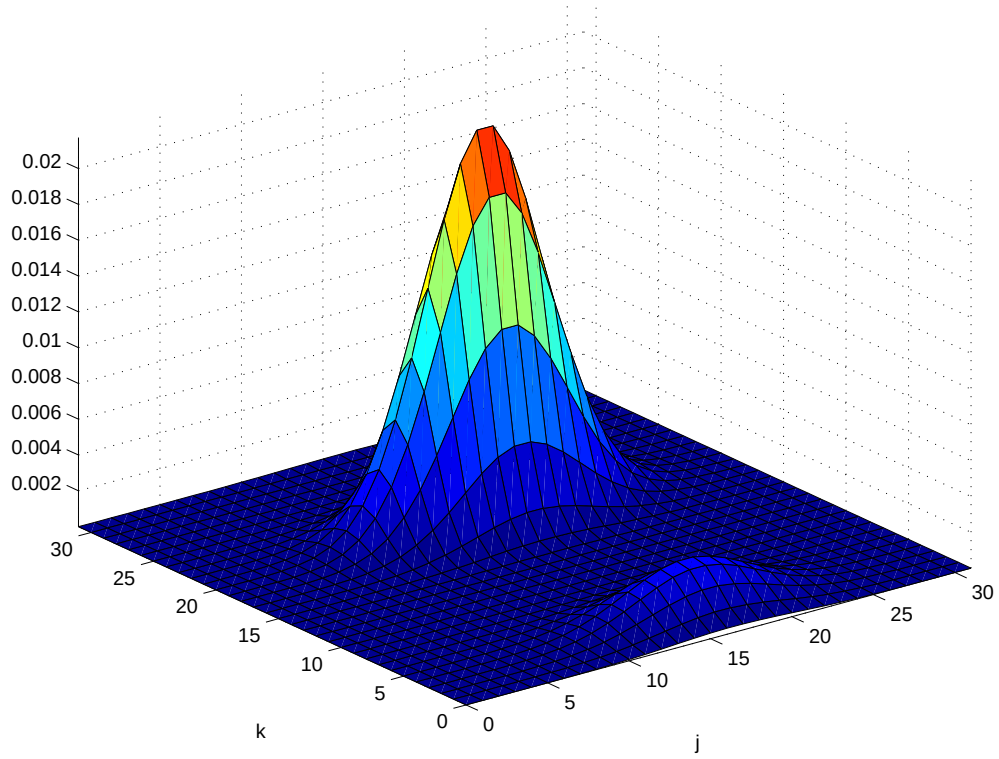

Figure 6.7: The Q-function in 32 dimensions of the $\hat{B}_5$ operator acting upon the $a = 3/4 + i/4$ coherent state.

mapped states have two "humps." One hump is centered at the correct point, while the other is centered at the point specified by the other half of the classical baker's map. While this behavior is not alarming *a priori* since the extra hump could vanish in the classical limit, we shall see in the forthcoming analysis that these humps do not, in fact, disappear in the classical limit. Therefore, this map cannot be said to have the correct limit.

Technically, this map must be treated separately because an assumption made in the previous section is no longer true. In particular, in Equation 6.37, we have taken the terms with prefactor D^{ϕ} as dominate. This clearly cannot now be the case

as $\phi = 0$. We must repeat the analysis taking the correct dominant terms. To this end, we shall assume that $n = N - r$ where r is constant. This allows us to study the map which has a fixed number of momentum bits r,

$$\hat{B}_{1,-r}\big|a_r \dots a_1 \bullet x_1 x_2 \dots x_{N-r}\big\rangle = \big|a_r \dots a_1 x_1 \bullet x_2 \dots x_{N-r}\big\rangle. \tag{6.61}$$

We see that in this case $2^n = D2^{-r}$ which for ease of reading we shall call D/R such that $R = 2^r$. Using Equation 5.24, we have

$$\begin{aligned}\hat{B}_{1,-r} = \frac{\sqrt{2}}{R}\sum_{x_1=0}^{1}\sum_{j,k=0}^{R-1}\sum_{l=0}^{2R-1}\sum_{m=0}^{D/(2R)-1}\Big|e_l + 2Re_m - \frac{R}{D}\Big\rangle\Big\langle e_k + x_1/2 + Re_m - \frac{R}{2D}\Big| \\ \times \exp\Big[\frac{\pi i D^2}{R}\Big(e_j e_l + R/D x_1 e_l - 2e_j e_k\Big)\Big].\end{aligned} \tag{6.62}$$

We are now set to find the matrix element:

$$\begin{aligned}\big\langle b\big|\hat{B}_{1,-r}\big|a\big\rangle = \frac{1}{\sqrt{D}R}\sum_{\mu,\nu=-\infty}^{\infty}\sum_{x_1=0}^{1}\sum_{j,k=0}^{R-1}\sum_{l=0}^{2R-1}\sum_{m=0}^{D/(2R)-1}\exp\Big[-\frac{\pi D}{2}\Big(|a|^2 + |b|^2 - a^2 - b^{*2}\Big) \\ + i\pi\Big(\mu - \nu\Big) - \pi D\Big(Re_m + x_1/2 - a + \mu + \frac{(k + 1/2 - R/2)}{D}\Big)^2 \\ - \pi D\Big(2Re_m - b^* + \nu + \frac{(l + 1/2 - R)}{D}\Big)^2 \\ + \pi i\Big(\frac{1}{R}(j + 1/2)(l + 1/2) + x_1(l + 1/2) - \frac{2}{R}(j + 1/2)(k + 1/2)\Big)\Big].\end{aligned} \tag{6.63}$$

Using the Poisson formula again, we replace the finite sum over the variable m with an integral over the interval $[0, (2R)^{-1}]$. It will be advantageous to quickly do a change of variable such that the integration interval will be $[0, 1/2]$. Having done

this and made some algebraic simplifications, the matrix element expression becomes

$$\begin{aligned}\langle b|\hat{B}_{1,-r}|a\rangle = \frac{\sqrt{D}}{R^2}\sum_{\mu,\nu,\kappa=-\infty}^{\infty}\sum_{x_1=0}^{1}\sum_{j,k=0}^{R-1}\sum_{l=0}^{2R-1}\int_0^{1/2} dy\,\exp\Big[-\frac{\pi D}{2}\Big(|a|^2+|b|^2-a^2-b^{*2}\Big)\\ +i\pi\Big(\mu-\nu-\kappa\Big)+\frac{2\pi i D}{R}y\kappa-\pi D\Big(y+x_1/2-a+\mu\Big)^2\\ -\pi D\Big(2y-b^*+\nu\Big)^2-2\pi\Big(y+x_1/2-a+\mu\Big)\Big(k+1/2-R/2\Big)\\ -2\pi\Big(2y-b^*+\nu\Big)\Big(l+1/2-R\Big)+\pi i\Big(\frac{1}{R}(j+1/2)(l+1/2)\\ +x_1(l+1/2)-\frac{2}{R}(j+1/2)(k+1/2)\Big)\Big].\end{aligned} \tag{6.64}$$

We will now do the method of steepest descent again on the following integral

$$\int_0^{1/2} dy\, f(y)\exp\Big[-\pi D g(y)\Big]$$

where

$$g(y)=\Big(y+x_1/2-a+\mu\Big)^2+\Big(2y-b^*+\nu\Big)^2-\frac{2iy\kappa}{R}, \tag{6.65}$$

$$\begin{aligned}f(y)=\exp\Big[&-2\pi\Big(y+x_1/2-a+\mu\Big)\Big(k+1/2-R/2\Big)\\ &-2\pi\Big(2y-b^*+\nu\Big)\Big(l+1/2-R\Big)\Big].\end{aligned} \tag{6.66}$$

After using the steepest descent formula, Equation A.3, we get

$$\begin{aligned}\langle b|\hat{B}_{1,-r}|a\rangle = \frac{1}{\sqrt{5}R^2}\sum_{\mu,\nu,\kappa=-\infty}^{\infty}\sum_{x_1=0}^{1}\sum_{j,k=0}^{R-1}\sum_{l=0}^{2R-1}\exp\Big[-\frac{\pi D}{2}\Big(|a|^2+|b|^2-a^2-b^{*2}\Big)\\ +i\pi\Big(\mu-\nu-\kappa\Big)-\frac{\pi D}{5}\Big(2A-B\Big)^2-\frac{2\pi i D\kappa}{5R}\Big(A+2B\Big)-\frac{\pi D\kappa^2}{5R^2}\\ -\frac{2\pi}{5}\Big(2(2A-B)+\frac{i\kappa}{R}\Big)\Big(k+1/2-R/2\Big)\\ -\frac{2\pi}{5}\Big(-(2A-B)+\frac{2i\kappa}{R}\Big)\Big(l+1/2-R\Big)\\ +\pi i\Big(\frac{1}{R}(j+1/2)(l+1/2)+x_1(l+1/2)-\frac{2}{R}(j+1/2)(k+1/2)\Big)\Big]\end{aligned} \tag{6.67}$$

where

$$A = x_1/2 - a + \mu \qquad B = -b^* + \nu.$$

The restriction for using this approximation is

$$0 < a_1 - x_1/2 - \mu + 2b_1 - 2\nu < \frac{5}{2}, \tag{6.68}$$

where again $a = a_1 + ia_2$ and $b = b_1 + ib_2$.

Now we use tricks similar to last time. We gather the leading terms of the matrix element and write out the real and imaginary parts. We find

$$\begin{aligned}
&\frac{1}{2}\Big(|a|^2 + |b|^2 - a^2 - b^{*2}\Big) + \frac{1}{5}\Big(2A - B\Big)^2 + \frac{2i\kappa}{5R}\Big(A + 2B\Big) + \frac{\kappa^2}{5R^2} \\
&= \frac{1}{5}\Big(b_1 - 2a_1 + x_1 + 2\mu - \nu\Big)^2 + \frac{1}{5}\Big(a_2 - 2b_2 + \frac{\kappa}{R}\Big)^2 \\
&\quad + \frac{i}{5}\Big(3a_1a_2 + 3b_1b_2 + 4a_1b_2 - 4a_2b_1\Big) - \frac{2i}{5}\Big(b_2 + 2a_2\Big)\Big(x_1 + 2\mu - \nu\Big) \\
&\quad + \frac{2i\kappa}{5R}\Big(x_1/2 - a_1 + \mu - 2b_1 + 2\nu\Big).
\end{aligned} \tag{6.69}$$

Once again, we have two rapidly decaying Gaussians. The matrix element is $O(1)$ when

$$b_1 = 2a_1 - x_1 - 2\mu + \nu \quad \text{and} \quad b_2 = \frac{1}{2}a_2 + \frac{\kappa}{2R}.$$

Equation 6.68 along with the range of a_1 values, implies that $\mu = \nu = 0$; thus, we arrive at the following semi-classical approximation for our propagator

$$\begin{aligned}
\big\langle b\big|\hat{B}_{1,-r}\big|a\big\rangle = \frac{1}{\sqrt{5}R^2}\sum_{\kappa=-\infty}^{\infty}\sum_{j,k=0}^{R-1}\sum_{l=0}^{2R-1} \exp\Bigg[&-\frac{\pi D}{5}\Big\{\big(2a_1 - b_1 - \lfloor 2a_1\rfloor\big)^2 \\
&+ \big(a_2 - 2b_2 + \kappa/R\big)^2 + i\big(3a_1a_2 + 3b_1b_2 + 4a_1b_2 - 4a_2b_1\big) \\
&- 2i\kappa\big(a_1 + 2b_1 - \lfloor 2a_1\rfloor/2\big)/R - 2i\lfloor 2a_1\rfloor\big(2a_2 + b2\big)\Big\} \\
&+ \frac{2\pi}{5}\big(2a - b^* - \lfloor 2a_1\rfloor\big)\big(2k - l + 1/2\big) - \frac{2i\pi}{5R}\big(k + 2l + 3/2\big)\kappa \\
&+ \frac{i\pi}{R}\Big\{\big(j + 1/2\big)\big(l + 1/2\big) + R\lfloor 2a_1\rfloor\big(l + 1/2\big) - 2\big(j + 1/2\big)\big(k + 1/2\big)\Big\}\Bigg]
\end{aligned}$$

The only restriction for the value of κ is that a_2 must be in the $(0,1)$ range; therefore,

$$b_2 = \frac{1}{2}a_2 + \frac{\kappa}{2R}, \quad -Ra_2 < \kappa < R(2-a_2). \tag{6.70}$$

Setting $\mu = \nu = 0$, we have that

$$b_1 = 2a_1 - x_1. \tag{6.71}$$

Substituting these facts, Equation 6.68 becomes

$$\frac{1}{2}x_1 < a_1 < \frac{1}{2} + \frac{1}{2}x_1$$

such that $x_1 = \lfloor 2a_1 \rfloor$.

The consequence of Equation 6.70 is the additional humps in momentum seen in Figures 6.6 and 6.7. In general, in the region $0 < b_1, b_2 < 1$, there will be $2R$ humps at the points defined by Equations 6.71 and 6.70.

For the simplest case, when $r = 0$, our semi-classical propagator is

$$\begin{aligned}\langle b|\hat{B}_{1,0}|a\rangle = \sqrt{\frac{4}{5}}\sum_{\kappa=0}^{1} \exp\Big[-\frac{\pi D}{5}\Big\{ \big(2a_1 - b_1 - \lfloor 2a_1 \rfloor\big)^2 + \big(a_2 - 2b_2 + \kappa\big)^2 \\ + i\big(3a_1a_2 + 3b_1b_2 + 4a_1b_2 - 4a_2b_1\big) - 2i\kappa\big(a_1 + 2b_1 - \lfloor 2a_1 \rfloor/2\big) \\ - 2i\lfloor 2a_1 \rfloor\big(2a_2 + b_2\big)\Big\} + i\pi\big(\lfloor 2a_1 \rfloor - \kappa\big)\Big] \\ \cos\left[\frac{i\pi}{5}\big(2a - b^* - \lfloor 2a_1 \rfloor\big) + \frac{\pi}{2}\big(\lfloor 2a_1 \rfloor + 1/2\big) - \frac{2\pi}{5}\kappa\right].\end{aligned} \tag{6.72}$$

This defines the two humps: one at a position specified by the classical baker's map,

$$(b_1, b_2) = \left(2a_1 - \lfloor 2a_1 \rfloor, \frac{a_2 + \lfloor 2a_1 \rfloor}{2}\right),$$

with an asymptotic size of

$$\big|\langle b(a)|\hat{B}_{1,0}|a\rangle\big|^2 = \frac{4}{5}\cos^2\left[\frac{\pi}{2}\big(a_2 - 1/2\big)\right]. \tag{6.73}$$

The other hump is located at the point specified by the other "half" of the classical baker's map, *i.e.* at the point

$$(b_1, b_2) = \left(2a_1 - \lfloor 2a_1 \rfloor, \frac{a_2 + 1 - \lfloor 2a_1 \rfloor}{2}\right).$$

It has asymptotic size

$$\left|\langle b(a)|\hat{B}_{1,0}|a\rangle\right|^2 = \frac{4}{5}\sin^2\left[\frac{\pi}{2}\big(a_2 - 1/2\big)\right]. \tag{6.74}$$

One interpretation of these equations could be that a *stochastic* mapping is implied in the classical limit: a point at (a_1, a_2) has the probability $\cos^2[\pi(a_2 - 1/2)/2]$ of obeying the classical baker's map, and probability $\sin^2[\pi(a_2 - 1/2)/2]$ of ending up at $(2a_1 - \lfloor 2a_1 \rfloor, (a_2 + 1 - \lfloor 2a_1 \rfloor)/2)$. Notice that there is now a smooth transition of probabilities as one crosses the lines $a_2 = 0, 1$.

Consider the size of our probabilistic humps in the general case. If we set $(b_1, b_2) = (2a_1 - \lfloor 2a_1 \rfloor, (a_2 + \kappa/R)/2)$, with κ fixed, then

$$\langle b(a)|\hat{B}_{1,-r}|a\rangle = \sqrt{\frac{4}{5}}\,\exp\left[\frac{i\pi D}{2R}\Big(2a_1\kappa + R\lfloor 2a_1\rfloor a_2 - \lfloor 2a_1\rfloor\kappa\Big)\right]\Psi_\kappa(a) \tag{6.75}$$

where

$$\Psi_\kappa(a) = \frac{1}{2R^2}\sum_{j=0}^{R-1}\frac{\cos^2\left[\pi R a_2\right]}{\sin\left[\pi\Big(a_2 - (j+1/2)/R\Big)\right]\sin\left[\frac{\pi}{2}\Big(a_2 - \lfloor 2a_1\rfloor + \kappa/R - \dfrac{j+1/2}{R}\Big)\right]}. \tag{6.76}$$

The probability associated with each hump is given by Ψ_κ^2, with $\sum_{\kappa=0}^{2R-1}\Psi_\kappa^2 = 1$, and is plotted for $r = 2$ in Fig. 6.8(a). The curve with the largest probabilities is that associated with the "correct" hump prescribed by the classical baker's map ($\kappa' = \lfloor 2a_1\rfloor R$). It takes maximum values of unity whenever $a_2 = (m + 1/2)/R$ ($0 < m < R - 1$), and as R becomes large, $\Psi_{\kappa'}^2 \to 1$ for all $0 < a_2 < 1$. Hence, as expected, we are left with a single hump located at the correct position. In figures 6.8(c) and (d), we have drawn the function $|\langle b|\hat{B}|a\rangle|^2$ and its semi-classical approximation (6.70), respectively, when $a = 3/4 + i/20$, $r = 2$ and $N = 8$. For such a

large dimension, $D = 2^8$, our semi-classical approximation becomes almost identical to the exact matrix element. One may also view our semi-classical propagator as an approximation to the Husimi function for the mapped state $\hat{B}|a\rangle$.

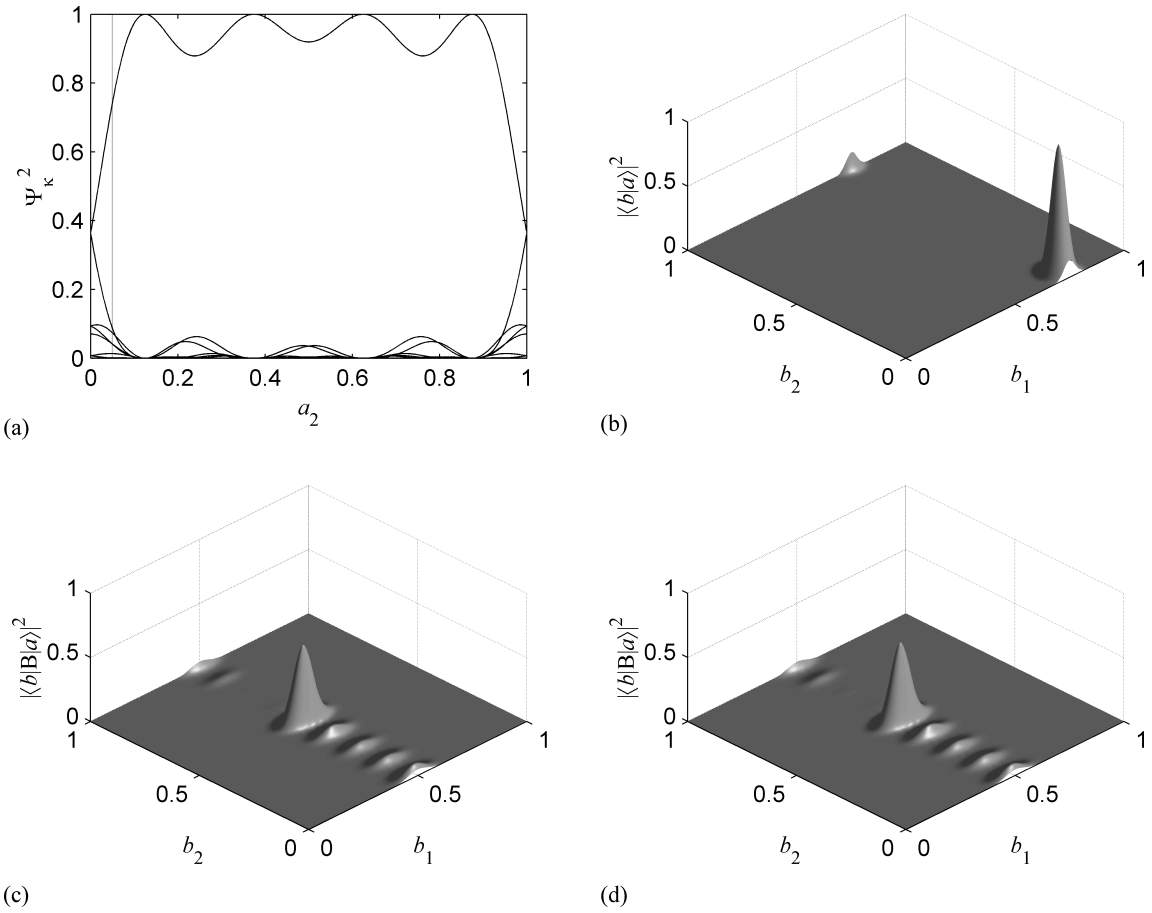

Figure 6.8: (a) The probabilities Ψ_κ^2 when $r = 2$. The Husimi functions of (b) the initial state $|a\rangle$ ($a = 3/4 + i/20$), (c) its mapping $\hat{B}|a\rangle$, and (d) our semi-classical approximation (6.70), when $r = 2$ and $N = 8$. The humps have the height $\frac{4}{5}\Psi_\kappa^2$ with $a_2 = 1/20$ (gray line in (a)).

Chapter 7

Conclusion

7.1 Summary of results

In this work, we have explored the transition from the quantum realm to the classical one. Using a favorite "toy" mapping from classical chaos, the baker's map, we have explored the boundary between the two realms in hopes of finding a general procedure for taking the classical limit. It was our hope that for the admittedly non-physical baker's map, the classical limit could be found without introducing extraneous elements like a decohering environment or resorting to a coarse graining program. Of course, one may argue that coarse graining and limit taking are equally mathematical[1] , but in such a pure system, one would like to recover classical behavior in the $\hbar \to 0$ limit.

Obviously before the classical limit program could be started, certain mathematical tools needed to be developed. We began in Chapter 2 with introducing the phase space for our finite-dimensional Hilbert space, $\mathcal{H}_D$. The fundamental objects

[1]Others would argue that the net effect of taking the classical limit is a coarse graining over phase space.

that this thesis is based on were the position eigenstates, $\left|e_j\right\rangle$. From them and the discrete Fourier transform, we created the momentum eigenstates, $\left|p_k\right\rangle$. Of course our choice of which eigenstates to start with was entirely arbitrary, but as position holds a special place in most physicists' hearts, we chose to label them as such.

Once the position and momentum eigenstates were established, we were able to create the phase space for our finite-dimensional Hilbert space. The position and momentum displacement operators allows one to associate an eigenvalue to each position and momentum eigenstate. From them, we construct our phase space as a grid of D^2 points each corresponding to a pair of position-momentum eigenvalues. When our coherent states were introduced in Chapter 4, we found it necessary to extend the phase space to all points in the QP area rectangle. Our original phase space grid is a sampling of this rectangle at the points $x = Q(j + \beta)/D$, $p = P(k + \alpha)/D$. This switching between a finite grid and a continuous set of points can be a little confusing, but as it is sometimes necessary to increase the resolution of a Q-function plot, it is seen as a necessary evil.

After defining the phase space, we then introduced the symmetry operations acting in this space. These operators would be paramount in explaining the form of the finite-dimensional Wigner function; therefore, they were given a context free introduction. The displacement, Fourier transform, and time reversal operators were all defined through their action upon the position eigenstates. Afterwards, the operators' action upon the momentum eigenstates was found using the discrete Fourier transform. Demanding that the result of these operations upon the momentum eigenstates be another eigenstate allowed us to infer a geometrical interpretation for these operators. As with the continuous case, the Fourier transform was found to be ninety degree rotation in the phase plane, while time reversal was found to be reflection through the position axis. Unfortunately, these definitions were valid only for the periodic and anti-periodic boundary conditions; therefore, these two bound-

ary conditions became the focus for the rest of the thesis. It was then shown that all other symmetry operations could be performed using combinations of Fourier transform and time reversal; it was unnecessary to consider any other operators.

In Chapter 3, a finite-dimensional Wigner function was found. There has been much research done on finding such a quasi-distribution, therefore the chapter began with a summary of the previous work. It was pointed out that there have been repeated discoveries of a function that would behave like the Wigner function in finite dimensions[2]; hence, the humorous title of that section. Our derivation of the Wigner function relied on the relationship between the finite-dimensional Hilbert space and the subspace of doubly periodic functions. Any wavefunction can be expanded in either the position or momentum basis with a simple relationship between each bases' expansion coefficients. We showed that this relationship had the same form in both $\mathcal{H}_D$ and for the doubly periodic functions; therefore, we could create an isomorphism from one space to the other. To make this isomorphism mathematically rigorous, we found it necessary to introduce windowing functions and perform some rather tedious analysis to prove they behaved correctly. Luckily, we found that the simple non-windowing form of the isomorphism produced a valid Wigner function, thus making a harder calculation unnecessary.

Once the isomorphism was established, we could find the characteristic function for a state in $\mathcal{H}_D$. We found it to be a discrete function which meant that it could be simply interpreted in the finite-dimensional Hilbert space as the expectation value of the symmetrically ordered displacement operator. Previous work on the finite Wigner function had used such an operator, so it was reassuring to find that we were going to have a similar form for our function. To find our Wigner function, it was then necessary to Fourier transform the characteristic function. Doing this calculation led to another discrete function, the interpretation of which was not as apparent.

[2]The author includes himself in the list of those re-inventing the wheel.

The phase space has D^2 points; therefore, most work had concentrated on finding a Wigner function with a value for each grid point. Even in previous work, however, it was found that it was not always possible to find such a function. In particular, when the dimension of the Hilbert space was even, some researchers had found it necessary to use a discrete function with $4D^2$ points. Our calculation found that the Wigner function could have $4D^2$ points for all dimensions. The question was why? The answer was found in the symmetry operations. With these additional points, our Wigner function is found to have the proper action under displacement, Fourier transform, and time reversal and therefore, all symmetry operations. Without these extra points, no defined Wigner function would behave properly in all dimensions; they are rejected as being unphysical.

Having a distribution in our phase space[3], it now seemed possible to begin a program which could explore the classical limit. The idea behind such a program relied on finding coherent states whose Wigner function's classical limit could be shown to be a delta function. This delta function limit would be conferred a classical point status. If the map being studied acted on this coherent state to create a Wigner function that also limited to a delta function, then the limit of the quantum map would be the classical function which mapped the first point to the second point. Looking for these coherent states began the work of Chapter 4. A literature search unearthed the idea of periodically continuing the Weyl coherent states. These states were fairly easy to work with and an analytical expression could be found for their Wigner function. Unfortunately, their classical limit was found to be uncooperative. The Wigner function for these state have "interference" terms which take the form of sharp peaks of alternating sign. In the limit, these peaks do not disappear as desired; instead, they oscillate with ever greater frequency, making the classical limit undefined.

[3]Even if it did have a bit too many points.

It was therefore necessary to try a different approach to find the classical limit. Having discussed this problem with colleagues, the author was encouraged to attempt a program which relied upon the coherent states in a different way. Instead of trying a geometrical approach where the states were found to limit to points in the plane, the coherent states could be used to find a representation of a quantum map's propagator. If this coherent state representation of the propagator was found to have a semi-classical "Van-Vleck" form, *i.e.* an exponentiation of the classical map's generating function, then the limit of the map would be verified. Unfortunately, there was still no guarantee of success since this program had not been tried for either the periodically continued coherent states or for a map defined in $\mathcal{H}_D$. Moreover, it had been shown in other cases that the Van-Vleck form was not always recovered.

Having decided that this new classical limit program was a worthy successor, it was necessary to study these coherent states in detail; therefore, the rest of Chapter 4 was born. First the method of finding the Fourier series expansion for the periodic pieces of the coherent state wavefunction was devised in order to show that these states have the expected momentum representation. Next, it was shown that a specific subset of these coherent states were complete. This allowed us to define a D^2 valued discrete Q-function for $\mathcal{H}_D$ which was later discovered to have all of the symmetry operations correctly defined for it. It was also easily shown that the squeezed states could be periodically continued in the same fashion. While these states were not needed in the classical limit program, their existence is intrinsically interesting and was included for future study. Finally, since the Wigner and Q-function had already been defined, it was natural to wonder if their interrelation had the same Gaussian convolution form of the continuous case. As the proof of this statement's veracity was determined without too much trouble, it was included here.

Once the coherent states were well understood, Chapter 5 was needed to introduce the quantum baker's map. As this work had mostly been done by other authors, this

chapter was necessarily a review of pertinent information. We began historically by first introducing the Balazs and Voros quantum baker's map. Given that their introduction to the map had been found by some to be lacking in clarity, we reformulated their map into a more active form using the Q-function. We showed that the action of their map is to take states which have good position and momentum localization to states whose localization is doubled in position and halved in momentum. In this way, their quantum baker's map recreates the classical one.

We then introduced the Schack-Caves class of baker's maps. Inspired by the active interpretation of the Balazs and Voros work[4], Schack and Caves created a whole set of partially Fourier transformed states which have varying position and momentum localizations. They then created a class of quantum baker's maps by setting up a correspondence from one set of states to the other. In this work, the details of these maps were thoroughly presented with special care given to the importance of the choice of anti-periodic boundary conditions. It was shown that only anti-periodic boundary conditions predicted the correct position centering of the partially Fourier transformed state. Finally, it was pointed out that the eigenvalues for one of the maps could easily be found since it was demonstrated that this map raised to the $4D$ power was equal to the identity operator.

Finally, in Chapter 6 the classical limit was found for the Schack-Caves class of baker's maps. The calculation to find the semi-classical expression for the quantum propagator had two important features. The first was that the Poisson formula could be used to replace the propagator's finite sums with a combination of infinite sums and finite integrals. Then the method of steepest descents[5] asymptotically expanded the finite integrals. The end result is that in most cases, this semi-classical propagator can be put in the Van-Vleck form; hence, we say that it has the proper classical limit.

[4]Later Saraceno would help improve the map.

[5]Or slight improvements upon the standard steepest descent formulae.

The localization of the Schack-Caves partially Fourier transformed states are dependent upon their number of position and momentum bits. We found that in taking the limit, we could control the rate at which the number of these bits approached infinity. Only in the case where the number of momentum bits was kept fixed was the correct classical limit not found. This seems to be a consequence of the fact that the localized states used to define the quantized Schack-Caves maps are not sufficiently localized in momentum if the number of momentum bits is kept constant in the limit. Presently, however, this remains only speculation. There may be the possibility of interpreting this map's limit as a stochastic version of the classical baker's map, but this also remains an open question.

7.2 Future work

When a theoretical calculation delights its creators by yielding a long sought after result, it is sometimes unappealing to consider creating further work. Such is the case here with the semi-classical program and its months of excruciatingly detailed algebraic work. But as Æsop said, "Do not invoke the gods without making some effort yourself. Otherwise you will invoke them in vain," [84] or as it is commonly translated "The gods help those who help themselves; the best prayer for good is right action."

To this end, the author has already found many open questions which could keep one busy for many months to come. The first question is obvious; can this technique be applied to other quantum maps. As was mentioned earlier, there has been evidence that other terms besides the Van-Vleck might be found in the semi-classical limit for more complicated maps. It then seems reasonable that instead of opening a favorite chaos book and sequentially attempting each map found inside, that it would be more productive to find a general classical limit theory. To call this

idea "ambitious" might be a bit of an understatement, as this has been the thrust of many research programs for many years. As of this time, the author is unsure of how to begin solving this problem, but hope springs eternal.

A problem which has a greater chance of being solved this century is the limit of the Schack-Caves, $\theta = 1$ quantum baker's map. While the interpretation of the limit being a stochastic map is the author's favorite, it remains a conjecture. Likewise, the easily assumed fault of insufficient momentum localization has not been tested. This idea could be verified by quantizing in terms of a different set of states. As was explained in Chapter 5, Schack and Caves defined their localized states by Fourier transforming the $N - n$ least significant qubits of a state. This created states which are strictly localized in position. An obvious variation of these states would be ones which are strictly localized in momentum. A whole different set of baker's maps could then be defined using these states. The expectation would be that the classical limit would be recovered for all cases in which the number of position bits is allowed to become infinite.

Another open question is that of the eigenvalue statistics. Much faith in the usefulness of these statistics has been espoused by other researchers. And while such a simple program for determining whether a quantum system is chaotic is appealing, the practical use of such statistics has proven to be troublesome. It was the author's intent to include in this work a study of the eigenvalue statistics for the Schack-Caves quantum baker's maps, the purpose of which was to demonstrate the difference in the $\theta = 1$ map, thus providing additional evidence for its improper classical limit. Upon researching the matter, however, it became clear the quantum baker's map seems to be singularly unsuited for such study. In their 1989 paper, Balazs and Voros asserted that the eigenvalue statistics for their map was dependent upon dimension [20]. In particular, for dimension $D = 2^N$ the eigenvalue statistics were found to be Poissonian, a characteristic found in non-chaotic systems. Obviously, this change

in character could be troubling for the Schack-Caves maps which are defined only for such dimensions. Later, Saraceno claimed that the introduction of anti-periodic boundary conditions would destroy the eigenvalues' dimensional dependence [21]. Indeed the eigenvalues were changed; numerical studies found that for anti-periodic boundary conditions, the eigenvalue statistics were neither Poissonian nor any of the types of statistics which are supposed to indicate chaos. It seems that more study will be needed before any claims about the eigenvalue statistics of the quantum baker's maps can be made.

Finally, the periodically continued squeezed states could be studied in detail. One needs only to examine the large body of literature on the continuous squeezed states to realize the usefulness of the existence of a discrete analog. In particular, there are many unanswered questions about their use in defining a squeezed Q-function. In the continuous case, the squeezed states can be used to define the probability density for the simultaneous measurement of position and momentum in the Arthurs-Kelly model[6]. It remains an open question as to whether this measurement model can be adapted to $\mathcal{H}_D$ given that position and momentum are not defined for it. Alternatively, the POVM defined from these finite squeezed states could be used to create position and momentum operators different from those discussed in Chapter 2.

[6]See Chapter 4 for references.

Appendix A

The method of steepest descents: A brief introduction

This Appendix serves as the briefest possible introduction to the method of steepest descents. For a more detailed explanation, the reader is urged to investigate one of the many available resources from books [85, 83] to online notes [86].

The method of steepest descents is a technique for finding the asymptotic expansion for certain types of integrals. We are interested in integrals of the form

$$\int dz\, \phi(z) \exp\left[-\lambda g(z)\right], \tag{A.1}$$

with the parameter $\lambda \to \infty$. Many times this technique is referred to as the saddle-point method or saddle-point approximation for reasons which will become clear shortly.

As a means of introducing the important concepts, let's first consider the case when $g(z)$ is a real function. In the case, we wish to find an asymptotic expression

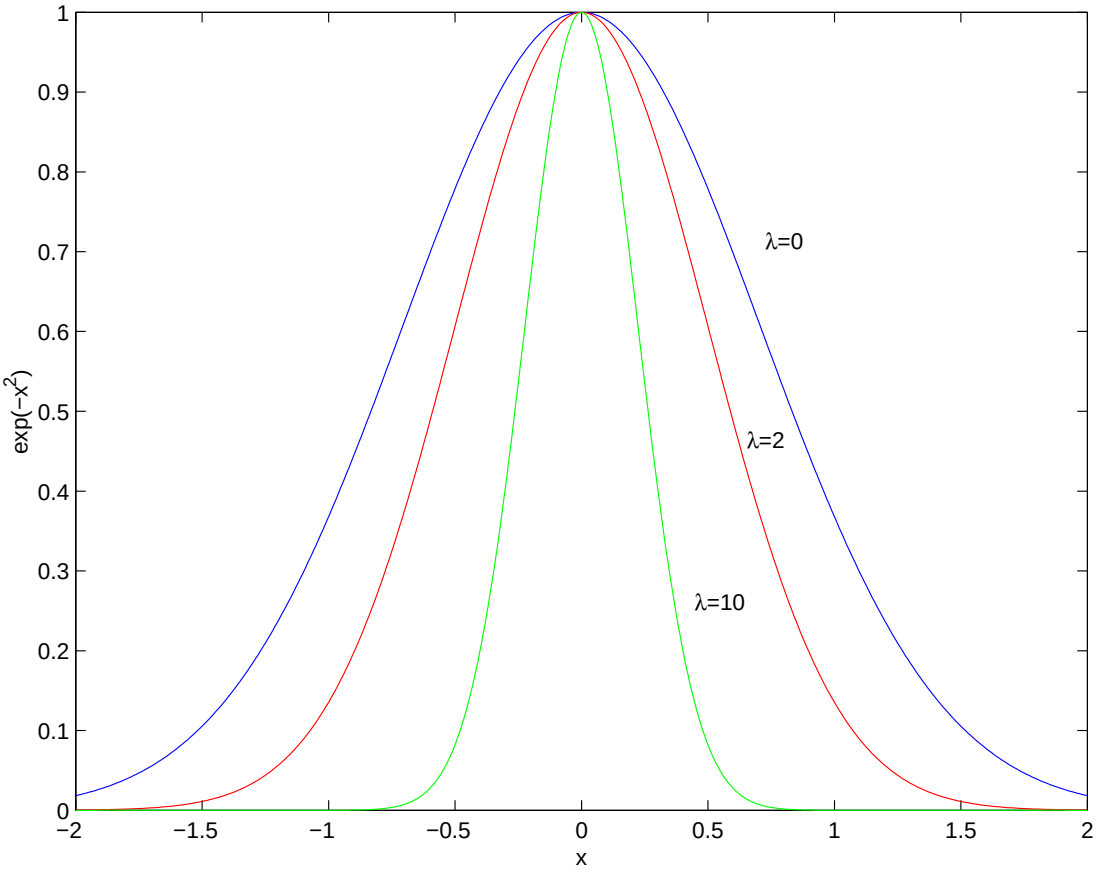

Figure A.1: Plots of $\exp(-\lambda x^2)$ showing the increase in localization as λ increases.

for the integral

$$\int_a^b dx\, f(x) \exp\left[-\lambda g(x)\right]. \tag{A.2}$$

The heuristic behind the method of steepest descent is quite simple in this case: If the function $g(x)$ has a maximum at the point x_0 somewhere in the range (a, b) then as $\lambda \to \infty$, $g(x_0)$ will dominate the integrand. Figure A.1 demonstrates this by plotting $\exp\left[-\lambda x^2\right]$ for increasing values of λ. To find an asymptotic expansion of the integral, we approximate $g(x) = g(x_0) + 1/2g''(x_0)(x - x_0)^2$ as a Gaussian and assume that the function is peaked enough to ensure that the function $f(x)$ can

be considered constant and that the tails of the Gaussian are unimportant to the integrals value. Using these approximations, we arrive at our asymptotic expansion,

$$\int_a^b dx\, f(x) \exp\left[-\lambda g(x)\right] = \sqrt{\frac{2\pi}{\lambda g''(x_0)}} \exp\left[-\lambda g(x_0)\right] \left[f(x_0) + O\big(\frac{\exp\left[-\lambda g(x_0)\right]}{\lambda^{3/2}}\big) \right]. \tag{A.3}$$

It is possible, even likely, that $g(x)$ will not have a maximum within the integral's range. In this case, one of the endpoints becomes the maximum. In the case when $g(x)$ has zero derivative at the endpoints, one can show[1] that the contribution to the asymptotic expansion is exactly half that of Equation A.3. Otherwise, the asymptotic expansion is found by using $g(x) \approx g(a) + g'(a)(x-a)$,

$$\int_a^b dx\, f(x) \exp\left[-\lambda g(x)\right] = -\frac{f(a)}{\lambda g(a)} \exp\left[-\lambda g(a)\right] \left[1 + O(1/\lambda)\right]. \tag{A.4}$$

A similar calculation for $x_0 = b$ gives the same results with the opposite sign.

In the case when $g(z)$ has an imaginary part, this simple heuristic argument will not work. As $\lambda \to \infty$, this imaginary part will create oscillations that could destroy the exponent's convergence. Instead, we use Cauchy's theorem[2] to deform the integral path to a contour in the complex plane where $\mathrm{Im}\left(g(z)\right)$ is constant. Then in the limit $\lambda \to \infty$, the dominating contribution to the integral will occur at the point along the contour where the value of $\mathrm{Re}\left(g(z)\right)$ is maximum, so we can approximate the integral using Equation A.3. Given that we integrate along paths where the imaginary part of $g(z)$ is constant, the maxima will be found at the points where the total derivative of the function is equal to zero, *i.e.*

$$\left.\frac{dg}{dz}\right|_{z=z'} = 0.$$

[1]The proof of this statement is fairly simple and relies upon "Watson's Lemma," but as the details are unimportant to the work here, we shall state it as fact. The details can be found in Bleistein [85].

[2]A reminder: Cauchy's theorem states that the value of a closed integral in the complex plane is $2\pi i$ times the sum of the residues.

This point is called the saddle point which is why this technique is often referred to as the saddle point approximation.

In the region of the saddle point, it can be shown that along the paths where $\mathrm{Im}\Big(g(z)\Big) = \text{constant}$, the value of $g(z)$ is always less than its value at the saddle point. Hence we are always descending from the saddle point; therefore, we call this path the steepest descent.

References

[1] J. H. Van Vleck. The correspondence principle in the statistical interpretation of quantum mechanics. *Proceedings of the National Academy of Science USA*, 14:178–188, 1928.

[2] A. Einstein. Zum quantensatz von Sommerfeld und Epstein. *Verhandlungen der Deutscher Physikalischer Gesellschaft*, 8:82–92, 1917.

[3] L. Brillouin. Remarques sur le méchanique ondulatoire. *Le Journal de Physique et le Radium*, 7:353–368, 1926.

[4] J. Keller. Corrected Bohr-Sommerfeld quantum conditions for nonseperable systems. *Annals of Physics*, 4:180–189, 1958.

[5] N. Hall, editor. *Exploring Chaos*. W.W. Norton & Company, New York, 1993.

[6] M. Hénon and C. Heiles. The applicability of the third integral of motion: Some numerical experiments. *Astronomical Journal*, 69:73–79, 1964.

[7] B. Chirikov. Universal instability of many-dimensional oscillator systems. *Physics Reports*, 52:263–379, 1979.

[8] G. Zaslavsky. Stochasticity in quantum-systems. *Physics Reports*, 80:157–198, 1981.

[9] M. Berry. Quantum chaology. *Proceedings of the Royal Society of London A*, 413:183–198, 1987.

[10] M. C. Gutzwiller. *Chaos in Classical and Quantum Mechanics*. Springer Verlag, New York, 1990.

[11] F. Haake. *Quantum Signatures of Chaos*. Springer-Verlag, Berlin, 1991.

[12] W. Zurek and J. Paz. Quantum chaos: A decoherent definition. *Physica D*, 83:300–308, 1995.

[13] R. Schack and C. Caves. Information-theoretic characterization of quantum chaos. *Physical Review E*, 53:3257–3270, 1996.

[14] B. Mirbach and H. Korsch. Phase-space entropy and global phase-space structures of (chaotic) quantum-systems. *Physical Review Letters*, 75:362–365, 1995.

[15] M. Gutzwiller. Phase-integral approximation in momentum space and the bound state of an atom. *Journal of Mathematical Physics*, 8:1979–2001, 1967.

[16] M. Berry and M. Tabor. Closed orbits and the regular bound spectrum. *Proceedings of the Royal Society of London A*, 349:101–123, 1976.

[17] O. Bohigas, M. Giannoni, and C. Schmit. Characterization of chaotic quantum spectra and universality of level fluctuation laws. *Physical Review Letters*, 52:1–4, 1984.

[18] T. Guhr, A. Müller-Groeling, and H. Weidenmüller. Random-matrix theories in quantum physics: common concepts. *Physics Reports*, 299:189–425, 1998.

[19] A. J. Lichtenberg and M. A. Lieberman. *Regular and Chaotic Dynamics*. Springer-Verlag, New York, 1992.

[20] N. L. Balazs and A. Voros. The quantized baker's transformation. *Annals of Physics*, 190:1–31, 1989.

[21] M. Saraceno. Classical structures in the quantized baker transformation. *Annals of Physics*, 199:37–60, 1990.

[22] J. Hannay, J. Keating, and A. Ozorio de Almeida. Optical realization of the baker's transformation. *Nonlinearity*, 7:1327–1342, 1994.

[23] R. Rubin and N. Salwen. A canonical quantization of the baker's map. *Annals of Physics*, 269:159–181, 1998.

[24] A. Lesniewski, R. Rubin, and N. Salwen. Classical limits for quantum maps on the torus. *Journal of Mathematical Physics*, 39:1835–1847, 1998.

[25] R. Schack. Using a quantum computer to investigate quantum chaos. *Physical Review A*, 57:1634–1635, 1998.

[26] T. Brun and R. Schack. Realizing the quantum baker's map on a NMR quantum computer. *Physical Review A*, 59:2649–2658, 1999.

[27] P. Pakoński, A. Ostruszka, and K. Życzkowski. Realizing the quantum baker's map on a NMR quantum computer. *Nonlinearity*, 12:269–284, 1999.

[28] R. Schack and C. M. Caves. Shifts on a finite qubit string: A class of quantum baker's maps. *Applicable Algebra in Engineering, Communication and Computing*, 10:305–310, 2000.

[29] A. N. Soklakov and R. Schack. Classical limit in terms of symbolic dynamics for the quantum baker's map. *Physical Review E*, 61:5108–5115, 2000.

[30] R. Griffiths. Consistent histories and the interpretation of quantum mechanics. *Journal of Statistical Physics*, 36:219–272, 1984.

[31] R. Omnès. Logical reformulation of quantum mechanics 1: Foundations. *Journal of Statistical Physics*, 53:893–932, 1988.

[32] M. Gell-Mann and J. B. Hartle. Classical equations for quantum-systems. *Physical Review D*, 47:3345–3382, 1993.

[33] H. Weyl. *The Theory of Groups and Quantum Mechanics*. Dover Press, New York, 1978.

[34] J. Schwinger. *Quantum Kinematics and Dynamics*. W.A. Benjamin, Inc., New York, 1970.

[35] A. Perelomov. *Generalized Coherent States and Their Applications*. Springer-Verlag, New York, 1986.

[36] R. Feynman and A. Hibbs. *Quantum Mechanics and Path Integrals*. McGraw-Hill, New York, 1964.

[37] A. Ozorio de Almeida and M. Saraceno. Periodic orbit theory for the quantized baker's map. *Annals of Physics*, 210:1–15, 1991.

[38] B. Eckhardt and F. Haake. Periodic orbit quantization of baker's map. *Journal of Physics A: Mathematics and General*, 27:4449–4455, 1994.

[39] M. Saraceno and A. Voros. Towards a semiclassical theory of the quantum baker's map. *Physica D*, 79:206–268, 1994.

[40] F. Dittes, E. Doron, and U. Smilansky. Long-time behavior of the semiclassical bakers map. *Physical Review E*, 49:R963–R966, 1994.

[41] A. Lakshminarayan. On the quantum baker's map and its unusual traces. *Annals of Physics*, 239:272–295, 1995.

[42] M. da Luz and A. Ozorio de Almeida. Path integral for the quantum baker's map. *Nonlinearity*, 8:43–64, 1995.

[43] L. Kaplan and E. Heller. Overcoming the wall in the semiclassical baker's map. *Physical Review Letters*, 76:1453–1456, 1996.

[44] F. Toscano, R. Vallejos, and M. Saraceno. Boundary contributions to the semiclassical traces of the baker's map. *Nonlinearity*, 10:965–978, 1997.

[45] G. Tanner. Periodic orbit action correlations in the baker map. *Journal of Physics A: Mathematics and General*, 32:5071–5085, 1999.

[46] J. H. Hannay and M. V. Berry. Quantization of linear maps on a torus - Fresnel diffraction by a periodic grating. *Physica D*, 1:267–290, 1980.

[47] W. K. Wootters. A Wigner-function formulation of finite-state quantum mechanics. *Annals of Physics*, 176:1–21, 1987.

[48] U. Leonhardt. Quantum-state tomography and discrete Wigner function. *Physical Review Letters*, 74:4101–4105, 1995.

[49] M. Kuś, F. Haake, and B. Eckhardt. Quantum effects of periodic-orbits for the kicked top. *Zeitschrift Für Physik B- Condensed Matter*, 92:221–233, 1993.

[50] A. J. Scott and G. J. Milburn. Periodic orbit quantization of a hamiltonian map on the sphere. *Journal of Physics A: Mathematics and General*, 34:7541–7562, 2001.

[51] Chang Shau-Jin and Kang-Jie Shi. Time evolution and eigenstates of a quantum iterative system. *Physical Review Letters*, 55:269–272, 1985.

[52] M. Baranger, M. de Aguiar, F. Keck, H. Korsch, and B. Schellhaaß. Semiclassical approximations in phase space with coherent states. *Journal of Physics A: Mathematics and General*, 34:7227–7286, 2001.

[53] K. Inoue, M. Ohya, and I. Volovich. Semiclassical properties and chaos degree for the quantum baker's map. *Journal of Mathematical Physics*, 43:734–755, 2002.

[54] W. Zurek. Environment-induced superselection rules. *Physical Review D*, 26:1862–1880, 1982.

[55] Giulini *et al. Decoherence and the Appearance of a Classical World in Quantum Theory*. Springer-Verlag, New York, 1997.

[56] S. Habib, K. Shizume, and W. Zurek. Decoherence, chaos, and the correspondence principle. *Physical Review Letters*, 80:4361–4365, 1998.

[57] T. Bhattacharya, S. Habib, and K. Jacobs. Continuous quantum measurement and the emergence of classical chaos. *Physical Review Letters*, 85:4852–4855, 2000.

[58] A. Scott and G. Milburn. Quantum and classical chaos for a single trapped ion. *Physical Review A*, 63:013401/1–7, 2000.

[59] A. de la Torre and D. Goyeneche. Quantum mechanics in finite dimensional hilbert spaces. `ArXive:quant-ph/0205159`, 2002.

[60] A. Messiah. *Quantum Mechanics Volume II*. John Wiley & Sons, Inc., 1966. Translated by J. Potter.

[61] E. P. Wigner. On the quantum correction for thermodynamic equilibrium. *Physical Review*, 50:749–759, 1932.

[62] U. Leonhardt. Discrete Wigner function and quantum-state tomography. *Physical Review A*, 53:2998–3013, 1996.

[63] D. Galetti and A. F. R. de Toledo Piza. An extended Weyl-Wigner transformation for special finite spaces. *Physica A*, 149:267–282, 1988.

[64] O. Cohendet, Ph. Combe, M. Sigurne, and M. Sigurne-Collin. Fokker-Planck equation associated with the Wigner function of a quantum system with a finite number of states. *Journal of Physics A: Mathematics and General*, 23:2001–2011, 1990.

[65] P. Bianucci, C. Miquel, J. P. Paz, and M. Saraceno. Discrete Wigner functions and the phase space representation of quantum computers. `ArXive:quant-ph/0106091`, 2001.

[66] I. Dana, M. Feingold, and M. Wilkinson. Band distributions for quantum chaos on a torus. *Physical Review Letters*, 81:3124–3127, 1998.

[67] A. Lakshminarayan. Semiclassical theory of the sawtooth map. *Physics Letters A*, 192:345–354, 1994.

[68] T. Opatrny, D. G. Welsch, and V. Bužek. Parameterized discrete phase-space functions. *Physical Review A*, 53:3822–3835, 1996.

[69] A. Luis and J. Peřina. Discrete Wigner function for finite-dimensional systems. *Journal of Physics A: Mathematics and General*, 31:1423–1441, 1998.

[70] C. Brif and A. Mann. A general theory of phase-space quasiprobability. *Journal of Physics A: Mathematics and General*, 31:L9–L17, 1998.

[71] P. Leboeuf and A. Voros. Chaos-revealing multiplicative representation of quantum eigenstates. *Journal of Physics A: Mathematics and General*, 23:1765–1774, 1990.

[72] S. Nonnenmacher. *Etats propres de systèmes classiquement chaotiques dans l'espace des phases*. Ph.d. thesis, Université Paris XI, 1998.

[73] E. Arthurs and J. Kelly. On the simultaneous measurement of a pair of conjugate variables. *The Bell System Technical Journal*, 44:725, 1965.

[74] E. Arthurs and M. Goodman. Quantum correlations: A generalized Heisenberg uncertainty relation. *Physical Review Letters*, 60:2447–2449, 1988.

[75] S. Braunstein, C. Caves, and G. Milburn. Interpretation for a positive P representation. *Physical Review A*, 43:1153–1159, 1991.

[76] M. Berry and M. Tabor. Level clustering in the regular spectrum. *Proceedings of the Royal Society of London A*, 356:375–394, 1977.

[77] E. Bogomolny, O. Bohigas, and P. Leboeuf. Distribution of roots of random polynomials. *Physical Review Letters*, 68:2726–2729, 1992.

[78] J. Hannah. Chaotic analytic zero points: exact statistics for those of a random spin state. *Journal of Physics A: Mathematics and General*, 29:L101–L106, 1996a.

[79] T. Prosen. Exact statistics of complex zeros for Gaussian random polynomials with real coefficients. *Journal of Physics A: Mathematics and General*, 29:4417–4423, 1996.

[80] P. Shukla. On the distribution of zeros of chaotic wavefunctions. *Journal of Physics A: Mathematics and General*, 30:6313–6326, 1997.

[81] A. Scott. *Classical and Quantum Nonlinear Dynamics*. Ph.d. thesis, University of Queensland, 2001.

[82] M. Tracy and A. Scott. The classical limit for a class of quantum baker's maps. *Journal of Physics A: Mathematics and General*, 35:8341–8360, 2002.

[83] R. Wong. *Asymptotic Approximations of Integrals*. Academic Press, Boston, 1989.

[84] Æsop. *Æsop, The Complete Fables*. Penguin Classics, Harmondsworth, Middlesex, England, 1998. Translated by Olivia and Robert Temple.

[85] N. Bleistein and R. Handelsman. *Asymptotic expansions of integrals*. Holt, Rinehart and Winston, New York, 1975.

[86] I. Avramidi. Lecture notes on asymptotic expansion. Available online at `www.nmt.edu/~iavramid`, 2000.